UNIVERSITY OF CAPE TOWN

Finite size effects in the thermodynamics of the free scalar field and the interacting SU(3) plasma (amended version)

by

Husam Mohamed

Supervisor: André Peshier

A thesis presented for the academic degree of Master of Science

in the

Faculty of Science

Department of Physics

October 2017

Declaration of Authorship

I, Husam Mohamed (student number: MHMHUS003), declare that this thesis and the work presented in it are my own. I confirm that:

- I know that plagiarism is wrong. Plagiarism is to use another's work and to pretend that it is one's own.
- Each significant contribution to, and quotation in, this project from the work of other people has been been cited and referenced.
- This report is my own work.
- I have not allowed, and will not allow, anyone to copy my work with the intention of passing it off as his or her own work.

Signed: Signed by candidate

Date: 10/9/2017

UNIVERSITY OF CAPE TOWN

Abstract

Faculty of Science
Department of Physics

Master of Science

by Husam Mohamed
Supervisor: André Peshier

In this thesis, we study the thermodynamic properties of the free scalar field and the thermodynamics of the interacting SU(3) plasma when these systems are away from the thermodynamic limit, i.e., at finite volume.

In the first part of the thesis, we study the thermodynamic properties of the free scalar field in a variety of finite-size geometries (the cube, the cuboid and the parallel-plates geometries) when the field is subjected to Dirichlet and periodic boundary conditions; we also give a brief review of the thermodynamic properties of the free scalar field on discretized Euclidian space-time lattices.

In the second part of the thesis, we discuss briefly the thermodynamic properties of the quark-gluon plasma in the continuum and thermodynamic limits, and then we use a quasi-particle model of the SU(3) plasma to shed some light on the interplay of finite-size and generic interaction effects in the context of lattice QCD calculations.

Acknowledgements

I would first like to thank my thesis advisor Professor André Peshier of the Department of Physics at the University of Cape Town. The door to Prof. Peshier's office was always open whenever I ran into a trouble or had a question about my research or writing. He has given his knowledge and put in effort at all times for the benefit of this thesis.

I also wish to thank my colleagues Greg Jackson and Dr. Sylvain Mogliacci who were kind enough to offer many useful comments on my thesis as I was researching and writing it.

Finally I would like to thank the African Institute for Mathematical Sciences (AIMS), the University of Cape Town (UCT) and the Head of Physics Department at UCT, Professor Andy Buffler, for providing me with generous bursaries that helped me complete this thesis.

Author

Husam Mohamed

Contents

Chapter 1

Introduction

Quantum field theory is the union of Einstein's Special Relativity and Quantum Mechanics. It is the foundation of the Standard Model of Particle Physics which describes all known elementary particles and their interactions, with the exception of gravity [1]. Quantum field theory is thus widely applied in the theoretical description of Heavy-ion collision experiments, as well as to a wide range of questions in cosmology (e.g. the origin of dark matter, and the observed matter-antimatter asymmetry) [2]. It is also used for constructing quasi-particle models in condensed matter physics [3].

However, the thermodynamics of quantum field theories are often calculated in the infinite volume limit [4], [5]. The assumption of infinite volume perhaps has its roots in our conceptualizing of the Universe to be unbounded, or at least too large in stretch that it is effectively infinite (often times the word "infinite" is used to mean "sufficiently large", which is fairly well-justified when referring to the size of the universe). Furthermore, the assumption of infinite volume is greatly convenient from a theoretical point of view since integrals are easier to evaluate than sums, and thus it permits more often an analytic investigation of the quantities of interest (e.g. the pressure, energy and entropy) that leads to closed form results, or at least simplifies the calculations.

For example, the assumption of infinite volume allows for a simple, closed-form evaluation of the partition function of a free massless scalar field and the partition function of a massless non-interacting fermionic field [4]. Also, in the theories of Quantum Electrodynamics (QED) and Quantum Chromodynamics (QCD), the perturbative evaluation of the partition function is usually done in the infinite volume limit [4], [5].

Though the assumption of infinite volume is theoretically convenient, some phenomenon require a consideration of finite-volume effects[1]. For example, particle accelerators probe

[1] We will often use the words "volume" and "geometry" interchangeably.

only finite-size systems, also, in the numerical simulations of QCD thermodynamic properties, space-time is approximated by finite, discretized space-time lattice (where the lattice spatial volume is $\sim 10^4$ Fermis^3) [6] [7] [8], not to mention that the universe in its entirety may be finite in volume. Furthermore, finite volume can result in the emergence of an observable contribution to the pressure and energy density of a quantum field from vacuum fluctuations (the Casimir effect) [9], [10].

Also in the situations relevant to Heavy-ion collisions, where typical temperatures are a few hundred Megaelectron-volts and typical length are a few Fermis, generic interaction effects can be of similar order of magnitude to finite-size effects [7].

A study of the interplay of finite-size and generic interaction effects on the thermodynamics of field theories and a quantification of such effects are therefore needed. In this thesis, we endeavor to study some aspects of finite-size effects on the thermodynamics of the free scalar field and attempt to shed some light on the interplay between finite-size and interaction effects on the thermodynamics of the SU(3) plasma.

Outline

We divide this work into two parts:

Part 1 (chapter 2)

We devote this part to a discussion of finite-size effects on the thermodynamics of the free scalar field: We first discuss the energy-momentum spectrum of a free scalar in infinite volume, we then discuss how this energy-momentum spectrum is altered when the field is placed in finite geometries (cube, cuboid, parallel plates and spherical cavity geometries) and Dirichlet and periodic boundary conditions are imposed on the field. We then discuss the partition function of a free scalar field and illustrate how the Free energy density, energy density, pressure and entropy density of the field can be derived in any given geometry with given boundary conditions. Next, we discuss the renormalization of the divergent vacuum contributions (the Casimir effect), in the case of a massless field, first as they arise in the parallel plates geometry. We then discuss the Casimir effects in the cube and cuboid geometries and, in anticipation of interaction-generated masses that will be discussed in the second part of the thesis, analyze the effects of a non-zero mass on the Casimir effect. We then discuss the full (vacuum and finite-temperature) thermodynamic bulk properties of the field in these geometries as well as the effect of the non-zero mass on these bulk properties. We then discuss the entropy density of the

free scalar field in these geometries and boundary conditions. Finally, we discuss the thermodynamic bulk properties of the free scalar field on a discretized space-time (a finite Euclidian lattice). The formalism and methodology used in this first part of the thesis will be re-applied to the discussions in the second part of the thesis.

Part 2 (chapter 3)

In this part, we discuss the general properties of quarks and gluons; we then discuss the partition function of QCD and its perturbative evaluation. Thereafter, to motivate the quasi-particle model, we discuss the propagation of gluons in a QCD plasma, and derive the gluon thermal mass and the dispersion relations of the transverse gluon quasi-particles in the plasma. We then discuss briefly lattice calculations of the thermodynamic bulk properties of pure gauge systems. We then review a quasi-particle model in infinite volume and attempt to use it to gain some insight into the continuum-extrapolation of lattice QCD results. In the final section, we extend the quasi-particle model to finite lattices (this will lead us to a divergence of the gluon thermal mass at leading order in the coupling, for which will propose a regulator) and attempt to use it to gain some insight into the interplay of finite-size and interaction effects in lattice QCD calculations.

System of units

We use the *natural units* system: $c = \hbar = 1$. Temperature, momentum and mass have the dimensions of energy, and length has the dimensions of inverse energy. The unit of energy is Megaelectron-volt (MeV) and the unit of length is Fermi (fm) with 1 fm^{-1} = 200 Mev.

Chapter 2

Free scalar field thermodynamics in infinite and finite volumes

We begin by a discussion of the effects of finite volume (geometry) on the thermodynamics of the free scalar field as the scalar field can serve as a prototype theory for many of the physical features that appear in more complicated theories such as QCD.

2.1 Free scalar field in an infinite space

Consider a free scalar field ϕ in infinite four-dimensional Minkowski space-time ($x = x^\mu = \{t, x^1, x^2, x^3\} = \{t, r\}$ and $x_\mu = g_{\mu\nu}x^\nu = \{t, x_1, x_2, x_3\} = \{t, -r\}$). The equation of motion of this field is the Klein-Gordon equation

$$\frac{\partial^2\phi}{\partial t^2} - \nabla^2\phi + m^2\phi(x) = 0 \,, \tag{2.1}$$

where m is the mass of the field. This equation of motion can be derived from action

$$S[\phi] = \int d^4x \mathscr{L}(x) = \int d^4x \left[\frac{1}{2}\Big(\frac{\partial\phi}{\partial t}\Big)^2 - \frac{1}{2}\Big(\nabla\phi\Big)^2 - \frac{m^2}{2}\phi^2\right] \tag{2.2}$$

via the Euler-Lagrange equation. The Klein-Gordon equation (2.1) has positive- and negative-frequency solutions

$$\phi_k^{(\pm)}(t, r) = \frac{1}{\sqrt{2\omega_k}}\frac{1}{(2\pi)^3}e^{\mp i(\omega_k t - k\cdot r)} \,, \tag{2.3}$$

where

$$k = (k_1, k_2, k_3) \ , \tag{2.4}$$

$$\omega_k = \sqrt{k^2 + m^2} \ , \tag{2.5}$$

are the momentum vector and the energy (frequency), respectively.

The solutions (2.3) satisfy the Ortho-normalization condition

$$\left(\phi_k^{(\pm)}, \phi_{k'}^{(\pm)}\right) = i \int_V dV \left(\phi_k^{(\mp)} \, \partial_t \phi_{k'}^{(\pm)} - \phi_{k'}^{(\pm)} \, \partial_t \phi_k^{(\mp)}\right) = \pm \delta^{(3)}(k - k') \ ,$$

where V is the volume of whole space and $\delta^{(3)}(k-k')$ is the three-dimensional Dirac delta function. The most general solution of the Klein-Gordon equation is a superposition of positive- and negative-frequency solutions, which reads

$$\phi(x) = \int d^3k \left[\phi_k^{(+)}(x) a_k + \phi_k^{(-)}(x) a_k^\dagger\right] \ , \tag{2.6}$$

where a_k and a_k^+ are the creation and annihilation operators of a particle with momentum k. The appearance of the creation and annihilation operators is a consequence of the fact that ϕ is a quantum field. The creation and annihilation operators satisfy the following commutation relations

$$[a_k, a_{k'}^\dagger] = \delta^{(3)}(k - k') \ , \qquad [a_k, a_{k'}] = [a_k^\dagger, a_{k'}^\dagger] = 0 \ . \tag{2.7}$$

2.2 Scalar field in finite space subjected to various boundary conditions

In the previous section we discussed the form of the solutions of the Klein-Gordon equation in infinite volume. In this section we are going to discuss the solutions that arise in finite volumes, and how boundaries alter the behavior of the field.

2.2.1 Scalar field in 1+1 dimensions with Dirichlet boundary conditions

Consider, as an elementary case, a scalar field ϕ in $1 + 1$ space-time ($t, x^1 = x$). The Klein-Gordon equation (2.1) simplifies to

$$\frac{\partial^2 \phi}{\partial t^2} - \frac{\partial^2 \phi}{\partial x^2} + m^2 \phi(t, x) = 0 \ . \tag{2.8}$$

Let's study, as a particular situation, the properties of the field on a finite interval $0 < x < L$, and impose the following *boundary conditions* (BCs) on the field

$$\phi(t,0) = \phi(t,L) = 0 \,, \tag{2.9}$$

i.e., the field vanishes at the boundaries. These conditions are called Dirichlet BCs. An example of Dirichelt BCs would be the vanishing of an Electromagnetic field at the boundaries of a perfect conductor. Equation (2.8) can now be solved by separation of variables. Let the solution be

$$\phi(t,x) = \psi(t)\chi(x) \,. \tag{2.10}$$

Substituting this into (2.8) gives

$$\frac{1}{\psi(t)}\frac{\partial^2\psi(t)}{\partial t^2} + m^2 - \frac{1}{\chi(x)}\frac{\partial^2\chi(x)}{\partial x^2} = 0 \,, \tag{2.11}$$

from which

$$\frac{1}{\psi(t)}\frac{\partial^2\psi(t)}{\partial t^2} + m^2 = -(k_n^D)^2 \,, \tag{2.12}$$

$$\frac{1}{\chi(x)}\frac{\partial^2\chi(x)}{\partial x^2} = -(k_n^D)^2 \,. \tag{2.13}$$

Here the constant k_n^D can be interpreted as the momentum vector, the superscript D stands for Dirichlet. The meaning of the index n will become apparent shortly. Equations (2.12) and (2.13) are simple harmonic oscillator differential equations, however the second, spatial one is subject to Dirichlet BCs. By solving (2.12) and (2.13), one obtains the general solution

$$\psi(t) = Ae^{\pm i\omega_n^D t} \,, \qquad \omega_n^D = \sqrt{(k_n^D)^2 + m^2} \,, \tag{2.14}$$

$$\chi(x) = B\cos\left(k_n^D x\right) + C\sin\left(k_n^D x\right) \,, \tag{2.15}$$

where A, B and C are constants. Let us now see how the spatial part (2.15) can be made to satisfy the BCs (2.9): The cosine does not vanish at $x = 0$ and thus $B = 0$, and the sine vanishes at $z = L$ only if

$$k_n^D L = n\pi \to k_n^D = \frac{n\pi}{L} \,, n = \pm 1, \pm 2, \ldots \,. \tag{2.16}$$

Thus, unlike in infinite volume, the energy-momentum spectrum of the field in a finite volume is discrete and is determined by the geometry (here the length of the interval

L). The solution satisfying the BCs (2.9) becomes

$$\phi_n^{(\pm)}(t,x) = Ae^{\mp i\omega_n^D t}\sin\left(k_n^D x\right) , \tag{2.17}$$

where we have absorbed the constant C into A. Now, these solutions must satisfy the following Ortho-normalization condition

$$(\phi_n^{(\pm)}, \phi_{n'}^{(\pm)}) = i\int_0^L dx\left[\phi_n^{(\mp)}\,\partial_t\phi_{n'}^{(\pm)} - \phi_{n'}^{(\pm)}\,\partial_t\phi_n^{(\mp)}\right] = \pm\delta_{n,n'} . \tag{2.18}$$

We note that, unlike in the case of infinite space discussed in the previous section, the integral is only over $[0, L]$, and that the Dirac delta is replaced with a Kronecker delta. The condition (2.18) enables us to calculate the constant A, and thus we obtain

$$\phi_n^{(\pm)}(t,x) = \frac{1}{\sqrt{L\omega_n^D}}e^{\mp i\omega_n^D t}\sin\left(k_n^D x\right) , \qquad n = 1, 2, 3, \dots . \tag{2.19}$$

We note that negative modes in (2.16) are dropped as positive modes are sufficient to complete the basis (the negative sign can be absorbed into the normalization constant A).

And so we see that finite volume, together with BCs, alter the field's frequency-momentum spectrum in such a way that only certain frequencies and momenta are allowed. Physically, momenta correspond to wave-lengths, and so only those waves that one can "fit" inside the finite volume are allowed.

2.2.2 Scalar field in 1+1 dimensions with periodic boundary conditions

Consider a scalar field in $1+1$ space-time (t, x) and let this field have a period L in the spatial dimension, i.e.

$$\phi(t,x) = \phi(t, x+L) . \tag{2.20}$$

The BCs (2.20), for obvious reasons, are called periodic BCs (topologically speaking, the field is on a torus). Periodic BCs are often more convenient to study and are used in imaginary-time formalism and in lattice calculations, as we shall see later in this thesis. Subject to (2.20), the Klein-Gordon equation (2.8), with the Ortho-normalization condition (2.18), has positive- and negative-frequency solutions

$$\phi_n^{(\pm)}(t,x) = \frac{1}{\sqrt{L\omega_n^P}}e^{\mp i(\omega_n^P t - k_n^P x)} \tag{2.21}$$

with

$$\omega_n^P = \sqrt{(k_n^P)^2 + m^2}\,, \tag{2.22}$$

$$k_n^P = \frac{2\pi n}{L}\,, \qquad n = 0, \pm 1, \pm 2, \pm 3, \ldots\,, \tag{2.23}$$

where P stands for periodic. As with Dirichlet BCs, the momenta in the compactified spatial direction are discrete, except now both positive and negative values of the momentum index are allowed. One should also note that the spacing between successive modes with periodic BCs (2.23), for a given L, is two times larger than with Dirichlet BCs (2.16), this to some degree compensates for the doubling of the number of terms with periodic BCs (see Figure 2.1).

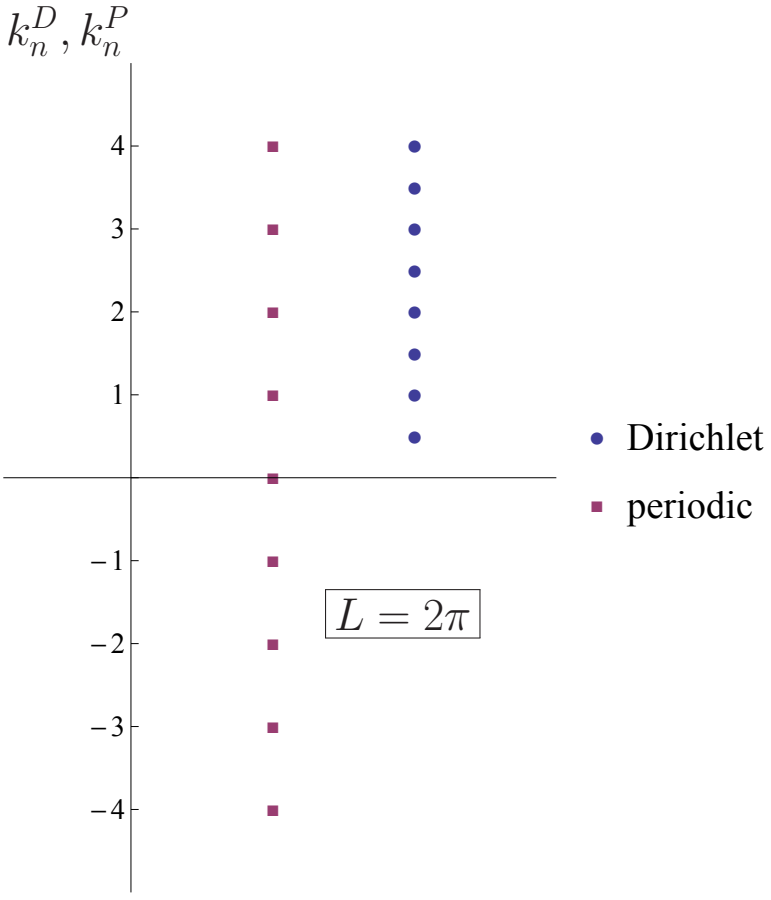

FIGURE 2.1: A visual representation of the momentum modes with Dirichlet and periodic BCs at $L = 2\pi$. The modes with Dirichlet BCs have only positive values, unlike with periodic BCs.

Though will not be discussed in this thesis, there exist several other BCs, for example, *Neumann* BCs where the *derivative* of the field vanishes at the boundaries (these are particularly useful BCs when discussing fermions) [10].

2.2.3 Scalar field in a three dimensional box with Dirichlet and periodic BCs

The most generic case of a three dimensional box is an anisotropic box with side-lengths (L_x, L_y, L_z). In this geometry, one can show, by factorization and along the lines of subsections 2.2.1 - 2.2.2, that the energy-momentum spectrum with Dirichlet BCs is

$$\omega^D_{nlp} = \sqrt{(k^D_{nlp})^2 + m^2}\,, \quad n, l, p = 1, 2, 3, \dots\,, \tag{2.24}$$

with

$$k^D_{nlp} = \sqrt{\left(\frac{\pi n}{L_x}\right)^2 + \left(\frac{\pi l}{L_y}\right)^2 + \left(\frac{\pi p}{L_z}\right)^2}\,. \tag{2.25}$$

And with periodic BCs, the energy-momentum spectrum is

$$\omega^P_{nlp} = \sqrt{(k^P_{nlp})^2 + m^2}, \quad n, l, p = 0, \pm 1, \pm 2, \dots\,, \tag{2.26}$$

with

$$k^P_{nlp} = \sqrt{\left(\frac{2\pi n}{L_x}\right)^2 + \left(\frac{2\pi l}{L_y}\right)^2 + \left(\frac{2\pi p}{L_z}\right)^2}\,. \tag{2.27}$$

We shall often consider special box geometries where the geometry depends only on one or two geometric parameters (e.g.,the side-length L), because it is easier to study the properties of the field in such special geometries and establish its generic features (for an anisotropic box, geometry depends on the three side-lengths (L_x, L_y, L_z) which is hard to study graphically and is also hard to visualize).

The simplest case of all box geometries is of course the cube (L, L, L). We will also consider the cuboid $((L, \xi L, \xi L), \xi \neq 1)$, and the limit of infinite parallel plates $((L, \xi L, \xi L), \xi \to \infty)$ (see Figure 2.2).

We see from the discussion in this subsection and subsections 2.2.1 - 2.2.2 that the energy-momentum spectrum of a scalar field in a finite geometry is determined by the interplay of geometry and BCs. In this chapter, we are going to study the effects of finite-volume on the properties of the free scalar field in various combinations of geometries and BCs.

Before we turn to study the effects of these rectangular geometries and BCs on the properties of the field, we review for completeness the spherical geometry as an example of other cases of relevance.

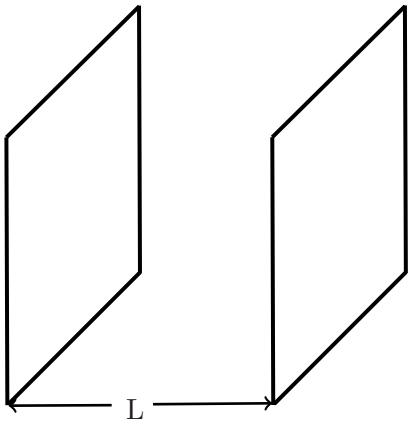

FIGURE 2.2: The infinite parallel plates geometry (the two plates are infinite in area).

2.3 Scalar field in a spherical cavity

The Klein-Gordon equation in spherical coordinates (t, r, θ, φ) follows from (2.1) by using the Laplace operator in spherical coordinates

$$\nabla^2 = \frac{1}{r^2}\frac{\partial}{\partial r}\left(r^2\frac{\partial}{\partial r}\right) + \frac{1}{r^2\sin(\theta)}\frac{\partial}{\partial\theta}\left(\sin(\theta)\frac{\partial}{\partial\theta}\right) + \frac{1}{r^2\sin^2(\theta)}\left(\frac{\partial^2}{\partial\varphi^2}\right) . \tag{2.28}$$

This equation can again be solved by separation of variables which gives, via superposition, the general solution

$$\phi(t, r, \theta, \varphi) = \frac{1}{\sqrt{2\omega_{n,l}}} e^{i\omega_{n,l}} \Phi_{n,l}(r)\ \mathrm{Y}_l^M(\theta, \varphi) , \tag{2.29}$$

where $\mathrm{Y}_l^M(\theta, \varphi)$ are the *spherical harmonics* and n, l, M are the radial index, orbital quantum number and magnetic quantum number, respectively. In infinite volume, these indices take the values

$$n = 1, 2, 3, \dots , \tag{2.30}$$

$$l = 0, 1, 2, ..., n , \tag{2.31}$$

$$M = -l, -l+1, \dots, 0, \dots, l-1, l , \tag{2.32}$$

Plugging the Ansatz (2.29) into the Klein-Gordon equation (2.1), we obtain for the radial part

$$\left[-\frac{1}{r^2}\frac{d}{dr}\left(r^2\frac{d}{dr}\right) - \frac{l(l+1)}{r^2}\right]\Phi_{n,l}(r) = (k_{n,l})^2\Phi_{n,l}(r) , \tag{2.33}$$

where $k_{n,l}$ is the momentum in the radial direction. The solutions of this equation are the spherical Bessel functions

$$\phi_{n,l}(r) = \sqrt{\frac{\pi}{2rk_{n,l}}} \mathrm{J}_{l+\frac{1}{2}}(rk_{n,l}) \,, \tag{2.34}$$

where $\mathrm{J}_{l+\frac{1}{2}}(rk_{n,l})$ is the ordinary Bessel function. The solutions (2.34) ensure that the radial wave function is regular at the origin

$$\lim_{r\to 0} \phi_{n,l}(r) \sim \sqrt{\frac{\pi}{2}} \left(\frac{rk_{n,l}}{2}\right)^2 \frac{1}{\Gamma(l+\frac{3}{2})} \,, \tag{2.35}$$

where Γ is Euler's Gamma function. Now let's see how the energy-momentum spectrum of the field in a finite spherical cavity looks like when BCs are imposed on it. We consider a spherical cavity of radius R (i.e., $r \in [0, R]$) and impose Dirichlet BCs on the radial component of the field, i.e. the field should vanish at $r = R$, which, from (2.34), gives

$$k^D_{n,l} = \frac{\chi_{\nu,n}}{R} \,, \tag{2.36}$$

where $\chi_{\nu,n}$ are the zeros of the Bessel function

$$\mathrm{J}_\nu(\chi_{\nu,n}) = 0 \,, \qquad \nu = l + \frac{1}{2} \,. \tag{2.37}$$

We see again that the momentum modes (2.36) are discrete and depend on the geometry (the radius R in particular). Similar to the energy-momentum spectrum in rectangular geometries discussed earlier, the momentum modes are roughly equidistant (see Figure 2.3), this is due to the asymptotic form of the Bessel function being

$$\mathrm{J}_\nu(z) \sim \sqrt{\frac{2}{\pi z}} \sin\left(z - \frac{(2\nu+3)\pi}{4}\right) \,, \tag{2.38}$$

which resembles the spatial part in (2.19).

Now that we have the allowed momenta, we can write down the energy-momentum spectrum of a free scalar field in a spherical cavity subject to Dirichlet BCs, which is

$$\omega^D_{n,l} = \sqrt{(k^D_{n,l})^2 + m^2} \,. \tag{2.39}$$

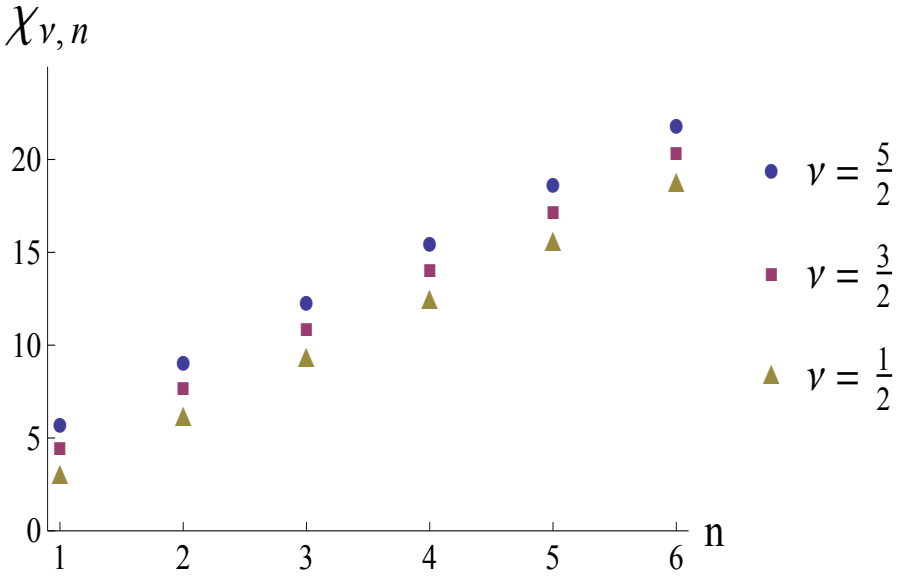

FIGURE 2.3: Some zeros of the Bessel function. Note the spectrum is approximately equidistant.

2.4 The partition function of the free scalar field

The prime object when doing thermodynamics is the partition function Z. Other thermodynamic properties can be derived directly from it. In particular

$$f = -\frac{T}{V}\ln(\mathrm{Z})\,, \tag{2.40}$$

$$e = \frac{T^2}{V}\frac{\partial \ln(\mathrm{Z})}{\partial T}\,, \tag{2.41}$$

$$p = T\frac{\partial \ln(\mathrm{Z})}{\partial V}\,, \tag{2.42}$$

$$s = \frac{1}{V}\frac{\partial}{\partial T}\Big[T\ln(\mathrm{Z})\Big]\,, \tag{2.43}$$

where f, e, p and s are the Free energy density, energy density, the pressure and entropy density, respectively.

The partition function of a free scalar in a volume V maintained in thermal equilibrium at a temperature T can be given as a functional integral [4]

$$\mathrm{Z} = N\int [d\phi] e^{-S_E(\phi)}\,, \tag{2.44}$$

where $S_E(\phi)$ is the *Euclidean action*, obtained from (2.2) via the Wick rotation $t \to i\tau$, with $\tau \in [0, 1/T]$. The field here is subject to periodic BCs in the imaginary time direction

$$\phi(0, x) = \phi(\beta, x) \tag{2.45}$$

where $\beta = 1/T$.

Integrating (2.44) by parts, and using the periodicity of ϕ, we obtain for a free scalar field

$$S = -\frac{1}{2}\int_0^\beta d\tau \int d^3x\, \phi(-\frac{\partial^2}{\partial\tau^2} - \nabla^2 + m^2)\phi\,. \tag{2.46}$$

Due to its periodicity, the field has a Fourier decomposition

$$\phi = \sqrt{\frac{\beta}{V}}\sum_{l=-\infty}^{\infty}\sum_J e^{i(J\cdot x + \xi_l\tau)}\,, \tag{2.47}$$

where

$$\xi_l = 2\pi l T\,,\quad l = 0, \pm1, \pm2, \ldots \tag{2.48}$$

are the *Matsubara frequencies* and the J's are the momentum modes. Compare the way temperature appears in (2.48) to the way length appears in (2.23), the emergence of physics at non zero temperature can be seen as a boundary effect in the imaginary-time direction with periodic BCs.

The allowed momentum modes J's in (2.47) depend on the geometry and BCs, as discussed in sections 2.2 - 2.3. Substituting (2.47) into (2.46) and recalling that the field is real, we obtain

$$S = -\frac{1}{2}\beta^2 \sum_l \sum_J (\xi_l^2 + \omega_J^2)\phi_l(J)\phi_l^*(J) \ , \tag{2.49}$$

with $\omega_J = \sqrt{J^2 + m^2}$. The integrand in (2.44) thus depends only on the magnitude of the field, $|\phi_l(J)| = A_l(J)$. Integrating out the phases gives [4]

$$\begin{aligned} Z &= N \prod_l \prod_J \Big\{ \int_{-\infty}^{\infty} dA_l k e^{-\frac{1}{2}\beta^2(\xi_l^2+\omega_J^2)A_l(J)^2} \Big\} \ , & (2.50) \\ &= N \prod_l \prod_J (2\pi)^{1/2} \left[\beta^2(\xi_l^2 + \omega_J^2)\right]^{-\frac{1}{2}} \ , & (2.51) \end{aligned}$$

from which results

$$\ln(Z) = -\frac{1}{2} \sum_l \sum_J \ln\left[\beta^2(\xi_l^2 + \omega_J^2)\right] \ , \tag{2.52}$$

where we've dropped a term that is independent of temperature and volume. It is worth noting that the argument of the natural logarithm in (2.52), up to a factor of $1/\beta^2$, is the inverse of the free scalar propagator [4]

$$\Delta_0(\xi_l, \omega_J) = \frac{1}{\xi_l^2 + \omega_J^2} \ . \tag{2.53}$$

Using the following identities

$$\begin{aligned} \ln\left[(2\pi l)^2 + \beta^2\omega_J^2\right] &= \int_1^{\beta^2\omega_J^2} \frac{d\,\theta^2}{\theta^2 + (2\pi l)^2} + \ln\left[1 + (2\pi l^2)\right] \ , & (2.54) \\ \sum_{l=-\infty}^{\infty} \frac{1}{l^2 + (\theta/2\pi)^2} &= \frac{2\pi^2}{\theta}\left(1 + \frac{2}{e^\theta - 1}\right) \ , & (2.55) \end{aligned}$$

and dropping a temperature independent term gives [4]

$$\begin{aligned}\ln(Z) &= -\sum_J \int_1^{\beta\omega_J} d\theta \left(\frac{1}{2}+\frac{1}{e^\theta-1}\right) , \\ &= -\sum_J \left[\frac{1}{2}\beta\omega_J + \ln\left(1-e^{-\beta\omega_J}\right)\right] . \end{aligned} \tag{2.56}$$

Now we are in position to write down the partition function in any geometry/BCs. This we do by specifying the geometry and BCs, which determines the spectrum ω_J. For example, for a massive field in a cube with periodic BCs, (2.56) becomes

$$\ln(Z) = -{\sum_{n,l,p=-\infty}^{\infty}}' \left[\frac{1}{2}\frac{\omega^P_{nlp}}{T} + \ln\left(1-e^{-\frac{\omega^P_{nlp}}{T}}\right)\right] , \tag{2.57}$$

where ω^P_{nlp} was defined in (2.26).

In the limit $L\to\infty$ (the infinite volume or thermodynamic limit), the energy-momentum spectrum (2.26) becomes continuous and the sum in (2.57) simplifies to an integral over n, l and p

$$\begin{aligned} dn &= \frac{L dk_1}{2\pi} , \\ dl &= \frac{L dk_2}{2\pi} , \\ dp &= \frac{L dk_3}{2\pi} , \end{aligned} \tag{2.58}$$

and so we obtain the familiar partition function in infinite volume

$$\ln(Z) = -V\int \frac{d^3k}{(2\pi)^3}\left[\frac{1}{2}\frac{1}{T}\omega_k + \ln\left(1-e^{-\frac{\omega_k}{T}}\right)\right] , \tag{2.59}$$

with ω_k being as in equation (2.5).

From (2.59), the thermodynamic properties (2.40) - (2.43) in infinite volume are

$$\mathscr{f} = \frac{1}{2}\int\frac{d^3k}{(2\pi)^3}\omega_k + T\int\frac{d^3k}{(2\pi)^3}\ln\left(1-e^{-\frac{\omega_k}{T}}\right) , \tag{2.60}$$

$$\mathscr{e} = \frac{1}{2}\int\frac{d^3k}{(2\pi)^3}\omega_k + \int\frac{d^3k}{(2\pi)^3}f_B(\omega_k)\omega_k , \tag{2.61}$$

$$\mathscr{p} = -\frac{1}{2}\int\frac{d^3k}{(2\pi)^3}\omega_k + \frac{1}{3}\int\frac{d^3k}{(2\pi)^3}f_B(\omega_k)\frac{k^2}{\omega_k} , \tag{2.62}$$

$$\mathscr{s} = \int\frac{d^3k}{(2\pi)^3}\left[(1+f_B(\omega_k))\ln(1+f_B(\omega_k)) - f_B(\omega_k)\ln(f_B(\omega_k))\right] . \tag{2.63}$$

The calligraphic font is to indicate that these are the thermodynamic properties in the infinite volume limit, and f_B is the Bose function

$$f_B(\omega_k) = \frac{1}{e^{\omega_k/T} - 1} \,. \tag{2.64}$$

We see that all of the expressions (2.60) - (2.62) are divergent; specifically because the first term on the right hand side of each of them is divergent. That term is the zero temperature (vacuum) contribution. The entropy density (2.63) not having this contribution is a fulfillment of the third law of thermodynamics, which states that $s \to 0$ when $T \to 0$. We devote the next section to a discussion of these divergent vacuum contributions.

2.5 The divergence of vacuum contribution and various regulation procedures

2.5.1 The Casimir effect

The divergence of vacuum contributions has its origin in the implicit assumption that momentum modes in (2.57) can increase without bound. Revising this assumption can lead to finite vacuum contributions. For example, for an Electromagnetic field in parallel plates and subject to Dirichlet BCs, the vacuum pressure acting on the plates can be shown to be finite and have the form [9]

$$p_{vac}^{EM} = -\frac{\pi^2}{240 L^4} \,, \tag{2.65}$$

where L is the plates' separation. This phenomenon of attractive pressure between the plates is known as the Casimir effect.

In the following sections, we study some ways of *renormalizing* these divergences (i.e, extracting physical, finite quantities from them).

2.5.2 Regularization by ultra-violet cut-off

We find it most convenient to study these divergences first as they arise in the case of a massless field in the parallel plates geometry with Dirichlet BCs.

The partition function in parallel plates, with Dirichlet BCs, is given by

$$\ln(Z_{par}) = -A\sum_{n=1}^{\infty}\int\frac{d^2k_\perp}{(2\pi)^2}\left[\frac{1}{T}\frac{1}{2}\tilde{K}_n^D + \ln\left(1-e^{\frac{\tilde{K}_n^D}{T}}\right)\right], \tag{2.66}$$

where A is the (infinite) area of the plates, and

$$\tilde{K}_n^D = \sqrt{(k_{zn}^D)^2 + k_\perp^2} \tag{2.67}$$

where $k_{zn}^D = n\pi/L$ is the momentum component in the direction perpendicular to the plates, and $k_\perp$ is the momentum component parallel to the plates.

From equation (2.42), the pressure acting on the plates is

$$p_{par}^D = \frac{1}{L}\sum_{n=1}^{\infty}\int\frac{d^2k_\perp}{(2\pi)^2}\left[\frac{1}{2}\frac{(k_{zn}^D)^2}{\tilde{K}_n^D} + \frac{(k_{zn}^D)^2}{\tilde{K}_n^D}f_B(\tilde{K}_n^D)\right]. \tag{2.68}$$

The second term in the equation above is the thermal pressure and is finite at any T, and the first term is the vacuum pressure

$$\mathbf{p}_{par0}^D = \frac{1}{2}\frac{1}{L}\sum_{n=1}^{\infty}\int\frac{d^2k_\perp}{(2\pi)^2}\frac{(k_{zn}^D)^2}{\tilde{K}_n^D}, \tag{2.69}$$

which is divergent (the bold font is to indicate that it is divergent, and the subscript "0" is to indicate that it's a purely vacuum contribution). The divergence is because k_{zn}^D and $k_\perp$ increase without bounds. Here we ask a question: Can the momentum really increase without bounds? One would imagine that in the real world this is not so[1] and therefore there should be some ultra-violet cut-off, Λ, imposed on the momentum, e.g.[2]

$$p_{par0}^D = \frac{1}{2}\frac{1}{L}\sum_{n=1}^{\Lambda L/\pi}\int_0^{\Lambda}\frac{k_\perp dk_\perp}{(2\pi)}\frac{(k_{zn}^D)^2}{\tilde{K}_n^D}, \tag{2.70}$$

which renders the pressure finite. What happened here is that the pressure was *regulated*. Parameters like Λ will be referred to as *regularization parameters* or *regulators*, and we shall refer to any method of removing a divergence as a *regularization procedure*.

We note here that though the regularized pressure is finite, it clearly depends on the choice of the regularization parameter, Λ. But observables must not depend on the choice of regulators. To make the distinction clear: Regulated quantities do depend on regularization parameters, while *renormalized* quantities should not. We will explore

[1] There are many arguments one can advance to justify this, e.g., the walls of a perfectly conducting container would become transparent to such particle.

[2] Or we could have chosen a different cut-off for $k_\perp$, say, $\Lambda_\perp$.

in the following section other regularization procedures where the final, renormalized results do not depend on the regularization parameters.

2.5.3 Infinite volume's vacuum energy subtraction and the Abel-Plana formula

Since energy in quantum field theory is defined only with respect to an arbitrary constant or reference, only the *change* in energy with respect to that reference is observable. Let us thus consider the parallel plates again and choose our reference to be the vacuum energy per unit area of infinite volume

$$\mathscr{E}_{par0} = \frac{1}{2} L \int \frac{d^3k}{(2\pi)^3}\, k \ . \tag{2.71}$$

We then calculate the difference between this energy and the energy per unit area in parallel plates

$$\mathbf{E}^D_{par0} = \frac{1}{2} \sum_{n=1}^{\infty} \int \frac{d^2k_\perp}{(2\pi)^2} \tilde{K}^D_n \ . \tag{2.72}$$

The change in energy therefore is

$$\Delta E = \mathbf{E}^D_{par0} - \mathscr{E}_{par0} = \frac{1}{2} \sum_{n=1}^{\infty} \int \frac{d^2k_\perp}{(2\pi)^2} \tilde{K}^D_n - \frac{1}{2} L \int \frac{d^3k}{(2\pi)^3}\, k \ . \tag{2.73}$$

In order to evaluate this difference between an integral and a sum, we make use of the *Abel-Plana formula* [10]

$$\sum_{n=0}^{\infty} F(n) - \int_0^{\infty} dt F(t) = \frac{1}{2} F(0) + i \int_0^{\infty} \frac{dt}{e^{2\pi t} - 1} \left[F(it) - F(-it) \right] \ . \tag{2.74}$$

where $F(z)$ is an analytic function in the right half complex plane. In our case, from (2.73), the function to be summed/integrated over is

$$F(z) = K^D_{\perp,z} = \sqrt{k_\perp^2 + z^2} = e^{\frac{1}{2}\ln\left(k_\perp^2 + z^2\right)} \ , \tag{2.75}$$

In the complex plane, this function has branch points $z_{1,2} = \pm i k_\perp$, and its discontinuity at the branch cut reads [11]

$$F(it) - F(-it) = 2i \sqrt{t^2 - k_\perp^2}\ \theta(t - k_\perp) \ , \tag{2.76}$$

where $\theta(x)$ is the Heaviside step function

$$\theta(x) = \begin{cases} 1 & x \geq 0 \\ 0 & x < 0 \end{cases} . \tag{2.77}$$

And so the Abel-Plana formula in this case becomes

$$\sum_{n=0}^{\infty} F(n) - \int_0^{\infty} dt F(t) = \frac{1}{2}k_\perp - \frac{\pi}{L}\int_{\frac{k_\perp L}{\pi}}^{\infty} \frac{dt}{e^{2\pi t}-1}\sqrt{t^2 - \left(\frac{Lk_\perp}{\pi}\right)^2} . \tag{2.78}$$

Applying this to equation (2.73) gives

$$\Delta E = -\frac{1}{8\pi}\int_0^{\infty} dk_\perp k_\perp^2 - \frac{1}{2L}\int_0^{\infty} dk_\perp k_\perp \int_{\frac{k_\perp L}{\pi}}^{\infty} \frac{dt}{e^{2\pi t}-1}\sqrt{t^2 - \left(\frac{Lk_\perp}{\pi}\right)^2} , \tag{2.79}$$

and after making the substitution $y = Lk_\perp/\pi$ and reversing the order of integration, one obtains [10]

$$\Delta E = -\frac{1}{8\pi}\int_0^{\infty} dk_\perp k_\perp^2 - \frac{1}{1440}\frac{\pi^2}{L^3}. \tag{2.80}$$

To calculate the pressure, we note from relations (2.41) and (2.42) that if the pressure is temperature independent then

$$p = -\frac{\partial E}{\partial V} , \tag{2.81}$$

where E is the energy.

Now, although the first term on the right hand side of equation (2.80) is infinite, it is *volume independent* and so it does not influence the pressure which, from equation (2.81), is related to the energy density by a volume derivative. The pressure thus is

$$p^D_{par0} = -\frac{1}{A}\frac{\partial(A\,\Delta E)}{\partial L} = -\frac{1}{480}\frac{\pi^2}{L^4} . \tag{2.82}$$

which is finite. Note that the scalar Casimir pressure (2.82) is half the Electromagnetic pressure (2.65); this is because photons have two polarization degrees of freedom.

We will often work with energy density (energy per unit volume)[1]:

[1] as different to energy per unit area.

$$e^D_{par0} = \frac{\Delta E}{L} = -\frac{1}{1440}\frac{\pi^2}{L^4} \,, \tag{2.83}$$

where we've dropped the volume-independent term.

The energy density (2.83) and pressure (2.82) are related via the equation of state

$$e^D_{par0} = \frac{1}{3} p^D_{par0} \,. \tag{2.84}$$

2.5.4 Regularization by exponential cut-off

One implicit assumption in expression (2.72) is that the two plates are ideal and therefore reflect all waves. But, in the real world, metal plates are not ideal, and a wave with momentum high enough can penetrate partly or completely. Therefore, in the exponential cut-off regularization procedure, an *exponential cut-off* is introduced to reflect the fact that waves with higher momenta contribute less to the energy between the plates [10], and so the vacuum energy per unit area of the plates (2.72) becomes

$$\mathbf{E}^{D(\delta)}_{par0} = \frac{1}{2}\sum_{n=1}^{\infty}\int \frac{d^2k_\perp}{(2\pi)^2}\, \tilde{K}^D_n\, e^{-\delta \tilde{K}^D_n} \,, \tag{2.85}$$

where δ is the dimensionful cut-off parameter (a regulator). This integral can be evaluated by the substitution $u^2 = \sqrt{k_\perp^2 + (n\pi/L)^2}$ and it yields in terms of Polylogarithm functions[1]

$$\mathbf{E}^{D(\delta)}_{par0} = \frac{1}{2}\left[\frac{1}{\pi\delta^3}\mathrm{Li}_0(e^{-\frac{\delta\pi}{L}}) + \frac{1}{L\delta^2}\mathrm{Li}_{-1}(e^{-\frac{\delta\pi}{L}}) + \frac{\pi}{2L^2\delta}\mathrm{Li}_{-2}(e^{-\frac{\delta\pi}{L}})\right] \,. \tag{2.86}$$

Now this expression is obviously δ-dependent. Let's expand it in powers of δ

$$\mathbf{E}^{D(\delta)}_{par0} = \frac{3L}{2\pi^2\delta^4} - \frac{1}{4\pi\delta^3} - \frac{\pi^2}{1440L^3} + \mathcal{O}(\delta^2) \,. \tag{2.87}$$

Now, as in the previous section, we subtract from this the energy per unit area of infinite volume[2] in the region between the parallel plates

[1] The Polylogarithm function of order s, $s \in \mathbb{C}$, is defined as: $\mathrm{Li}_s(z) = \sum_{n=1}^{\infty} \frac{z^n}{n^s}$.

[2] The limit of $L \to \infty$ of (2.85).

$$E_0^{(\delta)} = L\frac{1}{2}\int \frac{d^3k}{(2\pi)^3} k e^{-\delta k} = \frac{3L}{2\pi^2\delta^4} \,, \tag{2.88}$$

and so the energy difference caused by the plates is

$$\Delta E = \mathbf{E}_{par0}^{D(\delta)} - E_0^{(\delta)} = -\frac{1}{4\pi\delta^3} - \frac{\pi^2}{1440L^3} + \mathcal{O}(\delta^2) \,, \tag{2.89}$$

and so we see that the only divergent term is the first term on the right hand side, but is volume independet and so does not influence the pressure. Calculating the pressure and taking the limit $\delta \to 0$ gives

$$p_{par0}^{D} = -\frac{\partial(\Delta E)}{\partial L} = -\frac{\pi^2}{480L^4} \,, \tag{2.90}$$

in agreement with the result (2.82).

2.5.5 Zeta-function regularization

Zeta function regularization is rather mathematical, and is an example of regularization procedures that lack direct, physical intuition. It relies on regulating the divergent expression and then analytically continuing in the regularization parameter. This is explained below.

Consider the vacuum energy per unit area (2.72). Let us modify the exponent of the momenta in the manner done below

$$\mathbf{E}_{par0}^{D} \longrightarrow \mathbf{E}_{par0}^{D(s)} = \frac{1}{2}\sum_{n=1}^{\infty} \mu^s \int \frac{d^2k_\perp}{(2\pi)^2} (\tilde{K}_n^D)^{(1-s)} \,. \tag{2.91}$$

The factor μ^s, where μ is a constant with the dimensions of energy, is needed to retain the dimensions of the energy per unit area [10]. This integral is well defined for $s > 3$ and yields (see Appendix A)

$$\mathbf{E}_{par0}^{D(s)} = \frac{1}{4\pi^{s-2}} \frac{1}{L^{3-s}} \frac{\mu^s}{-3+s} \sum_{n=1}^{\infty} n^3 \,. \tag{2.92}$$

By taking the limit $s \to 0$, we obtain

$$\mathbf{E}_{par0}^{D} = -\frac{\pi^2}{12}\frac{1}{L^3}\sum_{n=1}^{\infty} n^3 \,. \tag{2.93}$$

Here the sum over n is obviously divergent. To renormalize this divergence, we note that this sum can be expressed in terms of Riemann Zeta function

$$\zeta(x) = \sum_{n=1}^{\infty} \frac{1}{n^x} \, . \tag{2.94}$$

And so the energy per unit area of the plates (2.93) becomes

$$\mathbf{E}^D_{par0} = -\frac{\pi^2}{12}\frac{1}{L^3}\zeta(-3) \, . \tag{2.95}$$

The sum (2.94) is convergent only for $\mathrm{Re}[x] > 1$. The analytic continuation of this sum is done by using another definition of Riemann Zeta function that is finite at all points $\mathrm{Re}[x] < 1$ [10]

$$\zeta(x) = 2^x \pi^{x-1} \sin\Big(\frac{\pi x}{2}\Big)\Gamma(1-x)\zeta(1-x) \tag{2.96}$$

where Γ is Euler's Gamma function and the ζ on the right hand side is given in (2.94). With our $x = -3$, the ζ function on the right hand side is evaluated at 4 which is within its domain. Thus at $x = -3$, relation (2.96) gives

$$\zeta(-3) = \frac{1}{120} \, . \tag{2.97}$$

Extending the domain of a function in this way is called *analytic continuation* [10].

Using the result (2.97), the energy per unit area of the plates (2.95) becomes

$$E^D_{par0} = -\frac{1}{1440}\frac{\pi^2}{L^3} \, , \tag{2.98}$$

which is the same as the δ-independent terms in equation (2.87), and the pressure

$$p^D_{par0} = -\frac{\partial E^D_{par0}}{\partial L} = -\frac{1}{480}\frac{\pi^2}{L^4} \, . \tag{2.99}$$

is the same as in equations (2.82) and (2.90).

2.5.6 Dimensional regularization

Dimensional regularization relies on changing the dimensionality of momentum space, calculating the energy, and then returning the dimensions to their original number. As with Zeta-function regularization, it gives finite results but it lacks direct physical intuition.

Let us change the dimensionality of transverse space in (2.72). It becomes

$$\mathbf{E}^{D(d)}_{par0} = \frac{1}{2}\sum_{n=1}^{\infty}\mu^{2-d}\int\frac{d^dk_\perp}{(2\pi)^d}\,\tilde{K}^D_n\,, \tag{2.100}$$

where d is a real, or even complex, number of dimension. Carrying out the integral (see Appendix A), and taking the limit $d \to 2$, gives

$$E^D_{par0} = -\frac{\pi^2}{12}\frac{1}{L^3}\sum_{n=1}^{\infty}n^3 = -\frac{\pi^2}{12}\frac{1}{L^3}\zeta(-3) = -\frac{1}{1440}\frac{\pi^2}{L^3}\,, \tag{2.101}$$

and the pressure

$$p^D_{par0} = -\frac{\partial E^D_{par0}}{\partial L} = -\frac{1}{480}\frac{\pi^2}{L^4}\,, \tag{2.102}$$

in agreement with the results obtained by the previous regularization procedures.

We see that the various regularization procedures (exponential cut-off, Abel-Plana, Zeta-function, dimensional regularization) give the same final renormalized results. This raises confidence in their validity, although Zeta-function and Dimensional regularization may lack direct physical intuition.

2.6 Casimir pressure in three-dimensional box geometries with various BCs

In the previous subsection we studied various ways of renormalizing vacuum contributions in parallel plates. The regularization procedures used there (exponential cut-off, Zeta-function regularization, etc) can be also applied to other geometries [10]. In this section we are going study vacuum contribution in further geometries and BCs. We choose to discuss first the energy density and pressure of a massless field in the cube, then in the parallel plates geometry and then we compare the energy density and pressure of this massless field in the cuboid to their parallel plates limits, and finally we discuss the effect of a non zero mass on the energy density and pressure in the cube.

2.6.1 Vacuum energy density and pressure of a massless scalar field in a cube

In this section, we want to study the Casimir energy density and pressure in a cube as functions of the cube's volume.

The simplest case in this geometry is of a massless field with periodic BCs. The unrenormalized energy density is

$$\mathbf{e}^P_{cube0} = \frac{1}{L^3}\left(\frac{1}{2}\sum_{n,l,p=-\infty}^{\infty}{}' k^P_{nlp}\right) , \tag{2.103}$$

where k^P_{nlp} was defined in equation (2.27) and the prime means that the mode with all indices equal to zero (the zero momentum mode) is excluded (the reason why it has to be excluded will become apparent shortly). This energy density can be renormalized by noting that it can be written in terms of the Epstein zeta function [12]

$$\mathrm{Z}_3(1/L, 1/L, 1/L; s) = \sum_{n,l,p=-\infty}^{\infty}{}' \left[\left(\frac{n}{L}\right)^2 + \left(\frac{l}{L}\right)^2 + \left(\frac{p}{L}\right)^2\right]^{-s/2} . \tag{2.104}$$

Thus (2.103) becomes

$$\mathbf{e}^P_{cube0} = \frac{\pi}{L^3}\mathrm{Z}_3(1/L, 1/L, 1/L; s = -1) . \tag{2.105}$$

Now, the sum (2.104) is well-defined only for $s > 1$, but it can be analytically continued to negative s by using the reflection formula [12]

$$\mathrm{Z}_3(1/L, 1/L, 1/L; s) = \frac{L^3}{\pi^{3/2}}\frac{\Gamma[(-s+3)/2]}{\Gamma[s/2]}\mathrm{Z}_3(L, L, L; -s+3) \tag{2.106}$$

which provides an analytic continuation for all s except at the pole $s = 1$. Using the reflection formula (2.106) gives for the finite, renormalized Casimir energy density

$$e^P_{cube0}(L) = -\frac{1}{2\pi^2}\mathrm{Z}_3(L, L, L, 4) = -2\left(\frac{2\pi}{L^4}\right)^2 \sum_{n,l,p=-\infty}^{\infty}{}' \frac{1}{(k^P_{nlp})^4} . \tag{2.107}$$

Note that this energy density is negative[1]. Note also the contribution of the zero momentum mode: (2.103) is ultra-violet divergent and the zero momentum mode contributes zero, but after we analytically continue (2.103) and obtain the ultra-violet convergent expression (2.107), we can no longer include the zero momentum mode because, in (2.107), it results in a divergence. This divergence will be revisited in the next chapter of this thesis. The pressure follows via relation (2.81) and is

$$p^P_{cube0} = \frac{1}{3}\, e^P_{cube0} . \tag{2.108}$$

With Dirichlet BCs, the unrenormalized energy density is given by

[1] in fact, the Casimir energy density of scalar field is negative in all geometries/BCs [10].

$$\mathbf{e}^D_{cube0} = \frac{1}{L^3}\left(\frac{1}{2}\sum_{n,l,p=1}^{\infty} k^D_{nlp}\right) , \tag{2.109}$$

where k^D_{nlp} was defined in equation (2.25). The renormalization of this energy density is rather involved (for details, see [10]) and it gives[1]

$$\begin{aligned} e^D_{cube0}(L_x, L_y, L_z) =& \frac{1}{L_x L_y L_z}\Big[-\frac{\pi^2 L_y L_z}{1440 L_x^3} + \frac{\zeta(3)(L_y + L_z)}{32\pi L_x^2} - \frac{\pi}{96 L_x} \\ & - \frac{\pi}{2L_x}\Big(\mathrm{G}\left(\frac{L_y}{L_x}\right) + \mathrm{G}\left(\frac{L_z}{L_x}\right)\Big) - \frac{1}{L_x}\mathrm{R}\left(\frac{L_y}{L_x}, \frac{L_z}{L_x}\right)\Big)\Big] \end{aligned} \tag{2.110}$$

where

$$\mathrm{G}(z) = -\frac{1}{2\pi}\sum_{n=1}^{\infty}\sum_{l=1}^{\infty}\frac{n}{l}\mathrm{K}_1(2\pi n l z) , \tag{2.111}$$

$$\mathrm{R}(z_1, z_2) = \frac{z_1 z_2}{8}\sum_{n,l=-\infty}^{\infty}\sum_{j=1}^{\infty}\Big(\frac{j}{\sqrt{n^2 z_1^2 + l^2 z_2^2}}\Big)^{3/2}\mathrm{K}_{\frac{3}{2}}(2\pi j\sqrt{n^2 z_1^2 + l^2 z_2^2}) , \tag{2.112}$$

with K being a modified Bessel function of the second kind. Note that the first and second terms on the right hand side of (2.110) are proportional to the surface area $L_y L_z$ and "circumference" $L_y + L_z$, these two terms can be interpreted as the Casimir energy density that reside in these surface area and circumference [10]. Though the renormalized energy density (2.110) has positive and negative contributions to it, it is always negative [10]. The energy density and the pressure here are as well related via the equation of state

$$p^D_{cube0} = \frac{1}{3}\, e^D_{cube0} . \tag{2.113}$$

Our goal now is study the volume dependence of the energy densities and pressures. To do so, we evaluate the energy densities and pressures numerically. In doing the numerics, the sums appearing in the energy densities and pressures expressions are truncated at $n, l, p = N_{max} \gg 1$. This cut-off is not at the cost of accuracy, since the summands are exponentially small for $n, l, p \gg 1$. This cut-off will hold for the sums studied in the remainder of this section, unless otherwise is stated.

[1] for reasons that will appear in due course, we choose to present here the formula for a general box.

In Figure 2.4 we present our results for the energy densities (the pressures follow from the equations of state).

We see that both energy densities approach zero as the volume increases and they grow rapidly as volume decreases. The energy density with periodic BCs is larger (in magnitude), this is perhaps because the spectrum with periodic BCs has far more energy modes than the spectrum with Dirichlet BCs.

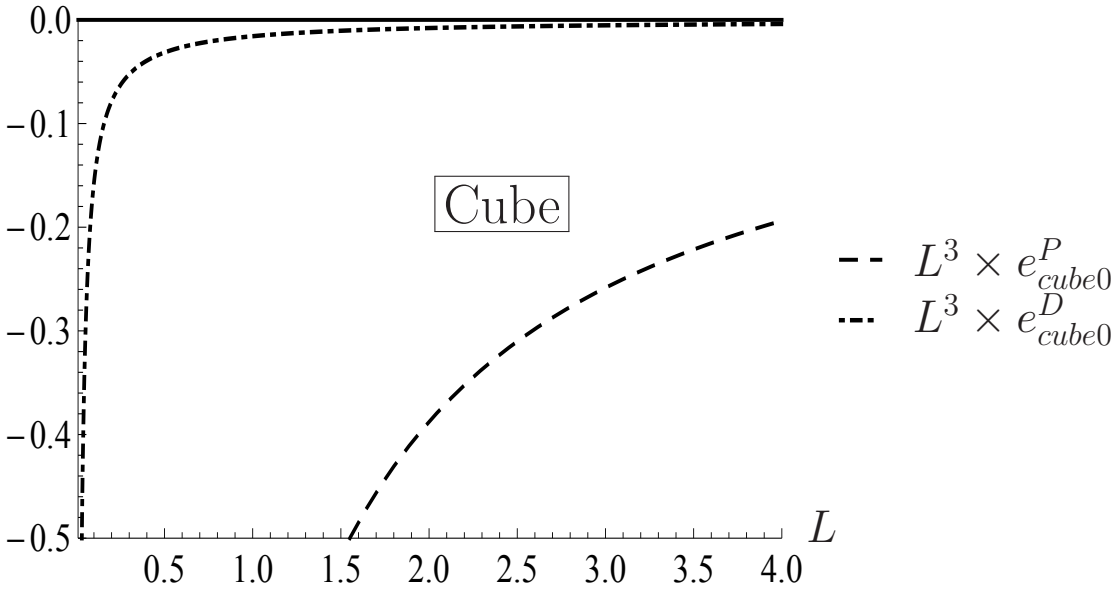

FIGURE 2.4: The energy densities in a cube with Dirichlet and periodic BCs.

2.6.2 The parallel plates as a limiting case of a cuboid

In section 2.5, we derived the renormalized vacuum energy density and pressure in parallel plates with Dirichlet BCs (see for example equations (2.83) and (2.82)). It is useful at this point to illustrate the connection between the cuboid and its parallel plates limit. The primary purpose of the discussion in this subsection is to develop some formulae that will be used in the following sections.

Let's consider first the allowed momenta in a cuboid. The allowed momenta can be obtained from (2.25) and (2.27) with the substitution $(L, L, L) \to (L, \xi L, \xi L)$. This gives

$$(k^D_{nlp})^2 \to (K^D_{nlp\xi})^2 = \left(\frac{\pi n}{L}\right)^2 + \left(\frac{\pi l}{\xi L}\right)^2 + \left(\frac{\pi p}{\xi L}\right)^2 , \tag{2.114}$$

$$(k^P_{nlp})^2 \to (K^P_{nlp\xi})^2 = \left(\frac{2\pi n}{L}\right)^2 + \left(\frac{2\pi l}{\xi L}\right)^2 + \left(\frac{\pi lp}{\xi L}\right)^2 . \tag{2.115}$$

Let's now plug the results (2.114) into equation (2.109) and take the limit $\xi \to \infty$ (the infinite parallel plates limit). This gives

$$\mathbf{e}^D_{par0} = \lim_{\xi\to\infty} \frac{1}{L(\xi L)^2} \left(\frac{1}{2} \sum_{n,l,p=1}^{\infty} K^D_{nlp\xi} \right) = \frac{1}{2}\frac{1}{L} \sum_{n=1}^{\infty} \int \frac{d^2k_\perp}{(2\pi)^2}\, \tilde{K}^D_n \, . \tag{2.116}$$

Similarly, one obtains for the energy density in parallel plates with periodic BCs

$$\mathbf{e}^P_{par0} = \lim_{\xi\to\infty} \frac{1}{L(\xi L)^2} \left(\frac{1}{2} {\sum_{n,l,p=-\infty}^{\infty}}' K^P_{nlp\xi} \right) = \frac{1}{2}\frac{1}{L} {\sum_{n=-\infty}^{\infty}}' \int \frac{d^2k_\perp}{(2\pi)^2}\, K^P_{\perp,n} \, . \tag{2.117}$$

The procedures for renormalizing the energy density and pressure in parallel plates with periodic BCs closely parallels the ones for renormalizing their Dirichlet counterparts discussed in section 2.5; however there is a slightly more elegant way [12]: By noting that the momentum modes, with Dirichlet and periodic BCs, that are perpendicular to the plates are related by

$$k^P_{zn} = 2\, k^D_{zn} \, , \tag{2.118}$$

and that the according sums are related by

$${\sum_{n=-\infty}^{\infty}}' = 2 \sum_{n=1}^{\infty} , \tag{2.119}$$

one can obtain the energy density and pressure with periodic BCs from the ones with Dirichlet BCs by the transformation $L \to L/2$, which gives

$$p^P_{par0}(L) = p^D_{par0}(L/2) = -\frac{\pi^2}{30L^4} , \tag{2.120}$$

$$e^P_{par0}(L) = e^D_{par0}(L/2) = -\frac{\pi^2}{90L^4} . \tag{2.121}$$

As with Dirichlet BCs, the energy density and pressure are related via the equation of state

$$e^P_{par0} = \frac{1}{3} p^P_{par0} . \tag{2.122}$$

Because the vacuum energy density and the pressure in parallel plates have simple closed forms, we will not present numerical results for them.

2.6.3 Vacuum energy density and pressure of a massless scalar field in a cuboid

Here we wish to see how the vacuum energy density and pressure in a cuboid compare to their parallel plates limits.

The renormalized energy density in a cuboid $(L, \xi L, \xi L)$ with periodic and Dirichlet BCs follows immediately from equations (2.107) and (2.110) with the substitution $(L, L, L) \to (L, \xi L, \xi L)$ and $(L_x, L_y, L_z) \to (L, \xi L, \xi L)$. The pressures follow via relation (2.81), however one must notice that, when applying relation (2.81), the side area of the cuboid $(\xi L)^2$ is treated as constant, in particular

$$\frac{\partial}{\partial V} \longrightarrow \frac{1}{(\xi L)^2} \frac{\partial}{\partial L} , \tag{2.123}$$

because this is how the change with respect to volume is to be calculated when calculating the pressure on the side area $(\xi L)^2$. This gives for the pressure with periodic BCs

$$p^P_{cuboid0} = \frac{1}{\pi^2} \left(\frac{1}{2} \mathrm{Z}_3(L, \xi L, \xi L) - 2L^2 {\sum_{n,l,p=-\infty}^{\infty}}' \frac{n^2}{(L^2 n^2 + \xi^2 L^2 (l^2 + p^2))^3} \right) . \tag{2.124}$$

This pressure can be positive, zero or negative, depending on the value of L, this is because the energy is a non monotonic function of L (which is in contrast to the case of the cube discussed in the previous subsection where the pressure is always negative).

The pressure with Dirichlet BCs can be calculated similarly, but because expression (2.110) is not a closed form, we calculate it numerically.

The energy densities and pressures are presented in Figures 2.5-2.7. The results depicted in the Figures depend only on the geometry parameter ξ as all L-dependences cancel. It is seen in the Figures that the energy densities and pressures approach their parallel plates limits as ξ increases.

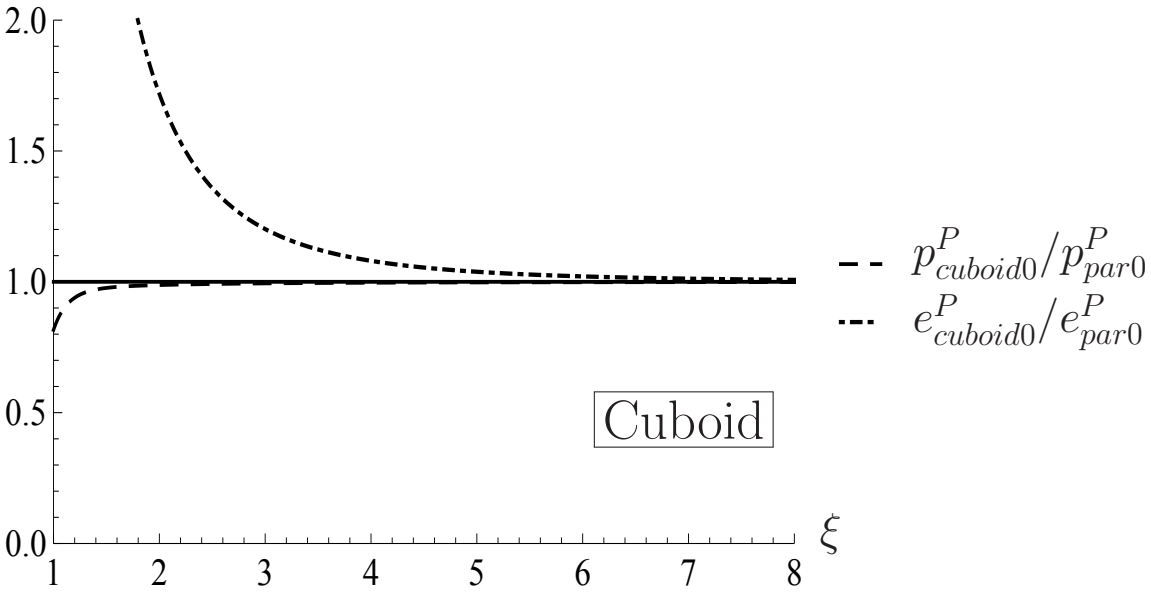

FIGURE 2.5: The ratio of the Casimir energy density and pressure in a cuboid with periodic BCs to their parallel plates limits.

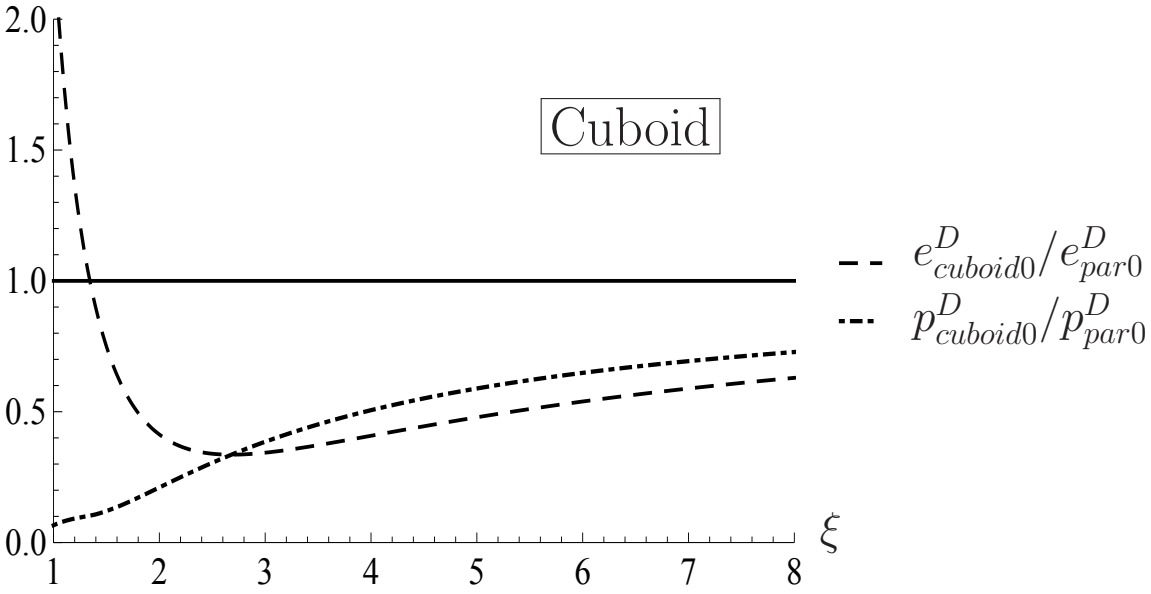

FIGURE 2.6: The ratio of the Casimir energy density and pressure in a cuboid with Dirichlet BCs to their parallel plates limits.

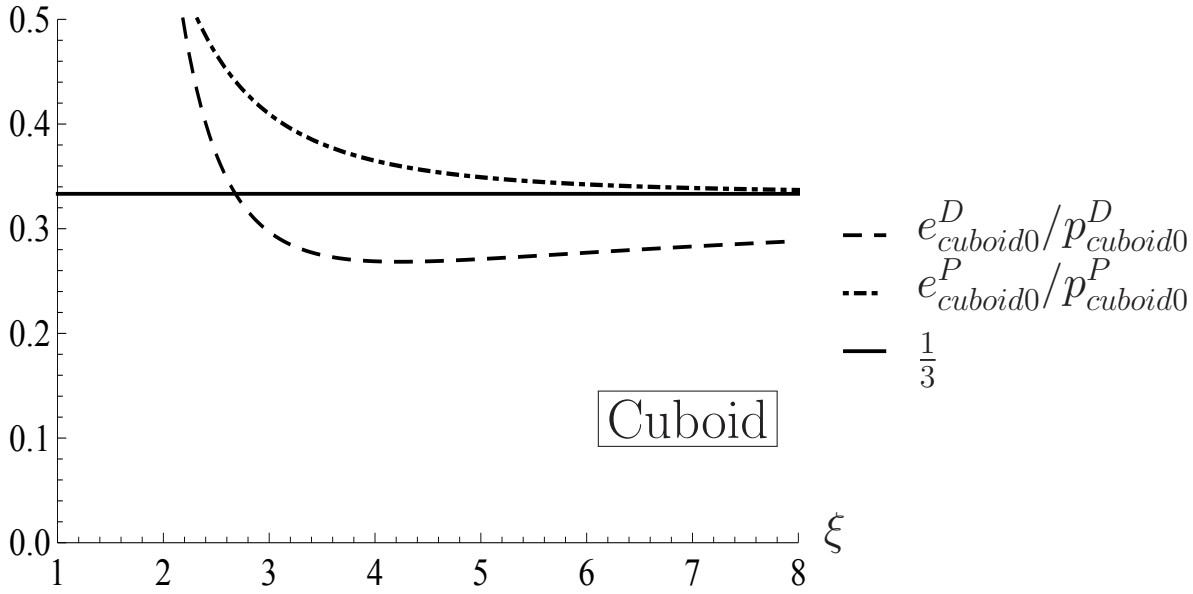

FIGURE 2.7: The ratios of the Casimir energy densities to pressures in a cuboid.

2.6.4 Vacuum energy density and pressure of a massive scalar field in a cube

Here we study the effect of introducing a mass on the vacuum energy density and pressure in a cube. The presence of a non zero mass will be relevant later in this thesis when we discuss interaction-generated masses. We restrict our selves to periodic BCs.

The unrenormalized vacuum energy density is

$$\mathbf{e}^{Pm}_{cube0} = \frac{1}{L^3}\left(\frac{1}{2}{\sum_{n,l,p=-\infty}^{\infty}}' \omega^P_{nml}\right) , \tag{2.125}$$

where ω^P_{nml} was defined in equation (2.26). The renormalization of this energy density gives (see Appendix B)

$$e^{Pm}_{cube0} = -\frac{1}{2}\frac{m^4}{(4\pi)^2}\left[\Gamma(-2) + 2{\sum_{n,l,p=-\infty}^{\infty}}' \frac{\mathrm{K}_2(\frac{mL^2}{2\pi}k^P_{nlp})}{(\frac{mL^2}{4\pi}k^P_{nlp})^2}\right] . \tag{2.126}$$

The first term corresponds to a constant energy density that is independent of L and can therefore be dropped [12]. The physically relevant energy density is thus

$$e^{Pm}_{cube0}(L,m) = -\frac{m^2}{L^4}{\sum_{n,l,p=-\infty}^{\infty}}' \frac{\mathrm{K}_2(\frac{mL^2}{2\pi}k^P_{nlp})}{(k^P_{nlp})^2} . \tag{2.127}$$

The pressure follows immediately via relation (2.81) and is

$$\begin{aligned} p^{Pm}_{cube0}(m,L) &= -\frac{1}{3}\frac{m^2}{L^2}{\sum_{n,l,p=-\infty}^{\infty}}' \frac{1}{(Lk^P_{nlp})^2}\left[\mathrm{K}_2(\frac{mL^2}{2\pi}k^P_{nlp}) + \frac{mL^2}{2\pi}k^P_{nlp}\mathrm{K}_1(\frac{mL^2}{2\pi}k^P_{nlp})\right] \\ &= \frac{1}{3}\left[e^{Pm}_{cube0}(L,m) - \frac{m^3}{2\pi L^2}{\sum_{n,l,p=-\infty}^{\infty}}' \frac{\mathrm{K}_1(\frac{mL^2}{2\pi}k^P_{nlp})}{k^P_{nlp}}\right] . \end{aligned} \tag{2.128}$$

To connect to the massless energy density (2.107) and pressure (2.108), we note that, for small arguments, the Bessel functions in the expressions above above behave as

$$x^3\,\mathrm{K}_1(x) \approx \mathcal{O}(x^2) , \; x \to 0 , \tag{2.129}$$

$$x^2\,\mathrm{K}_2(x) \approx 2 + \mathcal{O}(x^2) , \; x \to 0 . \tag{2.130}$$

Thus, in the limit $m \to 0$, and energy density (2.127) and the pressure (2.128) behave as

$$e^{Pm}_{cube0} \approx -2\left(\frac{2\pi}{L^4}\right)^2 {\sum_{n,l,p=-\infty}^{\infty}}' \frac{1}{(k^P_{nlp})^4} + \mathcal{O}(m^2)\,, \tag{2.131}$$

$$p^{Pm}_{cube0} \approx -\frac{2}{3}\left(\frac{2\pi}{L^4}\right)^2 {\sum_{n,l,p=-\infty}^{\infty}}' \frac{1}{(k^P_{nlp})^4} + \mathcal{O}(m^2)\,, \tag{2.132}$$

i.e, they indeed reduce to their massless counterparts.

Let's now investigate the dependence of these energy density and pressure on the volume and mass when compared to the massless limit. Since the Bessel functions in (2.127) and (2.128) are rapidly decreasing functions of their arguments, it suffices to truncate the sums at $n, l, p = N_{max} \gg (mL)^{-1}$. Also since, in the ratios of massive-to-massless energy density and pressure $e^{Pm}_{cube0}(L,m)/e^{P}_{cube0}(L)$ and $p^{Pm}_{cube0}(L,m)/p^{P}_{cube0}(L)$, m and L appear only as a product mL, we will plot our results for these rations as a function of this dimensionless product. The results are shown in Figures 2.8 and 2.9.

The observation that the energy density decreases with increasing mass (see Figure 2.8) is because the difference between successive energy modes decreases with increasing mass causing the energy-momentum spectrum to tend to the continuum limit which has zero renormalized energy density. The non-monotonic behavior of the pressure is because the summand in (2.128) contains products of increasing and decreasing functions.

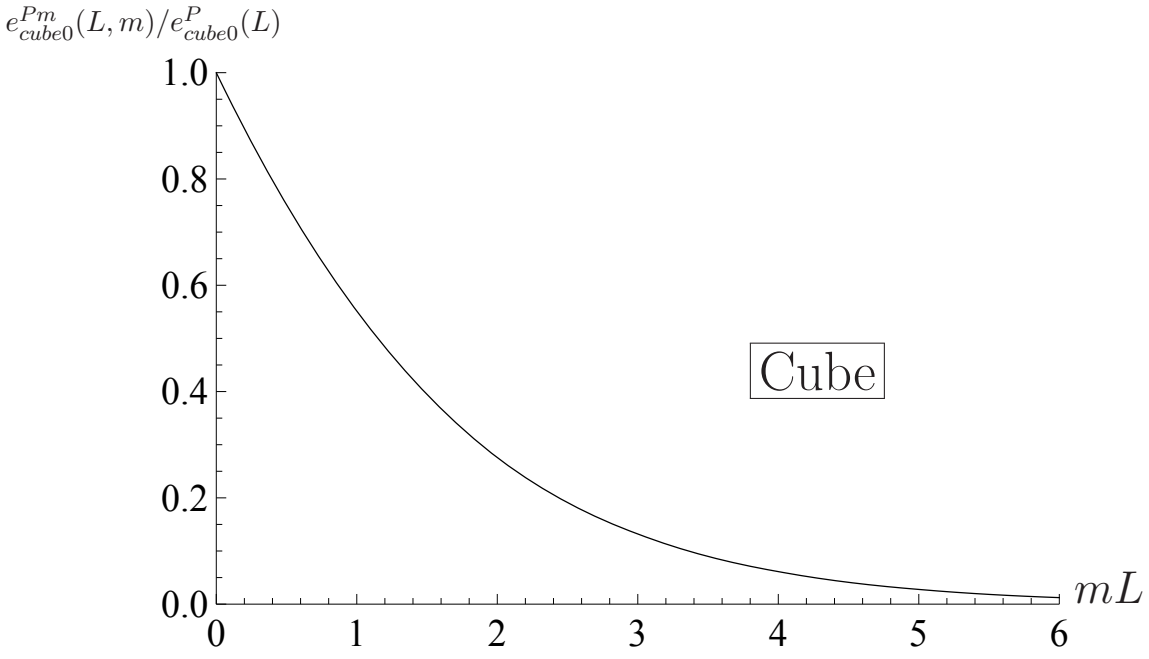

FIGURE 2.8: The ratio of the Casimir energy density of a massive field to massless field in a cube. The field is subject to periodic BCs.

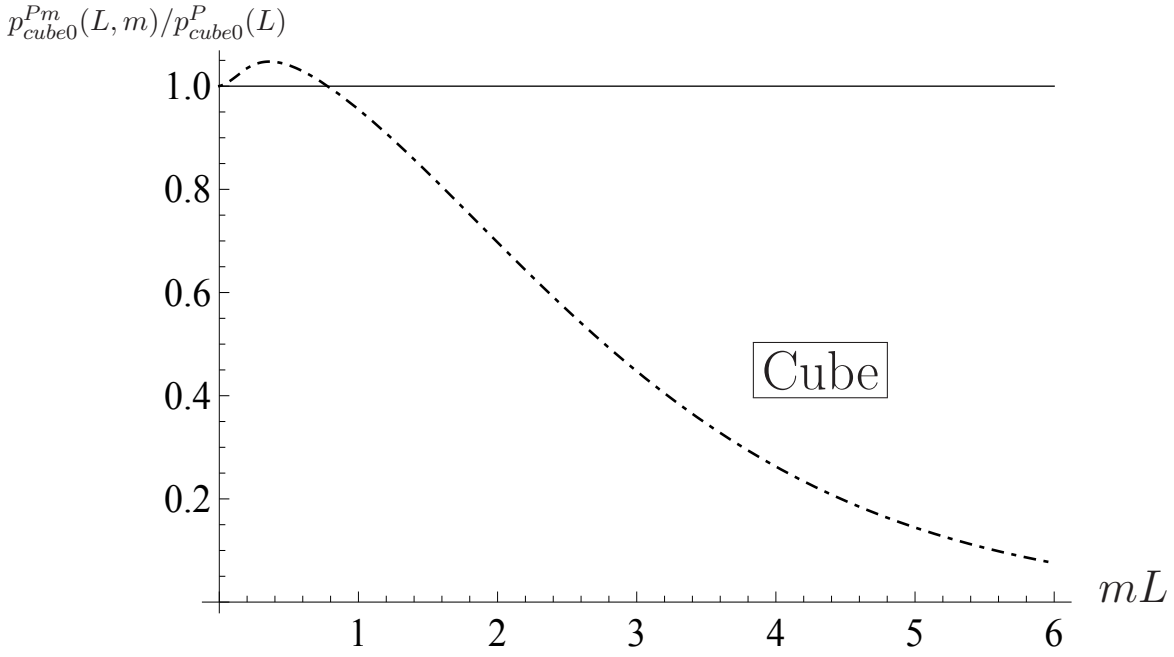

FIGURE 2.9: Same as Figure 2.8, except for the pressure.

2.7 Energy and pressure of a free scalar gas at non zero temperature

In the previous sections we obtained expressions for the renormalized vacuum energy density and pressure in various geometries/BCs. In this section we go further and investigate the thermal energy density and pressure in these geometries and BCs. As in the previous section, we start first with a discussion of a massless field.

For the sake of the discussion that will follow, we briefly revisit the Free energy density, energy density and pressure in infinite volume (equations (2.60) - (2.62)). We have seen in the previous sections that renormalized vacuum contributions vanish when the volume becomes infinite. This, it was mentioned, is because infinite volume was *chosen* to be the reference point from which things are to be measured. Consequently, we drop the vacuum contributions in equations (2.60) - (2.62) which gives

$$\mathcal{P} = -\mathcal{F} = \frac{1}{3}\int \frac{d^3k}{(2\pi)^3} f_B(\omega_k)\frac{k^2}{\omega_k} , \tag{2.133}$$

$$\mathcal{E} = \int \frac{d^3k}{(2\pi)^3} f_B(\omega_k)\omega_k . \tag{2.134}$$

In particular, if the field is *massless*, we can carry out these integrals to obtain

$$\mathcal{E} = 3\mathcal{P} = -3\mathcal{F} = \frac{\pi^2}{30}T^4 . \tag{2.135}$$

It is worth noting that the relation $\mathcal{E} - 3\mathcal{P} = 0$ is also the trace of the energy-momentum tensor of a free massless scalar field in infinite volume [13].

In this section we are going to extend the discussion done in section 2.6 by including thermal contributions.

2.7.1 Casimir energy density and pressure in a cube at non zero temperature

In this subsection, we study the behavior of the energy density and pressure in a cube at non zero temperature. The energy density in a cube for a massless field with periodic BCs is given by

$$e^P_{cube}(L,T) = e^P_{cube0}(L) + \frac{1}{L^3}\sum_{n,l,p=-\infty}^{\infty} k^P_{nlp} f_B(k^P_{nlp}) , \tag{2.136}$$

where the first term is the renormalized vacuum contribution given in equation (2.107) and the second term is the thermal contribution obtained from the second term in the partition function (equation (2.57)) via relation (2.41).

Along the same lines, the energy density in a cube with Dirichlet BCs at non zero temperature reads

$$e^D_{cube}(L,T) = e^D_{cube0}(L) + \frac{1}{L^3}\sum_{n,l,p=1}^{\infty} k^D_{nlp} f_B(k^D_{nlp}) \; . \tag{2.137}$$

As with their counterparts at zero temperature, the energy densities above are related to the pressures via the equations of state

$$e^P_{cube}(L,T) = 3\, p^P_{cube}(L,T) \; , \tag{2.138}$$

$$e^D_{cube}(L,T) = 3\, p^D_{cube}(L,T) \; . \tag{2.139}$$

Numerical analysis reveals that it is appropriate to truncate the sums appearing in the thermal contributions (thermal energy density and thermal pressure) at $N_{max} \gg LT/\pi$ for Dirichlet BCs, and at $N_{\max} \gg LT/(2\pi)$ for periodic BCs (just by looking at second terms on the right hand sides of (2.136) and (2.137) one can see that large momentum modes don't contribute significantly since the Bose function decreases exponentially). This cut-off will hold for all thermal contributions discussed in the remainder of this section.

In Figure 2.10 we show our results for the ratios of the energy densities in a cube at non zero temperature to the continuum energy density (2.135) (note that the dimensionless variable here is LT), which, from (2.135) and (2.139), are the same as the corresponding pressures ratios.

The energy densities are negative when vacuum contributions dominate and are positive when thermal contributions dominate, with the crossover being at $LT \sim 0.8$ for both Dirichlet and periodic BCs.

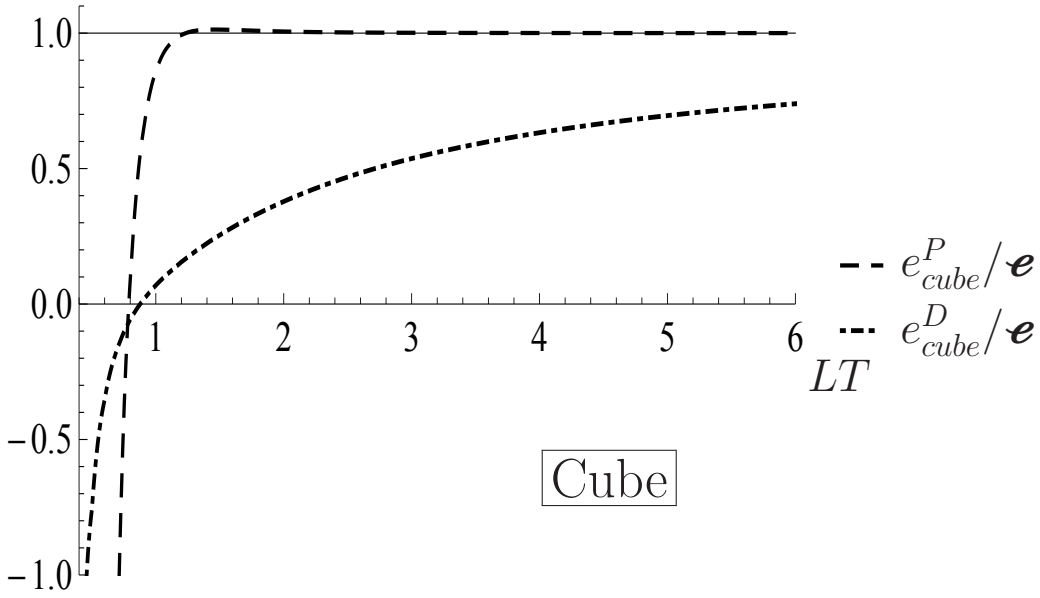

FIGURE 2.10: The ratios of the energy densities in a cube at non zero temperature to the energy density in infinite volume.

2.7.2 Energy density and pressure in parallel-plates at non zero temperature

The energy density of a massless field in parallel plates, subject to Dirichlet BCs, is given by

$$e^D_{par}(L,T) = e^D_{par0}(L) + \frac{1}{L}\sum_{n=1}^{\infty}\int_0^{\infty}\frac{dk_\perp\, k_\perp}{2\pi}\tilde{K}^D_n f_B(\tilde{K}^D_n)\,,$$

where the first term is the renormalized vacuum energy density given in equation (2.83) and the second term is the thermal energy density obtained from (2.66) via relation (2.41). Carrying out the integral gives

$$\begin{aligned} e^D_{par}(L,T) &= e^D_{par0}(L) + \frac{T^3}{2\pi L}\sum_{n=1}^{\infty}\left[\left(\frac{k^D_{zn}}{T}\right)^2 \mathrm{Li}_1\left(e^{-\frac{|k^D_{zn}|}{T}}\right)\right. \\ &\quad \left. + 2\frac{|k^D_{zn}|}{T}\mathrm{Li}_2\left(e^{-\frac{|k^D_{zn}|}{T}}\right) + 2\mathrm{Li}_3\left(e^{-\frac{|k^D_{zn}|}{T}}\right)\right]\,, \end{aligned} \tag{2.140}$$

Similarly, one obtains for the pressure

$$\begin{aligned} p^D_{par}(L,T) &= p^D_{par0}(L) + \frac{1}{L}\sum_{n=1}^{\infty}\int_0^{\infty}\frac{dk_\perp\, k_\perp}{2\pi}\frac{(k^D_{zn})^2}{\tilde{K}^D_n} f_B(\tilde{K}^D_n)\,, \\ &= p^D_{par0}(L) + \frac{T^3}{2\pi L}\sum_{n=1}^{\infty}\left(\frac{k^D_{zn}}{T}\right)^2 \mathrm{Li}_1\left(e^{-\frac{|k^D_{zn}|}{T}}\right)\,. \end{aligned} \tag{2.141}$$

The energy density and pressure with Dirichlet BCs can be obtained from the ones above by the transformation $L \to L/2$ [12]

$$e^P_{par}(L,T) = e^D_{par}(L/2,T) + \frac{T^3}{\pi L}\mathrm{Li}_3(1)\,, \tag{2.142}$$

$$p^P_{par}(L,T) = p^D_{par}(L/2,T)\,, \tag{2.143}$$

where the additional term on the right hand side is the $n = 0$ contribution. The pressure does not have a corresponding contribution from $n = 0$ because this mode describes the particles that are traveling parallel to the plates and hence exerting no pressure on them.

In Figures 2.11 and 2.12 we show how the energy density and pressure in parallel plates compare to the infinite volume limit. The discontinuity seen between the curves in Figures 2.13 and 2.14 is because each pressure has a zero in the region in between. The observation that the energy-to-pressure ratio is not constant (Figures 2.13 - 2.14) can be understood as follows: At zero temperature and finite volume, the energy density and the pressure are related by a factor of $\frac{1}{3}$, whereas at finite temperature and infinite

volume they are related by a factor of 3, and so, in the region in between, the relation between them has to be variable in order to allow for the transition from $\frac{1}{3}$ to 3.

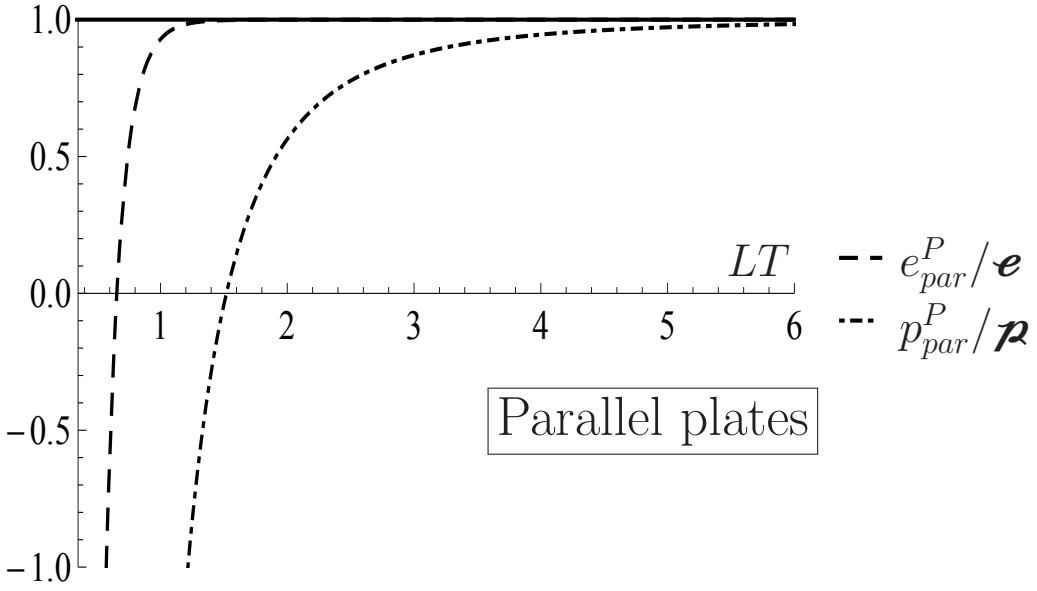

FIGURE 2.11: The ratios of the energy density and pressure in parallel plates with periodic BCs to the continuum limits.

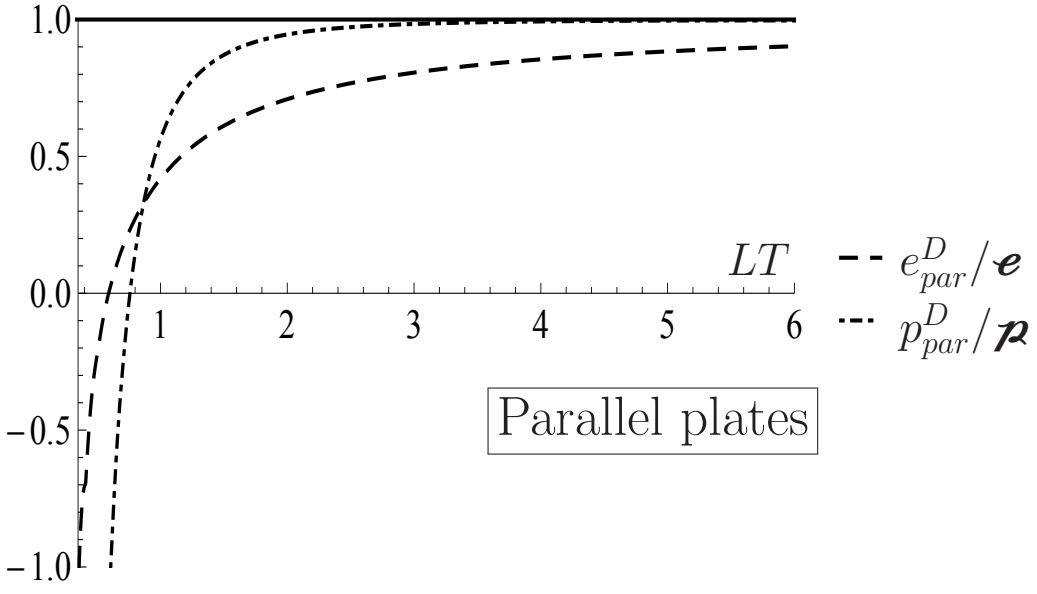

FIGURE 2.12: The ratios of the energy density and pressure in parallel plates with Dirichlet BCs to the continuum limits.

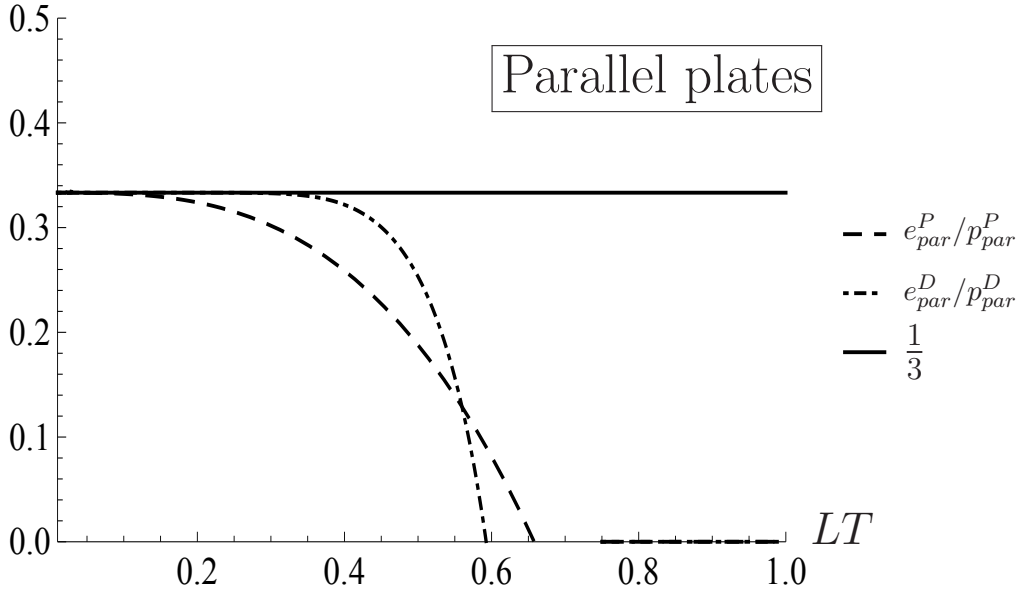

FIGURE 2.13: The ratios of the energy densities to the pressures in parallel plates for relatively small LT.

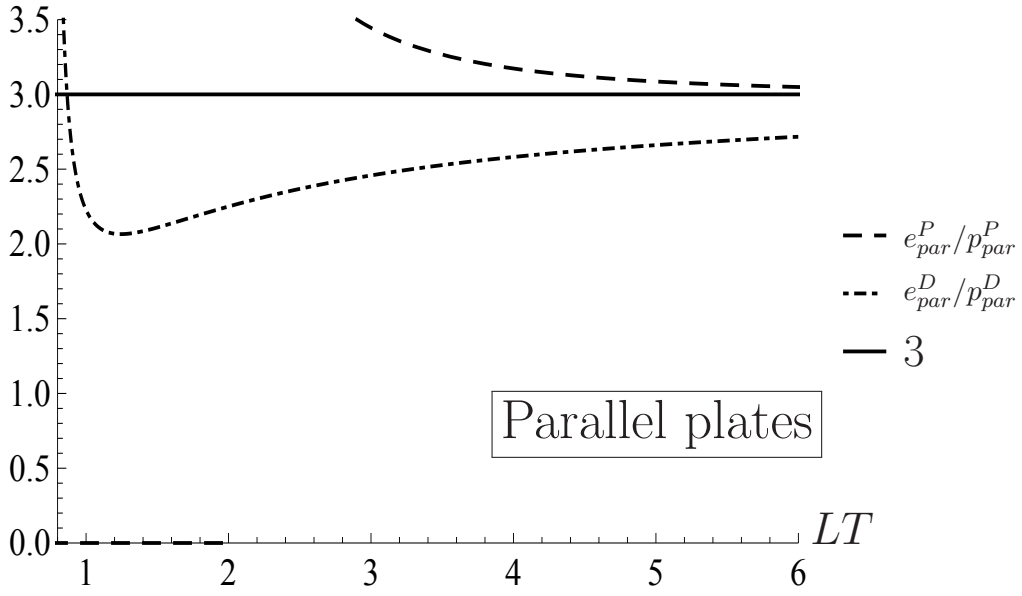

FIGURE 2.14: The ratios of the energy densities to the pressures in parallel plates for relatively large values of LT.

2.7.3 Energy density and pressure in a cuboid at non zero temperature

The energy density and pressure in a cuboid with periodic BCs are

$$e^P_{cuboid} = e^P_{cuboid0} + \frac{1}{\xi^2 L^3} \sum_{n,l,p=-\infty}^{\infty} K^P_{nlp\xi} f_B(K^P_{nlp\xi}) \,, \tag{2.144}$$

$$p^P_{cuboid} = p^P_{cuboid0} + \frac{1}{\xi^2 L^3} \sum_{n,l,p=-\infty}^{\infty} \frac{(k^P_{zn})^2}{K^P_{nlp\xi}} f_B(K^P_{nlp\xi}) \,. \tag{2.145}$$

And with Dirichlet BCs, the energy density and pressure are

$$e^D_{cuboid} = e^D_{cuboid0} + \frac{1}{\xi^2 L^3} \sum_{n,l,p=1}^{\infty} K^D_{nlp\xi} f_B(K^D_{nlp\xi}) \,, \tag{2.146}$$

$$p^D_{cuboid} = p^D_{cuboid0} + \frac{1}{\xi^2 L^3} \sum_{n,l,p=1}^{\infty} \frac{(k^D_{zn})^2}{K^D_{nlp\xi}} f_B(K^D_{nlp\xi}) \,. \tag{2.147}$$

We illustrate our results for the energy densities and pressures in Figures 2.15 - 2.22 (we illustrate the results for the values $LT = 1$ and $LT = 0.5$). In all Figures we see that the parallel plates limit is approached as ξ increases. However the way and the rapidity at which the curves approach the parallel plates limits strongly depends on LT, this is perhaps due to two factors: First, the parallel plates limits, at the small values of $LT = 0.5 - 1$, are rapidly varying functions, this is seen in Figures 2.12 - 2.14. Second, the vacuum contributions in a cuboid, with Dirichlet BCs, are non-monotonic functions of ξ, this is seen in Figures 2.6 - 2.7.

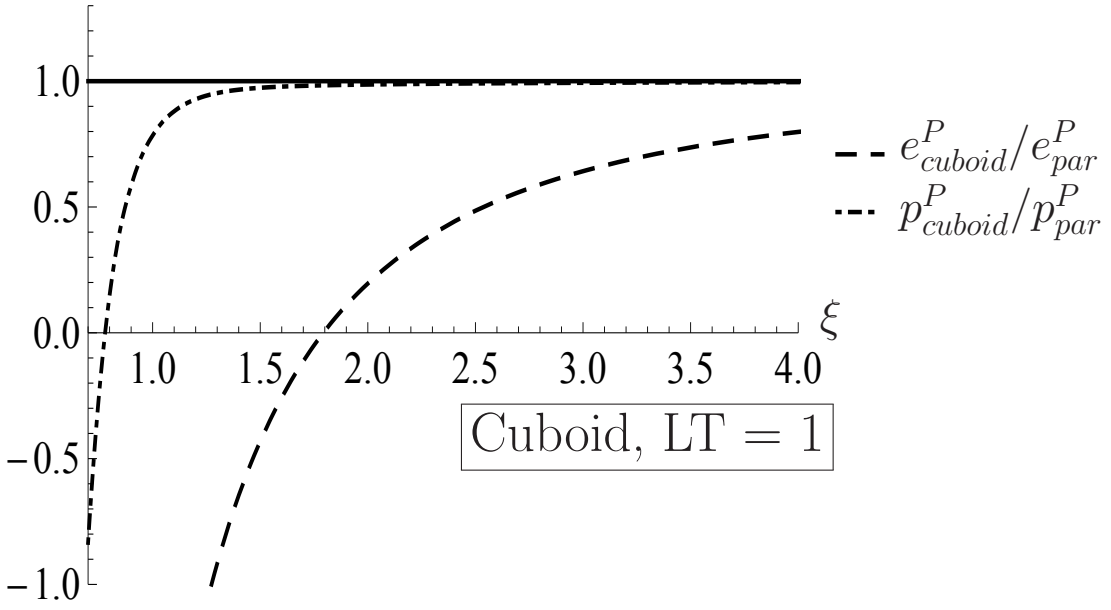

FIGURE 2.15: The ratios of the energy density and pressure in a cuboid with periodic BCs to their parallel plates limits.

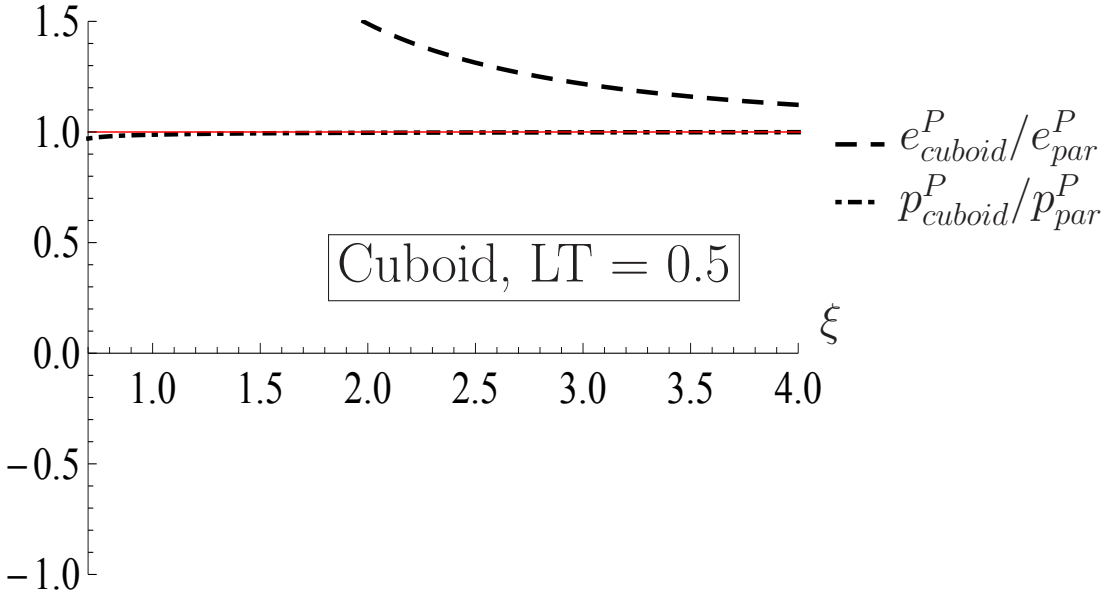

FIGURE 2.16: Same as Figure 2.15, except at $LT = 0.5$. The parallel plate limit is given the red color simply to distinguish it from the pressures ratio.

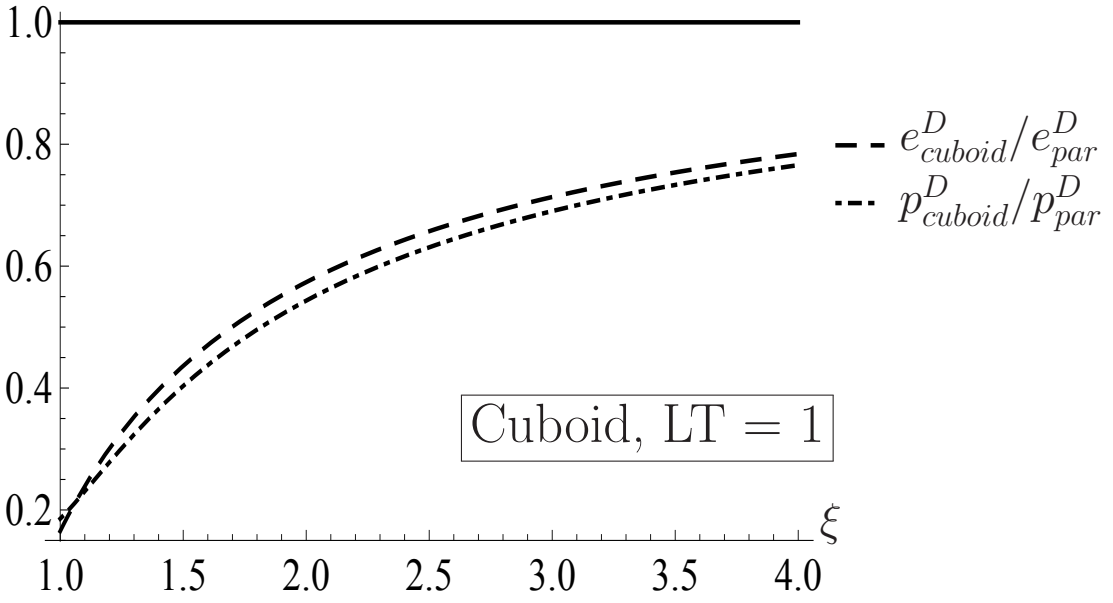

FIGURE 2.17: The ratios of the energy density and pressure in a cuboid with Dirichlet BCs to their parallel plates limits.

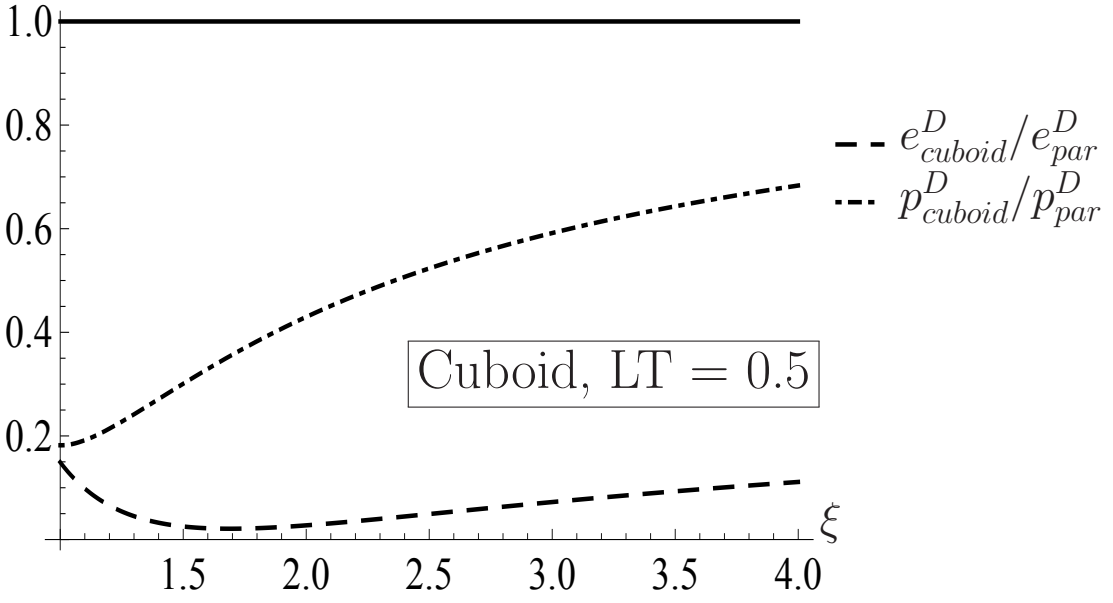

FIGURE 2.18: Same as Figure 2.17, except at $LT = 0.5$

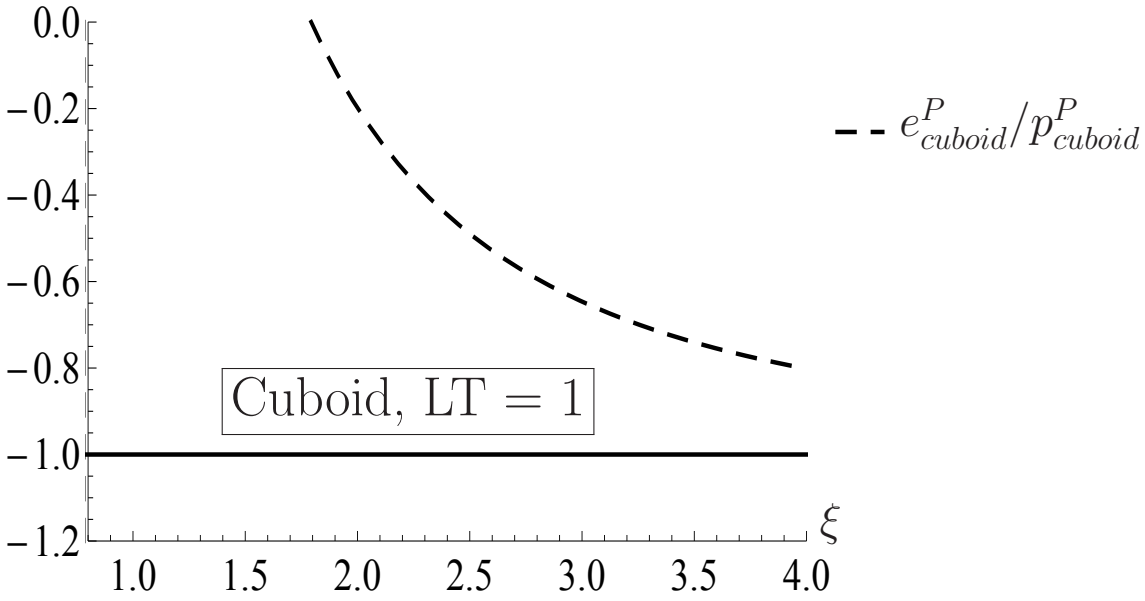

FIGURE 2.19: The ratio of the energy density to the pressure in a cuboid with periodic BCs. The horizontal line depicts the parallel plates limit at $LT = 1$.

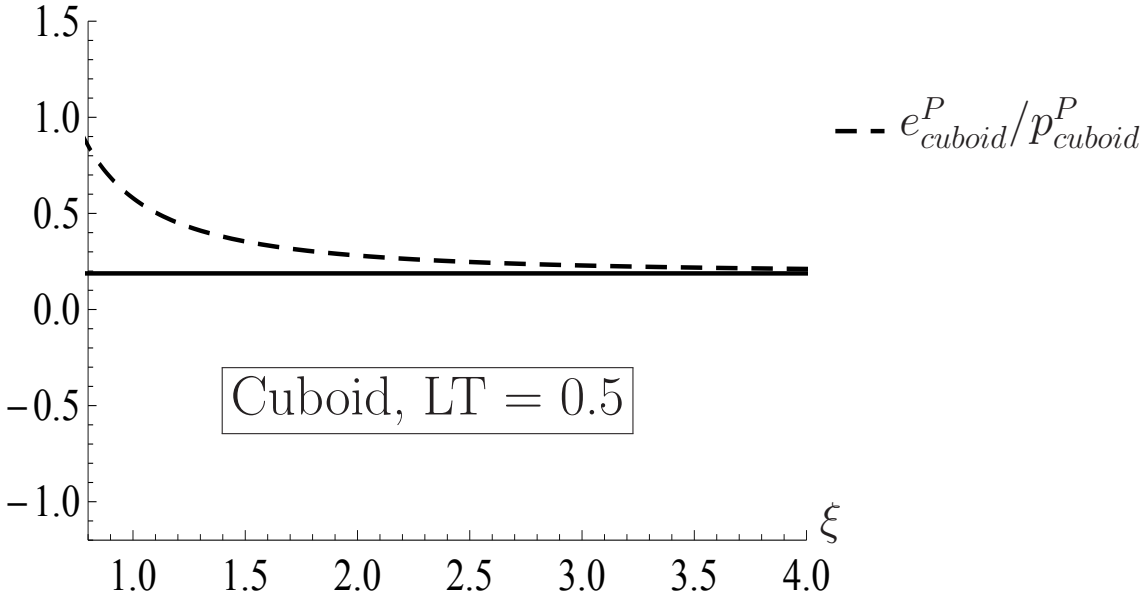

FIGURE 2.20: Same as Figure 2.19, except at $LT = 0.5$.

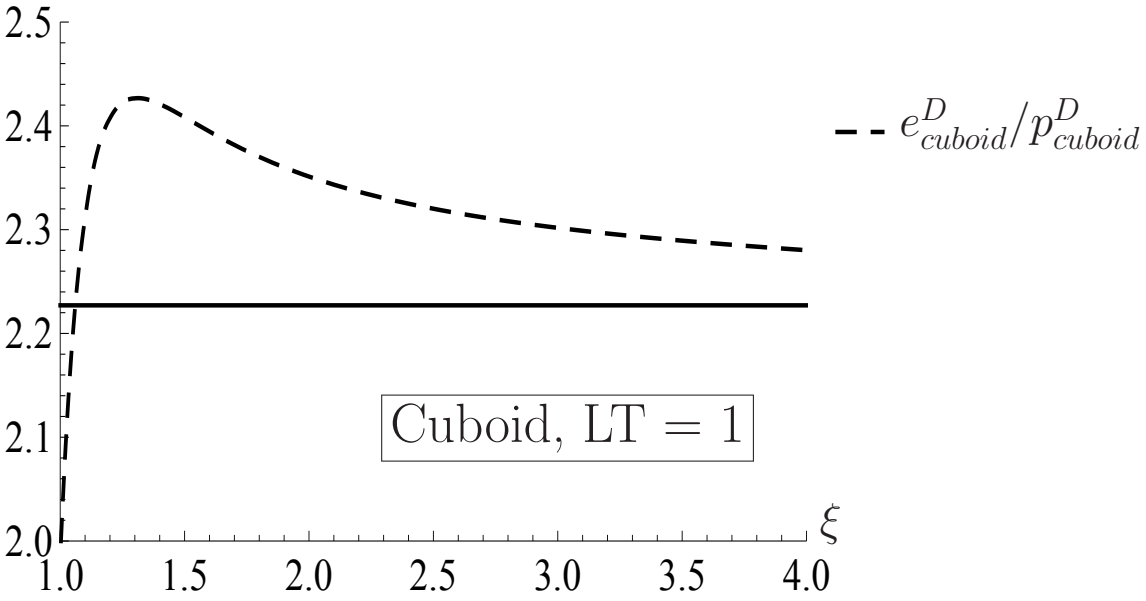

FIGURE 2.21: The ratio of the energy density to the pressure in a cuboid with Dirichlet BCs. The horizontal line depicts the parallel plates limit at $LT = 1$.

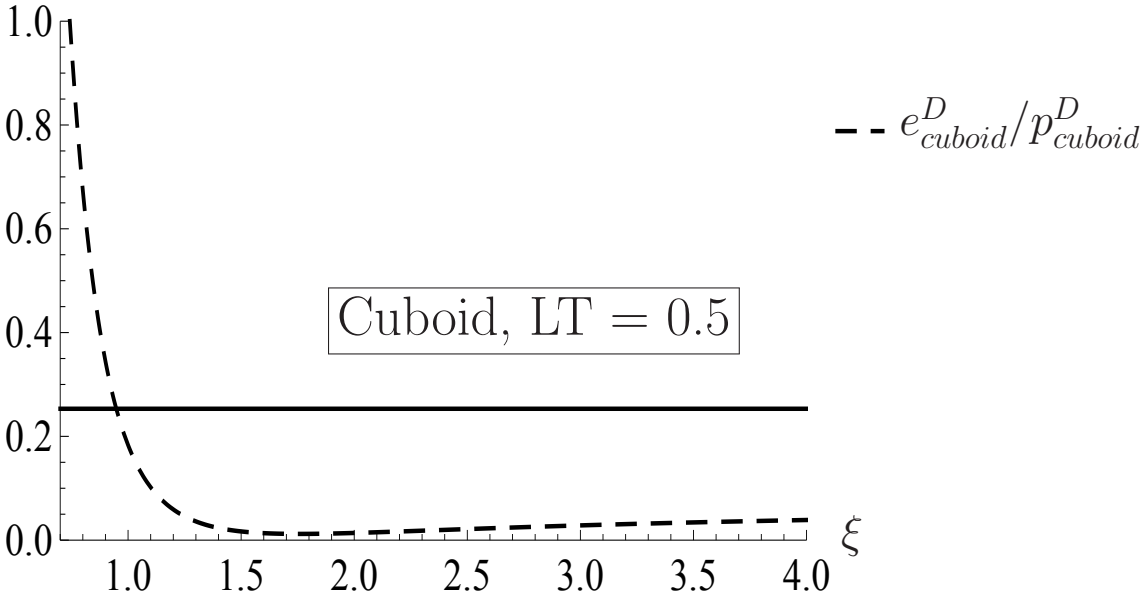

FIGURE 2.22: Same as Figure 2.21 except at $LT = 0.5$

2.7.4 Massive field in a cube at non zero temperature

In this section, we study the effects of a non zero mass on the energy density and pressure in a cube at non zero temperature. As in subsection 2.6.4, we restrict ourselves to periodic BCs. The energy density is obtained by generalizing (2.136)

$$e^{Pm}_{cube} = e^{Pm}_{cube0} + \frac{1}{L^3} \sum_{n,l,p=-\infty}^{\infty} \omega^P_{nlp} f_B(\omega^P_{nlp}) \ , \tag{2.148}$$

whereas, since (2.138) does not hold for a massive field, the pressure has to be calculated from the partition function, which gives

$$p^{Pm}_{cube} = p^{Pm}_{cube0} + \frac{1}{3}\frac{1}{L^3} \sum_{n,l,p=-\infty}^{\infty} \frac{(k^P_{nlp})^2}{\omega^P_{nlp}} f_B(\omega^P_{nlp}) \ . \tag{2.149}$$

We note that, for $m \to 0$, we have

$$\frac{1}{\omega^P_{nlp}} \approx \frac{1}{k^P_{nlp}} + \mathcal{O}(m^2) \ , \tag{2.150}$$

$$f_B(\omega^P_{nlp}) \approx f_B(k^P_{nlp}) + \mathcal{O}(m^2) \ , \tag{2.151}$$

thus, in the limit $m \to 0$, the energy density and the pressure reduce to their massless counterparts (2.136) and (2.138)

$$e^{Pm}_{cube} \approx e^{P}_{cube} + \mathcal{O}(m^2) \ , \tag{2.152}$$

$$p^{Pm}_{cube} \approx p^{P}_{cube} + \mathcal{O}(m^2) \ . \tag{2.153}$$

The results for the energy density and pressure are shown in Figures 2.23 and 2.24. The non uniformity of the curve in the first Figure is due to the opposing influences of vacuum and thermal contributions, whereas in the second Figure an additional factor is the non monotonic character of the vacuum pressure (Figure 2.9).

The reason why thermal contribution also decreases with increasing mass resides in the Bose function: The larger is the mass, the less is the average number of particles in a given energy level.

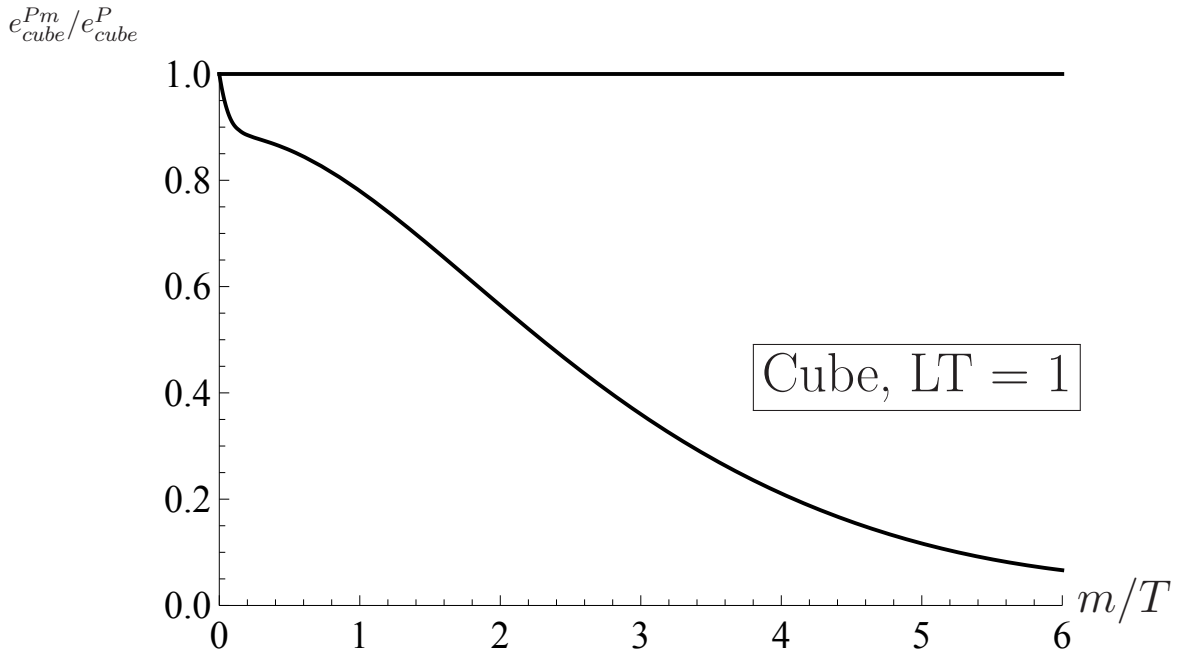

FIGURE 2.23: The ratio of the energy density of a massive field to massless field with periodic BCs.

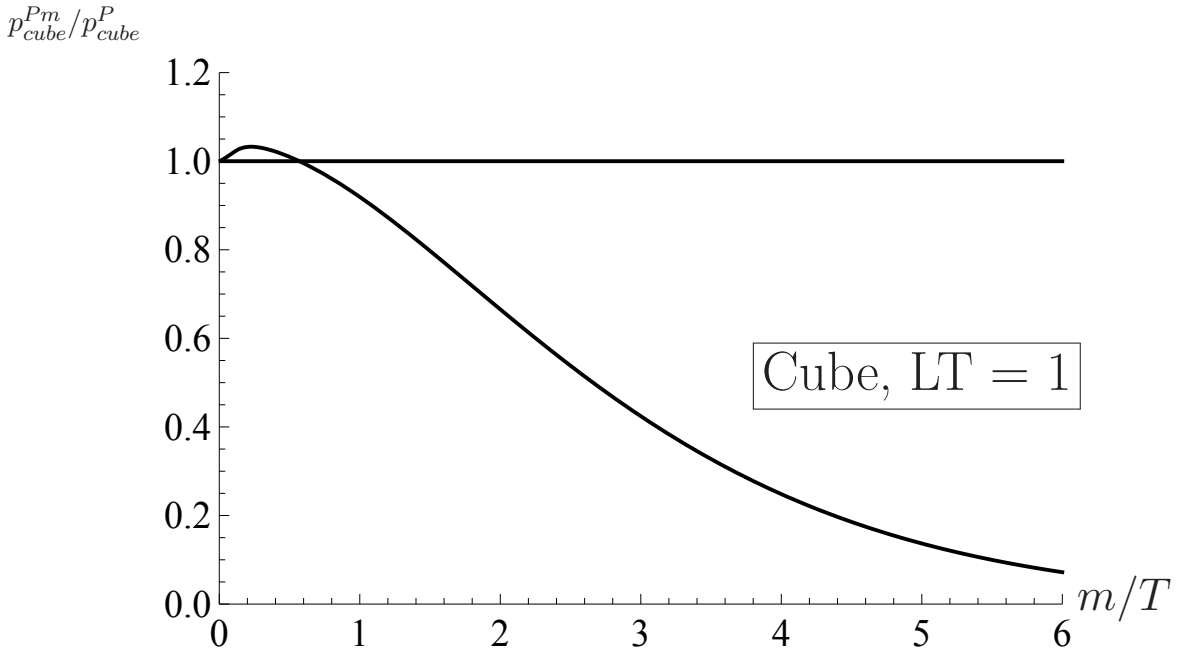

FIGURE 2.24: Same as Figure 2.23, except for the pressure.

2.8 Entropy of a free scalar gas

Finally in this section we discuss the behavior of the entropy density of the scalar field in finite volume. The entropy density will be greatly relevant to our discussion of a QCD quasi-particle model later in this thesis. As we've done with energy density and pressure, we discuss the volume-dependence of the entropy density first for a massless field in the cube, then in the parallel plates and the cuboid, and we finally discuss a massive field in a cube.

2.8.1 Entropy density in infinite volume

For the sake of the discussion that will follow, we briefly revisit the entropy density in infinite volume. Let us first first rewrite the continuum entropy density (2.63) in a more convenient form

$$\mathfrak{s} = \int \frac{d^3\,k}{(2\pi)^3}\sigma(\omega_k)\ , \tag{2.154}$$

where

$$\sigma(\omega_k) = \left[(1+f_B(\omega_k))\ln(1+f_B(\omega_k)) - f_B(\omega_k)\ln(f_B(\omega_k))\right]\ . \tag{2.155}$$

For a *massless* field, we can carry out the integral in (2.154) and we obtain

$$\mathfrak{s} = \frac{4\pi^2}{90}T^3\ . \tag{2.156}$$

2.8.2 Entropy density in a cube

It is now our goal to see how the entropy density looks like for a massless field in a cube when compared to the continuum limit. The entropy densities with Dirichlet and periodic BCs are

$$s^D_{cube} = \frac{1}{L^3}\sum_{n,l,p=1}^{\infty}\sigma(k^D_{nlp})\ , \tag{2.157}$$

$$s^P_{cube} = \frac{1}{L^3}{\sum_{n,m,l=-\infty}^{\infty}}'\sigma(k^P_{nlp})\ , \tag{2.158}$$

respectively.

In Figure (2.25) we show our results for the ratio of the entropy density in a cube to the continuum limit (2.154).

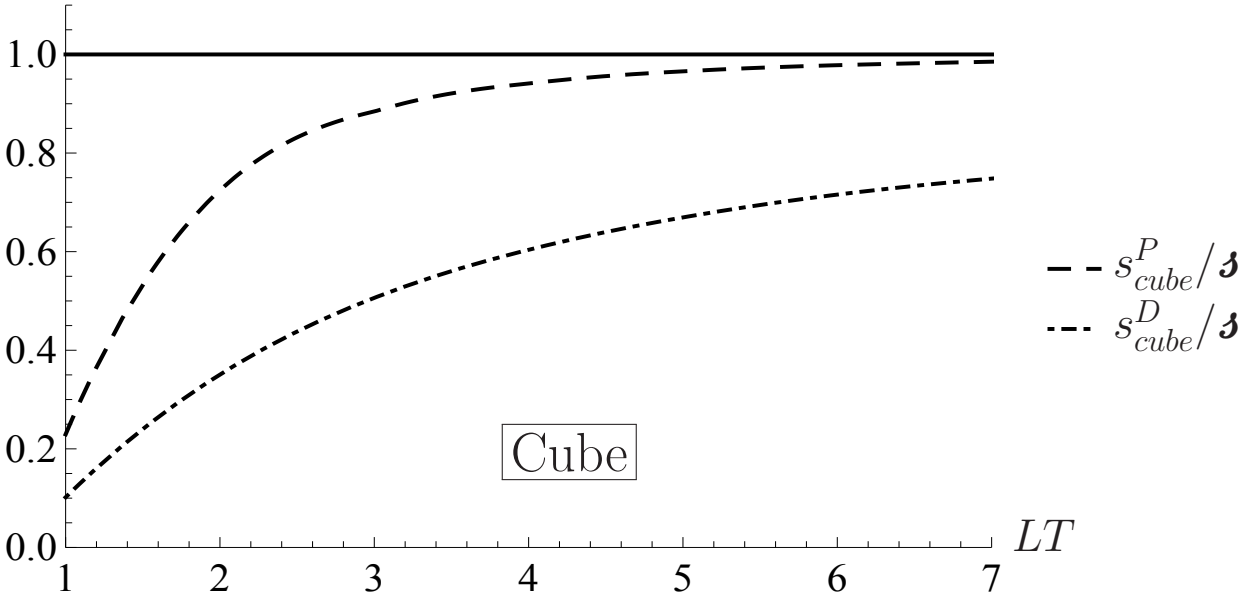

FIGURE 2.25: The ratios of the entropy density of a massless field in a cube with Dirichlet and periodic BCs to the continuum limit.

2.8.3 Entropy density in parallel plates

The entropy density in parallel plates, subject to Dirichlet BCs, is given by

$$s^D_{par} = \frac{1}{L}\sum_{n=1}^{\infty}\int \frac{d^2k_\perp}{(2\pi)^2}\sigma(\tilde{K}^D_n)\ . \tag{2.159}$$

Carrying out the integration, one obtains

$$s^D_{par} = \frac{1}{2\pi}\frac{T^2}{L}\sum_{n=1}^{\infty}\left\{\left(\frac{k^D_{zn}}{T}\right)^2 \mathrm{Li}_1(e^{-\frac{|k^D_{zn}|}{T}})+3\frac{|k^D_{zn}|}{T}\mathrm{Li}_2(e^{-\frac{|k^D_{zn}|}{T}})+3\mathrm{Li}_3(e^{-\frac{|k^D_{zn}|}{T}})\right\}\ . \tag{2.160}$$

The entropy density with periodic BCs can be obtained by similar calculations or by the transformation $L \to L/2$

$$s^P_{par}(L,T) = s^D_{par}(L/2,T) + \frac{3T^2}{2\pi L}\mathrm{Li}_3(1)\ . \tag{2.161}$$

We present our results in Figure 2.26.

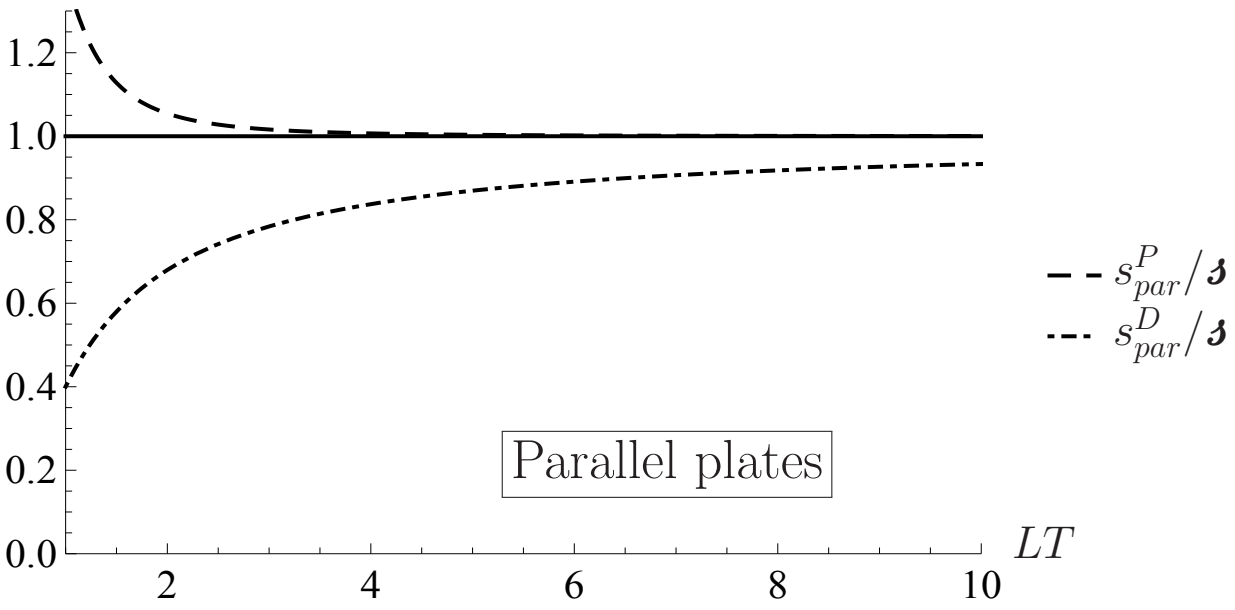

FIGURE 2.26: The ratio of the entropy density of a massless field in parallel plates with Dirichlet and periodic BCs to continuum limit.

2.8.4 Entropy density in a cuboid

Here we want to see how does the entropy density of a massless field in a cuboid compare to the entropy density in parallel plates.

The results for the entropy density in a cuboid with Dirichlet BCs, denoted by s^D_{cuboid}, and with periodic BCs, denoted by s^P_{cuboid}, are depicted in Figure 2.27.

2.8.5 Entropy density of a Massive scalar gas in a cube

Now we wish study the effects of introducing mass on the entropy density in a cube. The entropy density of a massive field will be denoted by s^{Pm}_{cube} and s^{Dm}_{cube} for periodic and Dirichlet BCs, respectively. We show our results in Figure 2.28.

The reason the entropy density decreases with increasing mass is that, as mass increases, more and more particle will be in energy levels with smaller k's; this creates more "order" and, therefore, reduces the entropy.

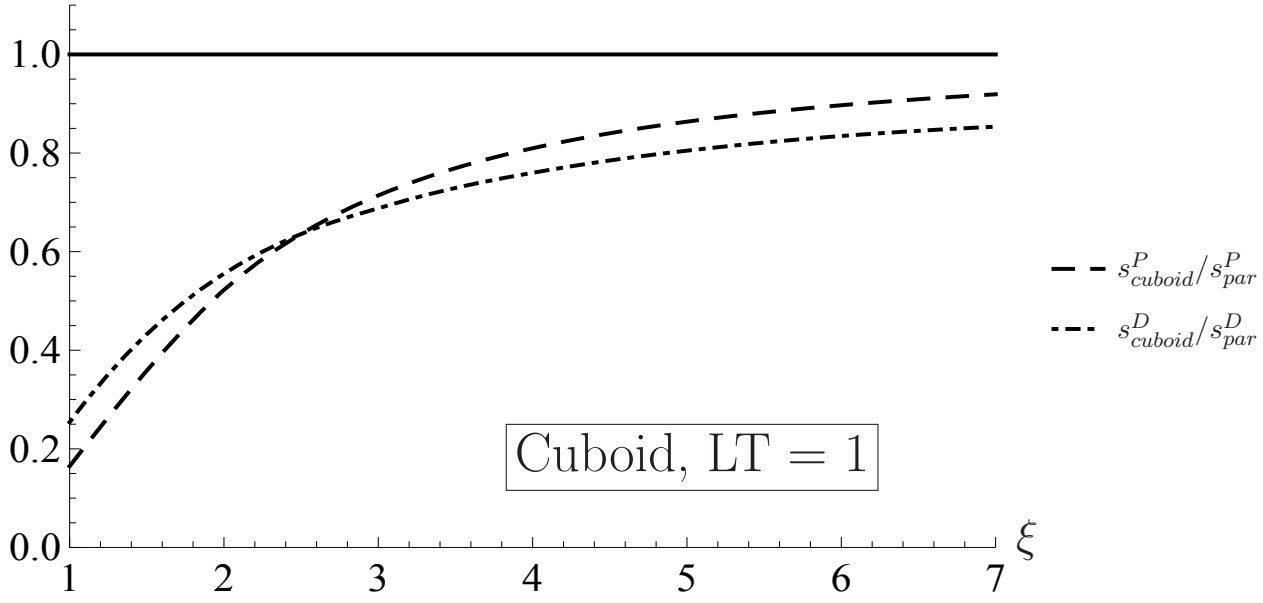

FIGURE 2.27: The ratio of the entropy density of a massless field in a cuboid with Dirichlet and periodic BCs to the parallel plates limit at $LT = 1$.

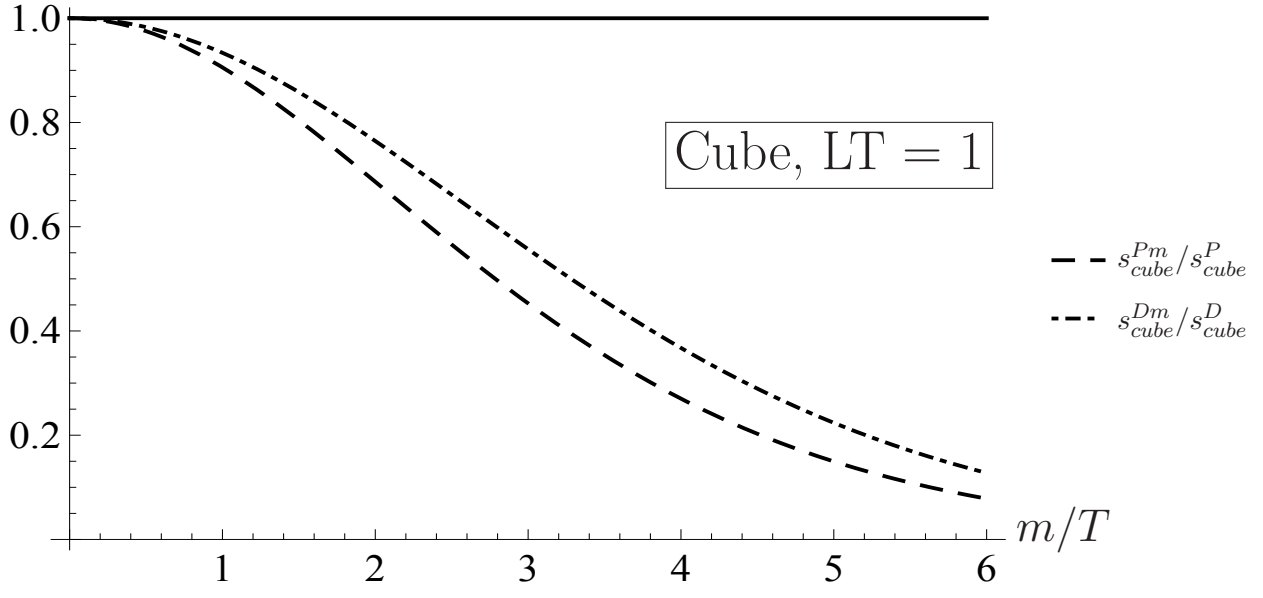

FIGURE 2.28: The ratios of the entropy densities of massive field in a cube with Dirichlet and periodic BCs to their massless limits.

2.9 Thermodynamics of a free scalar field on a finite Euclidean lattice

So far far we've been investigating the thermodynamics of a free scalar field with the natural assumption of continuous space coordinates, with the cut off on the momenta being a computational necessity. Also, in section 2.4, we have seen that the sum over Matsubara frequencies can be evaluated in a closed form, this was because we were dealing with the relatively simple theory of a free scalar field. In more complicated theories, such as Quantum Chromodynamics, evaluating such sums is, in general, not feasible (in fact, a functional integral (such as (2.44)) with a Lagrangian that contains terms other than quadratic in the field cannot be evaluated in a closed form [4]). In the numerical simulations of such theories, space-time is approximated by a finite, discretized lattice, which implies cut-offs on both Matsubara frequencies and spatial momenta [6]; this means that the lattice is a regulator, because it regulates ultra-violet divergences (in particular, it regulates the ultra-violet divergences of the vacuum contributions).

In this section, we are going to discuss the effects of this lattice discretization on the thermodynamic properties of the free scalar field.

On a finite lattice with N_τ lattice sites (nodes) in the imaginary time direction and N_σ sites in each of the spatial directions, and with according lattice spacings a_τ and a_σ, the position vector becomes [6]

$$x = (\alpha_0 a_\tau, \boldsymbol{\alpha} a_\sigma) \,, \tag{2.162}$$

with integer α_0 and $\boldsymbol{\alpha}$ ($\boldsymbol{\alpha}$ is written in bold font to indicate that it's a vector). The temperature and volume, assuming the cube geometry, become

$$T = \frac{1}{N_\tau a_\tau} \,, \qquad V = (N_\sigma a_\sigma)^3 \,, \tag{2.163}$$

and the partition function (equation (2.44)) becomes [6]

$$Z(N_\sigma, N_\tau, a_\sigma, a_\tau) = N' \int \prod_\alpha d\phi(x_\alpha) e^{-S(\phi)} \,, \tag{2.164}$$

where the product index α is a four-vector, and

$$N' = \left[\frac{a_\sigma^3}{2\pi a_\tau} \right]^{N_\sigma^3 N_\tau} \,, \tag{2.165}$$

$$S(\phi) = \frac{1}{2} a_\sigma^3 a_\tau \sum_\alpha \left[\sum_{\mu=1}^{3} \left(\frac{\phi(x_\alpha + e_\mu) - \phi(x_\alpha)}{a_\sigma} \right)^2 + \left(\frac{\phi(x_\alpha + e_0) - \phi(x_\alpha)}{a_\tau} \right)^2 + m^2 \phi^2(x_\alpha) \right] , \tag{2.166}$$

where $e_\mu, \mu = 1, 2, 3$ are the lattice unit vectors and the x_α's are the grid sites. This form of the normalization constant N' is to ensure the correct vacuum structure as we shall see later.

With the transformation [6]

$$\tilde{\phi}(x_\alpha) \equiv a_\sigma k^{-1/2} \phi(x_\alpha) , \tag{2.167}$$

$$k^{-1} \equiv 3\xi^{-1} + \xi + (m a_\sigma)^2 / 2\xi , \tag{2.168}$$

$$\xi \equiv a_\sigma / a_\tau , \tag{2.169}$$

the partition function (2.164) becomes [6]

$$Z(\sigma, N_\tau, a_\sigma, \xi) = \bar{N}' \int \prod_\alpha d\tilde{\phi}(x_\alpha) e^{-S(\tilde{\phi})} , \tag{2.170}$$

with

$$\bar{N}' = [k\xi / 2\pi]^{N_\sigma^3 N_\tau / 2} , \tag{2.171}$$

$$S(\tilde{\phi}) = -\sum_\alpha \left[-\tilde{\phi}^2(x_\alpha) + K_\sigma \sum_{\mu=1}^{3} \tilde{\phi}(x_\alpha + e_\mu) \tilde{\phi}(x_\alpha) + K_\beta \tilde{\phi}(x_\alpha + e_0) \tilde{\phi}(x_\alpha) \right] . \tag{2.172}$$

In the following we impose periodic BCs on the spatial directions. Thus we go to the reciprocal lattice of the momentum coordinates and introducing the Fourier-transformed field variables

$$\phi_q = \frac{1}{\sqrt{N_\sigma^3 N_\tau}} \sum_\alpha e^{-iqx_\alpha} \tilde{\phi}(x_\alpha) , \tag{2.173}$$

$$\tilde{\phi}(x_\alpha) = \frac{1}{\sqrt{N_\sigma^3 N_\tau}} \sum_q e^{iqx_\alpha} \phi_q , \tag{2.174}$$

where the momentum $q = (q_0, q_\mu)$, in the first Brillouin zone of the reciprocal lattice, have the allowed values [6], [14]

$$q_0 = \frac{2\pi}{N_\tau a_\tau} j_0, \quad \text{with} \quad \begin{cases} j_0 = 0, \pm 1, \ldots, \pm(\frac{1}{2}N_\tau - 1), \frac{1}{2}N_\tau \ , & \text{For } N_\tau \text{ even} \ , \\ j_0 = 0, \pm 1, \ldots, \pm\frac{(N_\tau - 1)}{2} \ , & \text{For } N_\tau \text{ odd} \ , \end{cases} \tag{2.175}$$

$$q_\mu = \frac{2\pi}{N_\sigma a_\sigma} j_\mu, \quad \text{with} \quad \begin{cases} j_\mu = 0, \pm 1, \ldots, \pm(\frac{1}{2}N_\sigma - 1), \frac{1}{2}N_\sigma \ , & \text{For } N_\sigma \text{ even} \ , \\ j_\mu = 0, \pm 1, \ldots, \pm\frac{(N_\sigma - 1)}{2} \ , & \text{For } N_\sigma \text{ odd} \ . \end{cases} \tag{2.176}$$

Note that the allowed values of the indices j_0 and j_μ are not the same as in (2.48) and (2.26), note also the ultra-violet cut-offs $\sim 1/a_\sigma$ and $\sim 1/a_\tau$ on the momenta; these are some of the artifacts of lattice discretization.

With the Fourier decomposition of the fields and the completeness relation

$$\sum_\alpha e^{iqx_\alpha} = N_\sigma^3 N_\tau \delta_{q,0} \ , \tag{2.177}$$

the action becomes [6]

$$S = \frac{1}{2} k \xi^{-1} \sum_q \phi_q \phi_q^* G^{-1}(a_\sigma, \xi, q) \ , \tag{2.178}$$

where the fact that the field is real was used, i.e.

$$\phi_{-q} = \phi_q^* \ . \tag{2.179}$$

G is the dimensionless lattice propagator [6]

$$G^{-1}(a_\sigma, \xi, q) = a_\sigma^2 \, \Delta_{0L}^{-1} = (m a_\sigma)^2 + 4 \sum_{\mu=1}^{3} \sin^2\left(\frac{1}{2} q_\mu a_\sigma\right) + 4\xi^2 \sin^2\left(\frac{1}{2} q_0 a_\tau\right) \ . \tag{2.180}$$

with Δ_{0L} being the lattice propagator (the lattice version of (2.53)) [6].

Due to relation (2.179), the integration measure in (2.170) becomes [6].

$$\prod_\alpha d\tilde{\phi}(x_\alpha) = 2^{N_\sigma^3 N_\tau/2} \prod_{q \geq 0} d\phi_q \ . \tag{2.181}$$

Thus the partition function becomes a product of Gaussian integrals, which gives [6]

$$Z(N_\sigma, N_\tau, a_\sigma, \xi) = \xi^{N_\sigma^3 N_\tau} \prod_q G^{1/2}(a_\sigma, \xi, q) \ . \tag{2.182}$$

From this, via relation (2.40), one obtains the Free energy density

$$f_E = -\frac{T}{V} \ln(Z) = -\frac{1}{a_\tau a_\sigma^3} \ln(\xi) + \frac{1}{2N_\tau N_\sigma^3 a_\tau a_\sigma^3} \sum_q \ln G^{-1}(a_\sigma, \xi, q) \ . \tag{2.183}$$

Next, the Free energy density is renormalized by requiring that it vanishes in the vacuum (the limit $N_\tau \to \infty$). The Free energy density (2.183) is obviously ultra-violet finite, but the renormalization is done so that, if the lattice is removed (the limit $N_\sigma, N_\tau \to \infty$ and $a_\sigma, a_\tau \to 0$), the continuum renormalized Free energy density (2.134) will be recovered. The renormalization is done by subtracting from it its value in the vacuum (the limit $N_\tau \to \infty$) [6]:

$$f_v = \lim_{N_\tau \to \infty} f_E \ . \tag{2.184}$$

This limit can be evaluated in a closed form and gives [6]

$$f_v a_\sigma^4 = \xi \ln(2/\xi) + \frac{\xi}{2N_\sigma^3} \sum_j \int_{-1/2}^{1/2} dx \ln\Big(b(j)^2 + \xi^2 \sin(\pi x)^2\Big) \ , \tag{2.185}$$

where the integral is the $N_\tau \to \infty$ limit of the sum over the j_0's, and

$$b^2(j) = \left(\frac{1}{2} m a_\sigma\right)^2 + \sum_{\mu=1}^{3} \sin^2(\pi j_\mu / N_\sigma) \ . \tag{2.186}$$

Carrying out the integral gives the vacuum contribution

$$f_v a_\sigma^4 = -\xi \ln(\xi) + \frac{\xi}{N_\sigma^3} \sum_j \ln\Big(b(j) + \sqrt{\xi^2 + b^2(j)}\Big) \ . \tag{2.187}$$

Thus the renormalized Free energy density is [6]

$$f a_\sigma^4 = a_\sigma^4 (f_E - f_v) \ . \tag{2.188}$$

The closed-form result (2.187) was possible because of the relatively simple structure of the free scalar partition function. In the numerical computations of more complicated systems, such as $SU(3)$ gauge theories which we will discuss later in this thesis, one cannot in general obtain the vacuum by taking the limit $N_\tau \to \infty$ [6]. Instead of this limit, the vacuum can be defined by choosing $N_\tau = N_\sigma$, with $N_\sigma \gg 1$

$$f_v = f_E \Big|_{N_\tau = N_\sigma}, \quad N_\sigma \gg 1 \ . \tag{2.189}$$

In other words, the vacuum is defined by a value of N_τ that is sufficiently large. The reason that that value is specified to be N_σ is because it is computationally convenient and because there is little benefit, in terms of accuracy, in choosing a larger value if N_σ is already $\gg 1$ (for a demonstration of the accuracy aspect, see [6]). Thus the vacuum contribution to the Free energy density becomes

$$f_v\, a_\sigma^4 = f_E\, a_\sigma^4\Big|_{N_\tau=N_\sigma} = -\xi\ln(\xi) + \frac{\xi}{2N_\sigma^4}\sum_q \ln G^{-1}(a_\sigma,\xi,q)\ . \tag{2.190}$$

Note that j_0 and j_μ will now have the same sum limits (see equations (2.175) and (2.176)), and the propagator is also evaluated with $N_\tau = N_\sigma$. Thus, using this renormalization scheme, we obtain for the renormalized Free energy density

$$f a_\sigma^4 = \frac{\xi}{2}\left[\frac{1}{N_\tau N_\sigma^3}\sum_q \ln G^{-1}(a_\sigma,\xi,q) - \frac{1}{N_\sigma^4}\sum_q \ln G^{-1}(a_\sigma,\xi,q)\right]\ . \tag{2.191}$$

where G was defined in (2.180). Note that for the case $m = 0$, the term with $q = 0$ has to be suppressed, since it leads to a divergence [6]. In the limit $N_\sigma \to \infty$ this infra-red (small momentum) divergence disappears because the phase space factor $(d^3k/(2\pi)^3)$ suppresses the integrand at small momenta.

Now that we have the Free energy density, we can calculate the energy density, the pressure and the entropy density from it via[1]

$$e = -T^2\frac{\partial}{\partial T}\left(\frac{f}{T}\right)\Big|_V\ , \tag{2.192}$$

$$p = -\frac{\partial}{\partial V}(Vf)\Big|_\beta\ , \tag{2.193}$$

$$s = -\frac{\partial f}{\partial T}\Big|_V\ . \tag{2.194}$$

On the lattice, the differential operators in the relations above become derivatives with respect to grid spacings a_σ and a_τ [6]

$$\frac{\partial}{\partial T}\Big|_V = -N_\tau a_\tau^2\frac{\partial}{\partial a_\tau}\Big|_{a_\sigma}\ , \tag{2.195}$$

$$\frac{\partial}{\partial V}\Big|_\beta = \frac{1}{3N_\sigma^3 a_\sigma^2}\frac{\partial}{\partial a_\sigma}\Big|_{a_\tau}\ . \tag{2.196}$$

Thus one obtains for the renormalized energy density on the lattice

$$e\, a_\sigma^4 = -\frac{\xi^3}{N_\sigma^3 N_\tau}\sum_j \frac{\sin^2(\pi j_0/N_\tau)}{b^2+\xi^2\sin^2(\pi j_0/N_\tau)} + \frac{\xi^3}{N_\sigma^4}\sum_j \frac{\sin^2(\pi j_0/N_\sigma)}{b^2+\xi^2\sin^2(\pi j_0/N_\sigma)}\ , \tag{2.197}$$

[1] These relations can be easily derived from (2.40) - (2.43).

and for the pressure

$$3\,p\,a_\sigma^4 = -\frac{\xi}{N_\sigma^3 N_\tau}\sum_j \frac{(\frac{ma_\sigma}{2})^2 + \xi^2\sin^2(\pi j_0/N_\tau)}{b^2+\xi^2\sin^2(\pi j_0/N_\tau)} + \frac{\xi}{N_\sigma^4}\sum_j \frac{(\frac{ma_\sigma}{2})^2 + \xi^2\sin^2(\pi j_0/N_\sigma)}{b^2+\xi^2\sin^2(\pi j_\mu/N_\sigma)}\,, \tag{2.198}$$

and finally the entropy density

$$s\,a_\sigma^3 = N_\tau\left[-\frac{1}{N_\sigma^3 N_\tau}\sum_j\left(\frac{4\,\xi^2\sin^2(\pi j_0/N_\tau)}{G^{-1}} + \frac{\ln\left(G^{-1}\right)}{2}\right) + \frac{1}{N_\sigma^4}\sum_j\left(\frac{4\,\xi^2\sin^2(\pi j_0/N_\sigma)}{G^{-1}} + \frac{\ln\left(G^{-1}\right)}{2}\right)\right]. \tag{2.199}$$

Note from (2.197) and (2.198) that in the limit $m \to 0$, the familiar continuum equation of state

$$e = 3p \tag{2.200}$$

is satisfied [6].

Though not used in lattice QCD calculations, it is useful for us to discuss as well the lattice energy density obtained with the renormalization (2.184). It is given by [6]

$$e\,a_\sigma^4 = -\frac{\xi^3}{N_\sigma^3 N_\tau}\sum_j \frac{\sin^2(\pi j_0/N_\tau)}{b^2+\xi^2\sin^2(\pi j_0/N_\tau)} + \frac{\xi^3}{N_\sigma^3}\sum_j (b\sqrt{\xi^2+b^2}+\xi^2+b^2)^{-1}. \tag{2.201}$$

When $m = 0$, the pressure corresponding to (2.201) is obtained via (2.200) as well [6].

Let us now compare the lattice energy densities (2.197) and (2.201) of a massless field to the energy density of a massless field in a cube with periodic BCs (2.136) and to the continuum energy density of a massless field (2.135). We will do the comparison for isotropic lattices ($a_\sigma = a_\tau = a$) because lattice QCD calculations are performed on such lattices, as we shall see in the next chapter. To do the comparison, let us note:

1. There are two renormalization schemes:

   A: The scheme given in equation (2.184) which corresponds to the energy density given in (2.201).

B: The scheme given in equation (2.189) which corresponds to the energy density given in (2.197).

2. On isotropic lattices, the dimensionless variable LT becomes

$$LT = N_\sigma a \times \frac{1}{N_\tau a} = \frac{N_\sigma}{N_\tau} \, . \tag{2.202}$$

3. As for the cube, since the lattice energy densities (2.197) and (2.201) are renormalized to be zero in the vacuum, it will be useful to discuss as well the energy density in a cube with periodic BCs without vacuum contribution. Thus let us drop the vacuum contribution from the energy density in a cube with periodic BCs (2.136), hence it becomes

$$e^P_{cube} \longrightarrow \tilde{e}^P_{cube} = \frac{1}{L^3} \sum_{n,l,p=-\infty}^{\infty} k^P_{nlp} f_B(k^P_{nlp}) \, . \tag{2.203}$$

4. It is useful to note that in the limit $N_\sigma \to \infty$ with large N_τ and when $m = 0$ and on an isotropic lattice, (2.197) and (2.198) admit the N_τ-expansion [7], [15]

$$\frac{e}{\boldsymbol{e}} = \frac{p}{\boldsymbol{p}} = 1 + \frac{30\pi^2}{63} \left(\frac{1}{N_\tau}\right)^2 + \mathcal{O}\left(\frac{1}{N_\tau}\right)^4 \, , \tag{2.204}$$

where $\boldsymbol{e}$ and $\boldsymbol{p}$ are the continuum energy density and pressure of a massless field, given in (2.135). Thus this asymptotic expansion can serve as a benchmark for our numerical results for the lattice energy density and pressure of a massless field on isotropic lattices, and we therefore expect our lattice results to be closest to this expression at large N_σ and N_τ with $N_\tau \ll N_\sigma$, i.e, at large N_σ with moderate LT. This asymptotic expansion will also be crucial when we discuss the continuum-extrapolation of lattice QCD results in the next chapter.

Figure 2.29 illustrates how the results for the $N_\sigma = 16$ and 32 lattices converge for small LT (the reason we choose $N_\sigma = 16, 32$ is because these two values are used in the lattice QCD calculations that we will discuss in the next chapter).

From the Figure we note the following:

1. For renormalization scheme A, lattice results agree with the cube without vacuum contribution (2.203), but not with the analytic expansion (2.204).

2. For large LT, finite-size effects are small but discretization artifacts become pronounced.

3. While the analytic expansion (2.204) is reasonably accurate for $N_\sigma = 32$ and $2 \precsim LT \precsim 6$, it is hardly useful with $N_\sigma = 16$ in any interval of LT.

4. With renormalization scheme B, there are sizable differences to the cube results even for $LT \precsim 2$: while the lattice energy vanishes at $LT = 1$ (corresponding to $N_\tau \to N_\sigma$) by construction, the cube energy density vanishes at a somewhat lower argument, $e^P_{cube}(\kappa) = 0$ with $\kappa \approx 0.8$. This fact motivates us to put forward a third renormalization scheme:

   C: the vacuum is defined to be at $N_\sigma/\kappa \approx 1.25 N_\sigma$.

We may improve the expansion (2.204) by taking into account the next to leading $\mathcal{O}(N_\tau^{-4})$ correction as well as finite-size modification at small LT [1], by using

$$\frac{e}{\mathscr{e}} = 1 + \frac{30}{63}\left(\frac{\pi}{N_\tau}\right)^2 + c_4\left(\frac{\pi}{N_\tau}\right)^4 + C\left(\frac{N_\tau}{N_\sigma}\right)^\nu \dots \tag{2.205}$$

We find the "Casimir parameters" $C \approx -0.21$ and $\nu \approx 6.9$ by matching the $N_\sigma = 32$ to the cube limit for $LT \simeq \kappa$ (using renormalization scheme C).[2] With the parameter $c_4 = 0.57$ matched to the $N_\sigma = 32$ at the very "moderately large" argument $LT = 4$ we find indeed a considerably improved agreement with the lattice results in case of $N_\sigma = 32$ even in the whole LT range considered, see Figure 2.30.

As mentioned in the introduction (chapter 1), in the situations relevant to Heavy-ion collisions, typical temperatures are a few hundred MeV and typical lengths are a few fm. This translates into $LT = \mathcal{O}(1)$. We see in Figure 2.29 that the deviations from the continuum at $LT = \mathcal{O}(1)$ are of order 10%, this was seen as well in the other geometries (the cuboid and the parallel plates) discussed in the previous sections.

In conclusion, lattice finite size effects on the thermodynamic properties, in particular on the energy density in the range $4 - 5.33\,LT$, which is the range used in the lattice QCD calculations in [7], are of order 10%.

[1] Here we make use of the fact that for small $LT = N_\sigma/N_\tau$ the lattice results are basically independent of N_σ.

[2] We mention that from the known cube result in vacuum, $e^P_{cube}(T = 0, L) = -0.83/L^4$ [12], corresponding to the expansion point $LT = 0$, we could only get a very crude estimate of these parameters.

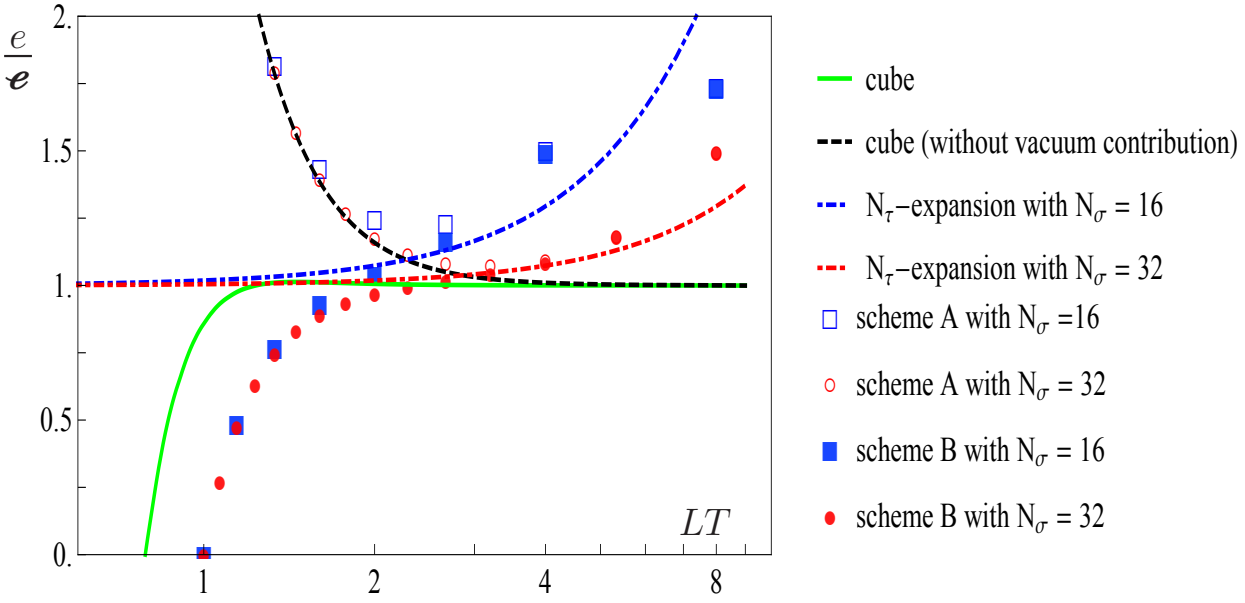

FIGURE 2.29: Energy density for a cube as a function of LT, comparing lattice results to the continuum limit and to the expansion (2.204).

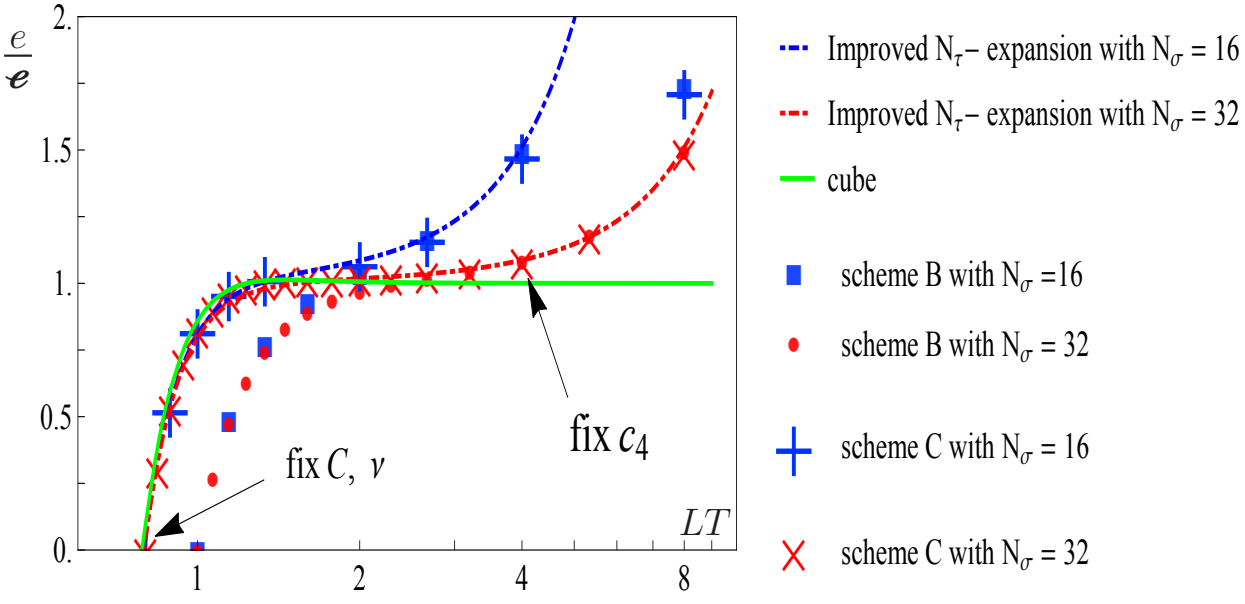

FIGURE 2.30: Lattice energy density with renormalization scheme C, compared to the cube limit and to our improved expansion (2.205) (the arrows indicate where the parameters were fixed).

Chapter 3

QCD Thermodynamics in Infinite and Finite Volume

3.1 Quantum Chromodynamics (QCD)

Quantum Chromodynamics (QCD) is the theory of the strong force (interaction) that binds quarks and gluons [4]. Quarks are spin-1/2 fermions, with fractional electric charge, and come in three colors: Red, Blue and Green, where color is a new quantum number. Quarks have different masses and they come in six "flavours" (see Table 3.1).

The strong interaction is mediated by gluons, which are massless spin-1 bosons. Gluons are also subject to the strong force because they, themselves, carry a color charge. The strong interaction increases at long distances, or small momentum transfers, which explains the non-observation of isolated quarks.

flavour		Electric charge	Baryon number	Mass
u	(up)	2/3	1/3	3 MeV
d	(down)	-1/3	1/3	7 MeV
s	(strange)	-1/3	1/3	120 Mev
c	(charm)	2/3	1/3	1.2 GeV
b	(bottom)	-1/3	1/3	4.25 GeV
t	(top)	2/3	1/3	175 GeV

TABLE 3.1: The various flavours of Quarks.[4]

3.2 Gluons

The color gauge group of QCD is $SU(3)$. It will be useful, however, to discuss a more general $SU(N)$ group, $N = 2, 3, \ldots$.

The generators of the group are thus written as G^a, with $a = 1, \ldots, N^2 - 1$. The generators satisfy the commutation relation

$$[G^a, G^b] = i f^{abc} G^c, \tag{3.1}$$

where the f^{abc} are the group structure constants, and a, b, c are the color indices. For $SU(3)$, the generators are the 3×3 Gell-Mann matrices [4]. The structure constants are antisymmetric, and they obey the identity

$$f_{acd} f_{bcd} = N \, \delta_{ab} \, . \tag{3.2}$$

The gauge (gluon) field strength tensor is given by

$$F_a^{\mu\nu} = \partial^\mu A_a^\nu - \partial^\nu A_a^\mu - g f_{abc} A_b^\mu A_c^\nu \, . \tag{3.3}$$

where g is the dimensionless QCD coupling[1].

Under an infinitesimal gauge transformation, $\alpha_a(x,t)$, the gluon field, up to $\mathcal{O}(\alpha^2)$, transforms as (different to photon field)[2]

$$A_a^\mu \to A_a^\mu + g f_{abc} A_b^\mu \alpha_c - \partial^\mu \alpha_a \, . \tag{3.4}$$

Opposed to QED, the field strength is not invariant under this gauge transformation

$$F_a^{\mu\nu} \to F_a^{\mu\nu} + g f_{abc} F_b^{\mu\nu} \alpha_c \, , \tag{3.5}$$

however, its square, $F_a^{\mu\nu} F^a_{\mu\nu}$, is invariant.

[1] The coupling is dimensionless only in $d = 3 + 1$ dimensions.

[2] The concepts of gauges and gauge transformations are assumed to be familiar to the reader.

3.3 The partition function of QCD

As mention earlier, quarks come in N colors, so the quark field, ψ, has a color index that runs from 1 to N, which will be suppressed in the following. The QCD Lagrangian is [4]

$$\mathscr{L} = \bar{\psi}(i\partial - M - gA_a G^a)\psi - \frac{1}{4}F_a^{\mu\nu}F^a_{\mu\nu} \; . \tag{3.6}$$

The first term in this Lagrangian is the kinetic energy of the quarks, M is the quark mass matrix, and the third term is the minimal coupling of the quarks to gluons. In order for the interaction to be gauge invariant, the quark field must transform as [4]

$$\psi \to \exp(igG^a\alpha_a)\psi \; . \tag{3.7}$$

In terms of this Lagrangian, the partition function can be written as functional integral (for details, see [4])

$$Z = \int [dA_a^\mu][d\bar{\psi}]d[\psi]\delta(F^b)\det\left(\frac{\partial F^c}{\partial \alpha_d}\right)\exp\left(\int_0^\beta \int d^3x(\mathscr{L} + \bar{\psi}\mu\gamma^0\psi)\right), \tag{3.8}$$

where μ is the quark chemical potential and F^b is a gauge fixing function. In the covariant gauge

$$F^a = \partial^\mu A^a_\mu - f^a(x,\tau) = 0 \; , \tag{3.9}$$

it can be shown that the partition function can be written as [4]

$$Z = \int [dA_a^\mu][d\bar{\psi}][d\psi][d\bar{C}_a][dC_a]\exp\left(\int d\tau \int d^3x \mathscr{L}_{eff}\right), \tag{3.10}$$

where $\bar{C}_a$ and C_a are ghost fields and

$$\mathscr{L}_{eff} = \mathscr{L} - \frac{1}{2\rho}(\partial^\mu A^a_\mu)^2 + gf^{abc}\bar{C}_a\partial_\mu A^\mu_b C_c + \bar{\psi}\mu\gamma^0\psi + \partial_\mu\bar{C}_a\partial^\mu C_a \; . \tag{3.11}$$

.

3.4 Perturbative evaluation of the partition function and Feynman rules of QCD

The QCD partition function (equation (3.10)) cannot be evaluated in a closed form [4]. The quantity $\ln(Z)$ can however be approximated by expanding it in a series in the coupling and then evaluating each of the terms in that series individually; if the coupling is sufficiently small, the first few terms may be sufficient to provide a good approximation for the full partition function.

The QCD coupling is energy (or temperature) dependent and, furthermore, in the high-energy (high-temperature) regime, it is small. Neglecting quark masses, it can be show that, in the high-temperature regime, the coupling, to leading order approximation, is given by [4]

$$\bar{\alpha} = \frac{\bar{g}^2}{4\pi} = \frac{12\pi}{(11N - 2N_f)\ln\left(\frac{M^2(T)}{\Lambda^2_{QCD}}\right)} , \tag{3.12}$$

where N_f is the number of "active" flavors and the renormalization scale $M(T)$ is the typical energy scale for the observable (e.g., energy density, pressure, entropy density) under consideration. The quantity Λ_{QCD} is the QCD scale. Note that if $M(T) \gg \Lambda_{QCD}$, then the coupling is small and a perturbative evaluation of the partition function is permissible. This phenomenon of decreasing coupling with increasing energies is known as *asymptotic freedom*. On the other hand if $M(T)$ is in the neighborhood of Λ_{QCD}, then the system is strongly coupled and the approximate form of the coupling (3.12) and the perturbative expansion become inadequate [4]. The numerical value of Λ_{QCD}, at higher orders in the coupling, depends on the the choice of the gauge and the renormalization scheme used for its calculation [4].

We turn now to a brief discussion of how this perturbative evaluation of the partition function is done.

To zero order in the coupling (i.e., in the absence of interaction), the QCD plasma is an ideal gas of quarks and gluons. If the quark chemical potential μ is zero, and the quarks are massless, the pressure, for example, is

$$p_0 = d_g \boldsymbol{\mathcal{P}} + d_q \frac{7\pi^2}{720} T^4 . \tag{3.13}$$

where the subscript 0 is to indicate it is the zero order pressure. The first term is the gluons contribution with $d_g = 2 \times N_g$ being the degeneracy (2 spin degrees of freedom times the number of SU(N) color degrees of freedom $N_g = N^2 - 1$) and $\boldsymbol{\mathcal{P}}$ is given in equation (2.135). In particular, for SU(3), one obtains $d_g = 16$. The second term is the

quark contribution, with $d_q = 2 \times 2 \times N \times N_f$ (spin, quark-antiqaurk, color and flavor degress of freedom, respectively)[1].

Higher order corrections to the ideal gas contribution are obtained by evaluating the higher order terms in the $\ln(Z)$ pertubative series. The evaluation of these terms can be done purely algebraically or with the aid of diagrams [4]. In the diagrammatic technique, each term is represented by one or more diagrams, known as Feynman diagrams, and then a set of rules, known as Feynman rules, is used to calculate the contribution of the given term from its diagram(s). Below we illustrate how these rules are used to calculate the leading order correction to the pressure.

The diagrams representing the leading order correction to the logarithm of the partition function are depicted in Figure 3.2, the prefactors account for the diagrams' multiplicities (the number of ways in which the same diagram can be assembled from its parts). Figure 3.1 shows the mathematical equivalent of each part of the diagrams.

Having drawn the relevant diagrams and determined the symmetry factor for each diagram, we use the following rules [4]

1. For each vertex, include the corresponding factor from Figure 3.1.
2. A factor of $\mathrm{T}\sum_n \int [d^3k/(2\pi)^3]\Delta$ for each line, where the sum is over the Matsubara frequencies and Δ is the propagator corresponding to that line.
3. Include a factor of $(2\pi)^3\beta\delta(k_{\mathrm{in}} - k_{\mathrm{out}})\delta_{\omega_{\mathrm{in}},\omega_{\mathrm{out}}}$, corresponding to momentum conservation. There will be a factor $\beta(2\pi)^3\delta(0) = \beta V$ left over.

Let us now apply these rules to the first diagram in Figure 3.2. From rule 1., we get

$$-\frac{1}{8}(g^2[f_{ade}f_{ebc}(g_{\alpha\beta}g_{\delta\gamma} - g_{\alpha\gamma}g_{\delta\beta}) + f_{abe}f_{edc}(g_{\alpha\delta}g_{\beta\gamma} - g_{\alpha\gamma}g_{\delta\beta}) + f_{ace}f_{edb}(g_{\alpha\delta}g_{\beta\gamma} - g_{\alpha\beta}g_{\delta\gamma})]) \,. \tag{3.14}$$

The factor 1/8 is the symmetry factor. Suppose we use the Feynman gauge ($\rho = 1$), then the gluon propagator (see Figure 3.1) becomes

$$D^{\mu\nu} = \frac{\delta_{ab}}{K^2} g^{\mu\nu} \,, \tag{3.15}$$

[1]The quark contribution can be derived from the scalar partition function by replacing the Bose function that appears in it with the Fermi function $f_f = 1/(e^{k/T} + 1)$, together with multiplying the quantity $\ln(Z)$ by the degeneracy factor d_q.

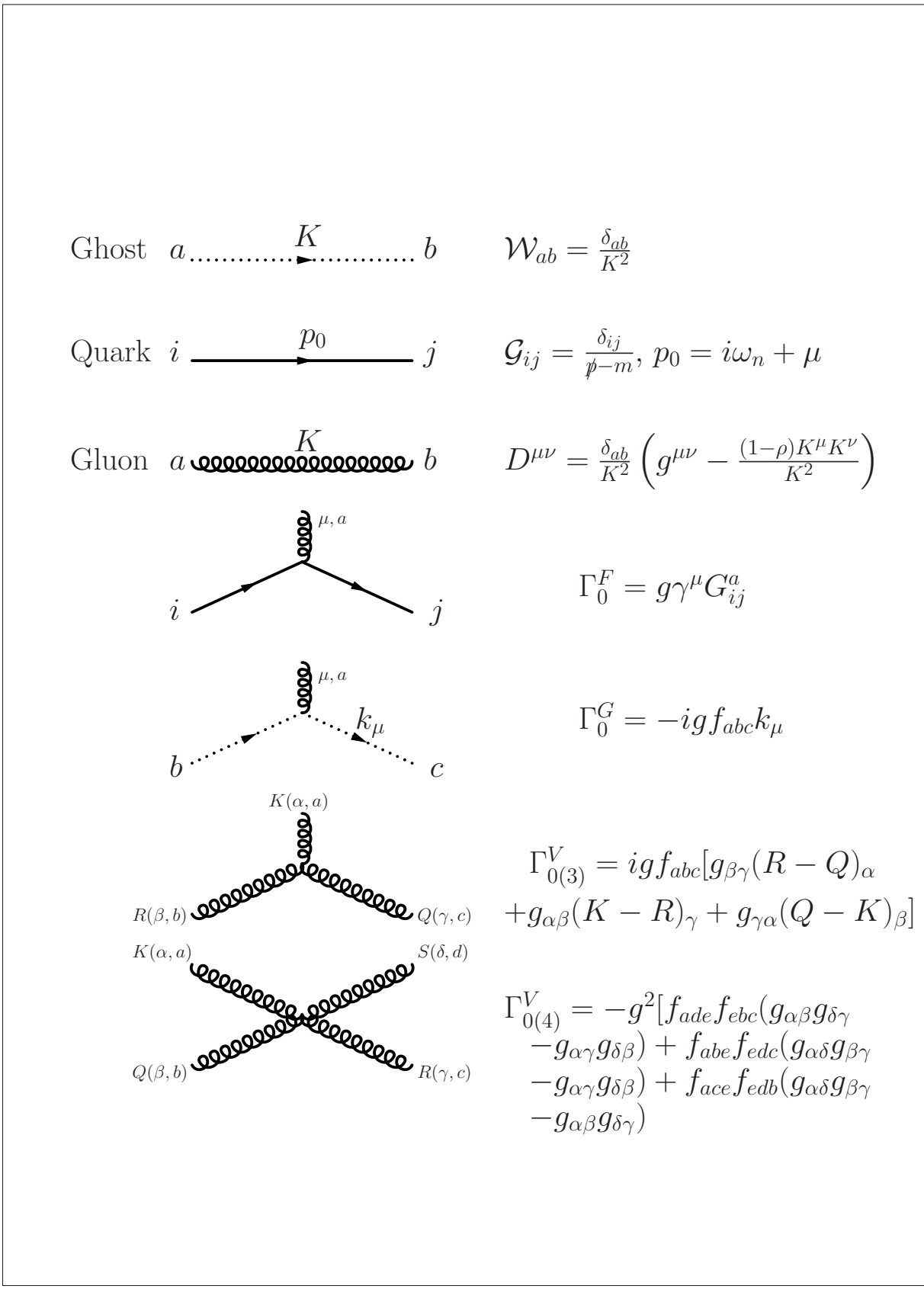

FIGURE 3.1: Feynman rules for free propagators and vertices in covariant gauges [4].

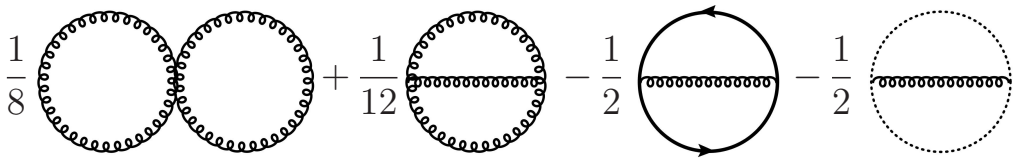

FIGURE 3.2: The leading order correction to the logarithm of the QCD partition function.

where $K = (\xi_n, k)$ is the Euclidean four-momentum and ξ_n's are the Matsubara frequencies (2.48). Thus from the second and third rules, and after some color algebra, we get

$$\ln(Z_1)^* = -3\, g^2 N N_g \beta V T^2 \left[\sum_n \int \frac{d^3k}{(2\pi)^3} \frac{1}{K^2} \right]^2 . \tag{3.16}$$

The subscript "1" is to indicate that this is the leading order correction to the logarithm of the partition function and the star is a reminder that it is the contribution of only one of the diagrams. Using relation (2.55), the sum over the Matsubara frequencies can be carried out, and it gives

$$\ln(Z_1)^* = -3\, g^2 N N_g \beta V \left(\frac{1}{2} \int \frac{d^3k}{(2\pi)^3} \frac{1}{k} + \int \frac{d^3k}{(2\pi)^3} \frac{1}{k} \frac{1}{e^{k/T} - 1} \right)^2 . \tag{3.17}$$

The first integral is the divergent vacuum contribution and is discarded. The second integral is the finite thermal contribution. Carrying out the thermal contribution integral gives

$$\ln(Z_1)^* = -3\, g^2 N N_g \beta V \frac{T^4}{144} . \tag{3.18}$$

The leading order correction to the pressure follows from this via relation (2.42), and is

$$p_1^* = -3\, g^2 \frac{N N_g}{144} T^4 . \tag{3.19}$$

Calculating the contributions from the remaining diagrams and adding them to (3.19) gives for the total leading order correction to the pressure

$$p_1 = -\frac{g^2\, N\, N_g}{144} T^4 . \tag{3.20}$$

The individual diagrams are gauge dependent, but the final result (3.20) is not [4].

So what about the renormalization scale $M(T)$ (see equation (3.12) and the comments below it)?: If one has the full expression of $\ln(Z)$, then the choice of $M(T)$ would be arbitrary, i.e., $\ln(Z)$ (and consequently the thermodynamics bulk properties) would be

completely independent of the form of $M(T)$, this is one of the main results of *Renormalization Group theory.* But since, as we've mentioned, the QCD partition function cannot be evaluated in a closed form and since only a finite number of terms in the perturbative expansion of $\ln(Z)$ can be calculated, one should choose $M(T)$ in such a way as to minimizes the contributions from higher order terms. The optimal form is [4]

$$M(T) = bT \ , \tag{3.21}$$

where the coefficient b is of order unity [4]. Physically, the renormalization scale (3.21) represents a thermal average of the energies

$$M(T) = bT \sim \langle k \rangle \ , \tag{3.22}$$

where $\langle k \rangle$ is a thermal average of the momenta.

3.5 Collective excitations in a QCD plasma

At low temperatures, where the coupling is large, the properties of a dilute QCD system can be described in terms of quark-gluon bound states (referred to as Hadrons if the system contains quarks, and glueballs if the systems involves gluons only). At high temperatures, we have seen, the coupling becomes small, and thus quarks and gluons that are otherwise strongly bound together roam quasi freely, giving rise to the quark-gluon plasma (or to the SU(N) plasma if the system involves gluons only). Since interaction does not cease completely, the properties of quarks and gluons in the plasma are different than in absolute vacuum (the bare properties are modified by the medium). For example, they acquire, due to interaction, an effective mass that is different from their masses in vacuum. Thus one speaks of quasi-particles in reference to these "modified" particles [5].

The quasi-particles are characterized by a dispersion relation $\omega(k)$ that gives their energies ω as functions of their momenta k. Also, these quasi-particles have finite life times, as opposed to stable particles in vacuum. Thus another characteristic of these quasi-particles is their decay (or damping) rate $\gamma(k)$ [5].

From *linear response theory*, the poles of the propagator give the dispersion laws and damping rates for waves traveling in the plasma; specifically, the real part of the poles gives the dispersion relation while the imaginary part gives the damping rate [5]. In the next two sections, we discuss briefly the gluon dispersion relation and damping rate in the plasma.

3.6 The gluon propagator and self-energy

The gluon self-energy $\Pi_{\mu\nu}$ is given by Dyson's equation [4], [5]

$$\Pi_{\mu\nu} = \tilde{D}^{-1}_{\mu\nu} - D^{-1}_{\mu\nu} = FP^L_{\mu\nu} + GP^T_{\mu\nu} \,, \tag{3.23}$$

where $\tilde{D}_{\mu\nu}$ is the full gluon propagator and $D_{\mu\nu}$ is the bare gluon propagator. F and G are the transverse and longitudinal parts of the self-energy[1], and $P^L_{\mu\nu}$ and $P^T_{\mu\nu}$ are the transverse and longitudinal projectors, given in Euclidean space by

$$P^T_{44} = P^T_{4i} = 0, \quad P^T_{ij} = \delta_{ij} - \hat{\mathbf{q}}_\mathbf{i}\hat{\mathbf{q}}_\mathbf{j} \,, \tag{3.24}$$

$$P^L_{\mu\nu} = \delta_{\mu\nu} - \frac{Q_\mu Q_\nu}{Q^2} - P^T_{\mu\nu} \,, \tag{3.25}$$

with $Q_\mu = (\xi_n, q)$ and $\hat{\mathbf{q}}_\mathbf{i}$ being a unit vector in the direction of the gluon momentum. The longitudinal and transverse projectors obey the relations

$$(P^T)^2 = P^T, \quad (P^L)^2 = P^L, \quad P^T P^L = P^L P^T = 0 \,. \tag{3.26}$$

In a covariant gauge, the full propagator reads

$$\tilde{D}_{\mu\nu} = \frac{1}{G+Q^2}P^T_{\mu\nu} + \frac{1}{F+Q^2}P^L_{\mu\nu} + \frac{\rho}{Q^2}\frac{Q_\mu Q_\nu}{Q^2} \,, \tag{3.27}$$

where the value of the gauge parameter ρ depends on the choice of gauge. Thus obtaining the dispersion laws and damping rates requires the evaluation of F and G or, equivalently, $\Pi_{\mu\nu}$. The evaluation of $\Pi_{\mu\nu}$ will be done to one loop. The relevant Feynman diagrams are shown in Figure 3.3.

The evaluation of diagrams b, c and d in Figure 3.3 can be simplified by noting that, in the high-temperature limit, the dominant contribution to the loop integral comes from the momenta $k \sim T$ and that one can assume $q \ll T$ and that, in particular for diagram d, vacuum quark masses become negligible; this approximation is known as the Hard Thermal Loop (HTL) approximation [5].

[1] Transverse and longitudinal with respect to the direction of the gluon's momentum.

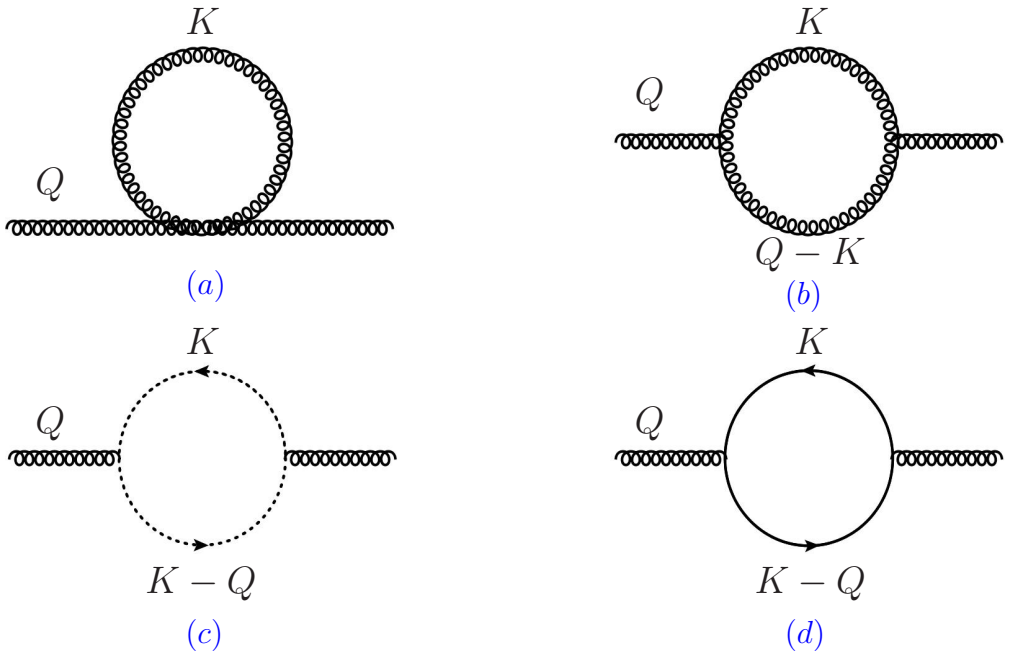

FIGURE 3.3: The leading order correction to the gluon self-energy.

Using the HTL approximation and adding the contributions from all four diagrams (see [4] or [5] for details), one obtains the approximate forms for G and F

$$G = m^2 \left(\frac{i\xi_n}{q}\right) \left[\left(1 - \left(\frac{i\xi_n}{q}\right)^2\right) Q_0\left(\frac{i\xi_n}{q}\right) + \frac{i\xi_n}{q}\right] , \tag{3.28}$$

$$F = -\frac{2m^2Q^2}{q^2} Q_1\left(\frac{i\xi_n}{q}\right) , \tag{3.29}$$

where Q_0 and Q_1 are Legendre functions of the second kind

$$Q_0(x) = \frac{1}{2}\ln\frac{x+1}{x-1} , \quad Q_1(x) = xQ_0(x) - 1 . \tag{3.30}$$

The quantity m is the gluon thermal mass and is gauge-invariant [5]. At this order in the coupling it is given by

$$m^2(T) = 2\,(N + \frac{1}{2}N_f)g^2\,T \sum_n \int \frac{d^3k}{(2\pi)^3} \frac{1}{\xi_n^2 + k^2} . \tag{3.31}$$

Note that the summand-integrand in (3.31) is the propagator of the free massless scalar field (see equation (2.53)). Carrying out the sum over the Matsubara frequencies and dropping the divergent vacuum contribution gives

$$m^2(T) = \frac{1}{6}(N + \frac{1}{2}N_f)g^2T^2 \ . \tag{3.32}$$

The reason it is called "thermal mass" will become apparent in the next section.

The formulae for F and G may be analytically continued from Euclidean to Minkowski space with the substitutions $i\xi_n \to \omega$ and $Q^2 \to -Q^2$, giving for G and F [5]

$$G = m^2\left(\frac{\omega}{q}\right)\left[\left(1-\left(\frac{\omega}{q}\right)^2\right)Q_0\left(\frac{\omega}{q}\right)+\frac{\omega}{q}\right] \ , \tag{3.33}$$

$$F = \frac{2m^2Q^2}{q^2}Q_1\left(\frac{\omega}{q}\right) \ , \tag{3.34}$$

and thus the retarded gluon propagator becomes

$$D^R_{F,\mu\nu} = \frac{i}{Q^2-G}P^T_{\mu\nu} + \frac{i}{Q^2-F}P^L_{\mu\nu} - i\frac{\rho}{Q^2}\frac{Q_\mu Q_\nu}{Q^2} \ . \tag{3.35}$$

3.7 The dispersion relations and damping rates

Let us first discuss the transverse gluons. Suppose that the transverse part of the retarded propagator has a simple pole located at [4]

$$\omega = \omega_T(q) - i\gamma_T(q), \text{ with } \gamma_T(q) \geq 0 \ , \tag{3.36}$$

where the subscript T is to indicate that these are the transverse dispersion relation and damping rate. The damping rate $\gamma_T(q)$ is assumed to be small, otherwise the transverse gluons would not propagate [4]. From (3.35), the poles of the transverse part of the propagator are given by

$$\omega(q)^2 = q^2 + G(\omega, q) \ . \tag{3.37}$$

Using (3.36), this equation can be decomposed into real and imaginary parts, giving

$$\omega_T = q^2 + \mathrm{Re}\, G(\omega_T, q) \ , \tag{3.38}$$

$$\gamma_T = -\frac{\mathrm{Im}\, G(\omega_T, q)}{2\omega_T} \ . \tag{3.39}$$

Thus it is seen from equation (3.39) that, since the imaginary part of this approximate form of G is zero, the damping rate of transverse gluons is zero in this approximation [5].

Equation (3.38) can be solved numerically (see Figure 3.4), or approximately in some limiting cases. For small values of q, the approximate form of $\omega_T(q)$ is

$$q \ll m: \qquad \omega_T^2(q) \approx \frac{2}{3}m^2 + \frac{6}{5}q^2 = \omega_p^2 + \frac{6}{5}q^2 \ , \tag{3.40}$$

where the plasma frequency, ω_p, has been defined

$$\omega_p = \sqrt{\frac{2}{3}}\, m \ . \tag{3.41}$$

For large values of q ($gT \ll q \ll T$), we get

$$q \gg m: \qquad \omega_T(q)^2 \approx q^2 + m^2 \ . \tag{3.42}$$

Note the similarity between this dispersion relation and (2.5).

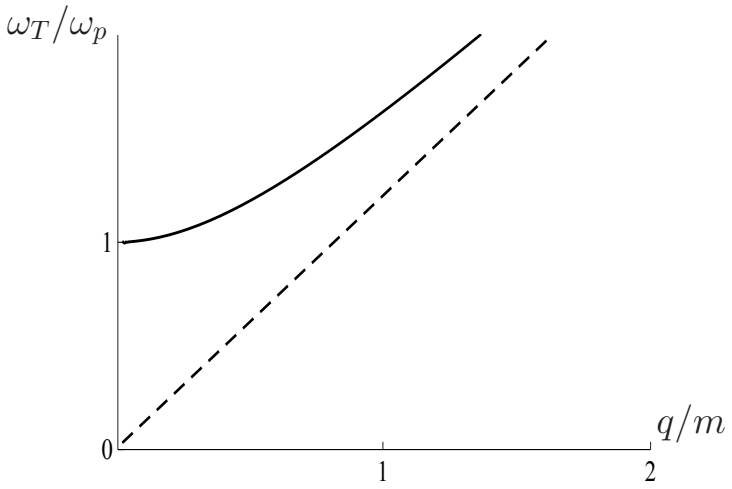

FIGURE 3.4: The transverse gluon dispersion relation (the dotted line shows the limit (3.42)).

Similar analysis can be done for longitudinal gluons (see [4] or [5]). However by studying numerically the full one-loop expression of the gluon self-energy, it was found in [16] (see also [17]) that, in the high-temperature regime, the dominant contributions to the gluon self-energy come from the large-momentum region of the transverse part of the gluon self-energy, while longitudinal gluons are there over damped, and that, furthermore, equation (3.42) holds even in the $q \sim T$ regime (which is our relevant regime, see equation (3.22)). Thus the transverse large-momentum dispersion relation (3.42) provides a good

framework for the calculations of the thermodynamic bulk properties of the plasma in the high-temperature regime.

In conclusion, gluons in the plasma propagate approximately as massive quasi-particles, with their mass being the thermal mass m, and relation (3.42) holds in the regime $q \sim T$.

3.8 Lattice QCD

It was mentioned in section 3.4 that the partition function of QCD cannot be evaluated in a closed form, and that one way of going around calculating the various thermodynamic properties is to evaluate it perturbatively. Another way that will be discussed in this section is to evaluate the thermodynamic properties numerically. The numerical calculations are done on discretized space-time lattices, the results are then extrapolated to the continuum limit [7].

In lattice QCD computations, it was found that a direct simulation of the partition function itself is not possible [7]. Thus what is usually evaluated on the lattice is the interaction measure $ia(T)$, which is related to the energy density and pressure via[1]

$$ia = e - 3p = T^5 \frac{\partial}{\partial T} \left(p/T^4 \right) \ . \tag{3.43}$$

The results for the interaction measure of the SU(3) (pure gauge) plasma, obtained in [7] on isotropic lattices ($a_\sigma = a_\tau = a$) with sizes $N_\sigma^3 \times N_\tau = 16^3 \times 4, 32^3 \times 6$ and $32^3 \times 8$, are shown in Figure 3.5 (all Figures shown in this section were obtained from [7]). From the interaction measure results, the pressure results are obtained via

$$\frac{p}{T^4} \ = \ \int_0^T d\,T' \frac{ia}{T'^5} \ , \tag{3.44}$$

and from the pressure results, the energy density results are obtain via

$$\frac{e}{T^4} \ = \ -\frac{1}{T^2} \frac{\partial}{\partial T} \left(\frac{p}{T} \right) \ . \tag{3.45}$$

Since lattice calculations are not performed down to $T = 0$ [2], the lower limit in the integral (3.44) is chosen to be some temperature below the critical temperature T_c where

[1] The relation $e - 3p = T^5 \partial / \partial T (p/T^4)$ can be derived from (2.41) - (2.42) if one assumes a large, homogeneous system, i.e., $\partial / \partial V \to 1/V$ [7].

[2] In fact they cannot be, since it would mean $a \to \infty$.

the interaction measure is sufficiently small [7]. The results for the energy density and pressure are shown in Figures 3.6 and 3.7 .

The results for the pressure are then extrapolated to the continuum limit. It is instructive for us to discuss in a bit of detail how this extrapolation is performed: Let us first rewrite (2.204) in a more relevant form

$$\left(\frac{e}{T^4}\right)_a = 3\left(\frac{p}{T^4}\right)_a = \frac{3\,d_g \not{p}}{T^4}\left[1 + \frac{30}{63}\left(\frac{\pi}{N_\tau}\right)^2 + \mathcal{O}(N_\tau^{-4})\right], \tag{3.46}$$

where the subscript a is to indicate lattice quantities and $\not{p}$ is the continuum pressure of the free scalar gas and d_g is gluon degeneracy factor (see equation (3.13)). By assuming interaction effects to be small, and thus considering (3.46), the continuum extrapolation is carried out by using the ansatz [7]

$$\left(\frac{p}{T^4}\right)_a = \frac{\tilde{p}}{T^4} + \frac{c_2(T)}{N_\tau^2}, \tag{3.47}$$

where $\tilde{p}$ is the continuum-extrapolated pressure and $c_2(T)$ is a temperature-dependent fit parameter. Note that the parameter $c_2(T)$ is not necessarily equal to the coefficient of the $\mathcal{O}(1/N_\tau^2)$ term in the ideal gas expansion (3.46); this is to reflect the fact that the QCD system in question is interacting. By plugging into (3.47) the temporal extents N_t of two lattices along with the uncorrected (un-extrapolated) pressures on these two lattices at a given temperature T, the coefficient $c_2(T)$ and the continuum-extrapolated pressure at that temperature can be obtained. Since higher-order corrections $\mathcal{O}(1/N_\tau^4)$ are large for the lattice $16^3 \times 4$ (see our discussion of Figure 2.29, in particular remark 3), the extrapolation in [7] was restricted to the $32^3 \times 6$ and $32^3 \times 8$ lattices.

After the pressure is extrapolated, the continuum-extrapolated energy density is obtained via (3.45), while the continuum-extrapolated entropy density is obtained via[1] [7]

$$\frac{\tilde{s}}{T^3} = \frac{\tilde{e} + \tilde{p}}{T^4}, \tag{3.48}$$

where $\tilde{s}$ and $\tilde{e}$ are the continuum-extrapolated entropy density and energy density, respectively. Figure 3.8 shows the continuum-extrapolated results.

The abrupt change in the thermodynamic properties at T_c the results show indicates a phase transition from gluon bound states ("glueballs") to the SU(3) plasma. It is also seen that, with increasing temperatures, the properties of the plasma asymptotically approach the free-gas limit, thus confirming the phenomenon of asymptotic freedom

[1] This relation can be derived from (2.41) - (2.43).

(see equation (3.12) and the comments below it). For SU(3), the critical temperature is ≈ 260 MeV. For temperatures relevant to Heavy-ion phenomenology (a few times T_c), interaction effects lead to $\mathcal{O}(10\%)$ deviations of thermodynamic bulk properties from their ideal gas values (except very close to T_c), see Figures 3.6 - 3.8. These interaction effects are thus of a similar order as the finite-size effects of the non-interacting Bose gas discussed in the previous chapter – which motivates us to investigate their interplay. To this end we utilize a quasi-particle model of the SU(3) plasma.

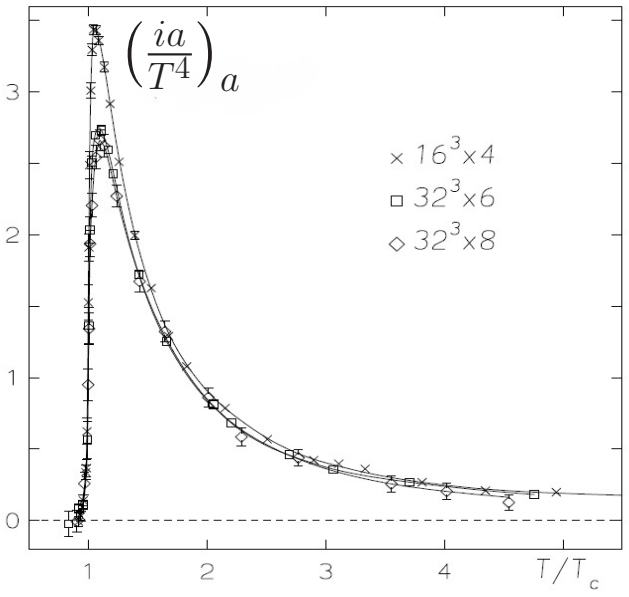

FIGURE 3.5: The interaction measure of the pure gauge plasma. Error bars are also depicted [7].

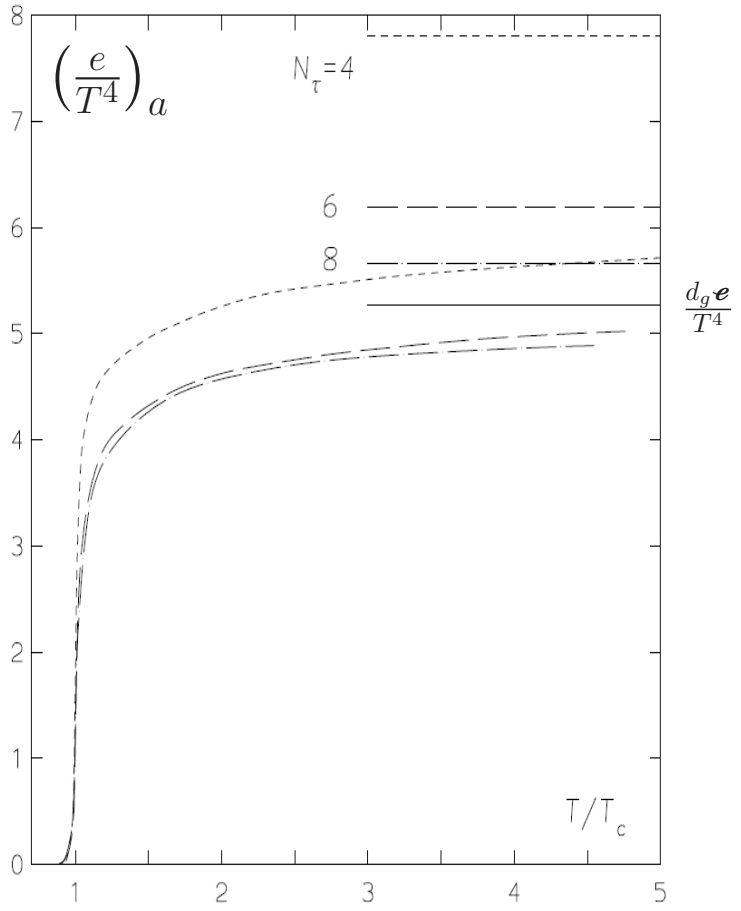

FIGURE 3.6: The pure gauge energy density (the horizontal lines show the ideal gas limits, the solid line in particular is the continuum ideal gas limit) [7].

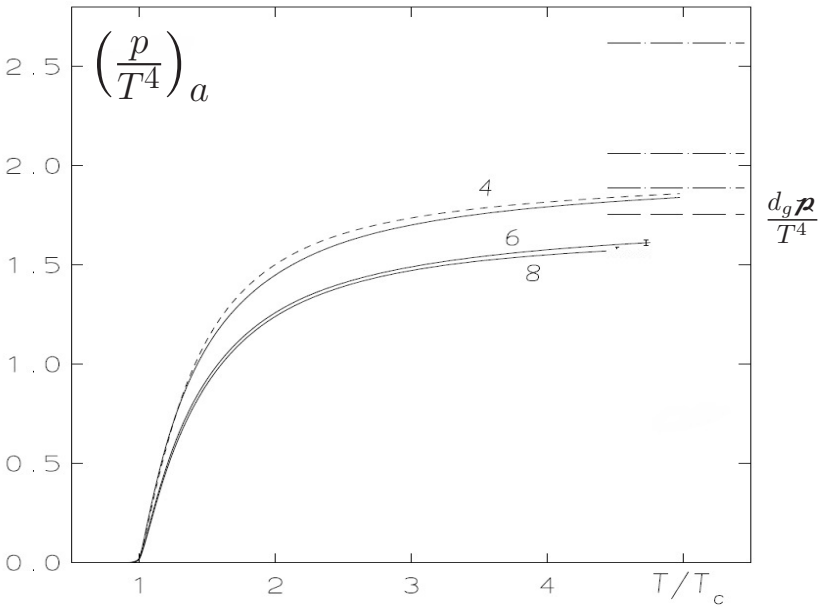

FIGURE 3.7: The pure gauge pressure (the two curves for the $N_\tau = 4$ correspond to two different techniques used in its calculation [7]).

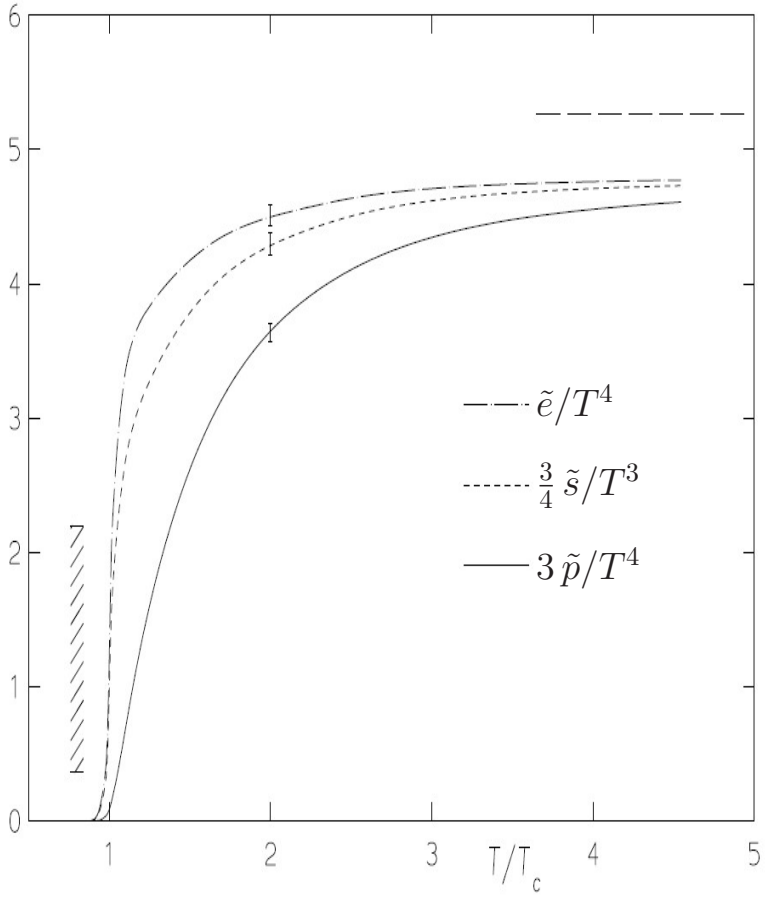

FIGURE 3.8: The continuum-extrapolated results [7].

3.9 The quasi-particle model of the SU(3) plasma

We have seen in section 3.7 that, at high temperatures, gluons in the plasma behave as massive quasi-particles, with the mass being the thermal mass of the gluons. Quasi-particle (QP) models attempt to reproduce, among other things, the thermodynamic properties of the plasma by modeling it as a gas of quasi-particles. The particular model we discuss here is the one developed by Peshier *et al* [16].

Since the approximate gluon dispersion relation (3.42) is identical to the free massive scalar dispersion relation (2.5), the plasma can be approximated as a gas of scalar quasi-particles. However, since the quasi-particle thermal mass (3.32) is not simply a constant but is temperature dependent, the quasi-particle gas won't be identical to a free massive scalar gas. Also, gluons have color and spin degrees of freedom and these must be taken into account as we shall see below. In this model, the entropy density of the plasma assumes the ideal gas form [16]

$$s^{QP} = d_g \; s^{id}(T, m(T)) \; , \tag{3.49}$$

where d_g is the gluon degeneracy (see (3.13) and the comments below it), and s^{id} given in (2.154)[1] is calculated with the temperature-dependent dispersion relation

$$\omega_k^2 = k^2 + m^2(T) \; , \tag{3.50}$$

which is the approximate gluon dispersion relation (3.42). The thermal mass (3.32), with $N = 3$ and $N_f = 0$, becomes

$$m^2(T) = \frac{1}{2} g^2(T) T^2 \; . \tag{3.51}$$

In order to account for the strong interaction effects near T_c, the effective coupling (3.12) is generalized to be [16]

$$g^2(T) \longrightarrow G^2(T) = \frac{48\pi^2}{11 \times 3 \ln\left[(\lambda \frac{T}{T_c} + \frac{T_s}{T_c})^2\right]} \; . \tag{3.52}$$

The parameter λ specifies the relation between the critical temperature T_c and Λ_{QCD}: $\Lambda_{QCD} = T_c/\lambda$. The parameter λ should be of order unity since T_c is very close to Λ_{QCD}.

[1] The superscript "*id*" is to indicate an ideal gas contribution.

T_s is a phenomenological regularization parameter[1] whose significance will be discussed later in this section. The pressure and energy density assume the forms [16]

$$p^{QP} = d_g\, p^{id}(T, m(T)) - B(T)\,, \tag{3.53}$$
$$e^{QP} = d_g\, e^{id}(T, m(T)) + B(T)\,, \tag{3.54}$$

where p^{id} and e^{id} are given in equations (2.198) and (2.197), respectively. The function B is a consequence of the temperature dependence of the mass (it represents a "residual interaction" between the quasi-particles). It is needed to ensure thermodynamic consistency while allowing for a temperature-dependent mass, i.e. to ensure

$$e + p = sT\,, \tag{3.55}$$
$$s = \frac{\partial p}{\partial T}\,. \tag{3.56}$$

To see this, let's apply relation (3.56) to equations (3.49) and (3.53). It yields

$$d_g\, s^{id}(T, m(T)) = d_g\, \frac{\partial p^{id}}{\partial T}\Big|_m + d_g\, \frac{\partial p^{id}}{\partial m^2}\Big|_T \frac{\partial m^2}{\partial T} - \frac{\partial B}{\partial T}\,. \tag{3.57}$$

The second term on the right hand size obviously arises because of the temperature-dependence of the mass. Thus preserving relation (3.56), i.e., preserving $s^{id} = \partial p^{id}/\partial T$, is achieved if

$$\frac{\partial B}{\partial T} = d_g\, \frac{\partial p^{id}}{\partial m^2}\Big|_T \frac{\partial m^2}{\partial T}\,. \tag{3.58}$$

The B function is to be determined by solving the above equation

$$B = B_0 + d_g \int_{T_0}^{T} dT'\, \frac{\partial p^{id}}{\partial m^2}\Big|_T \frac{\partial m^2}{\partial T'}\,, \tag{3.59}$$

where $B_0 = B(T_0)$ is the value of the B function at some reference temperature T_0.

In [16], the parameters d_g, λ and T_s were fitted to match the continuum-extrapolated entropy density results (Figure 3.8), and then B_0 was fixed by matching the QP pressure (3.53) to the continuum-extrapolated pressure (Figure 3.8). In this thesis, however, to get some understanding on the interplay of finite-size and interaction effects, we

[1] This parameter shifts the pole located at $T = \Lambda_{QCD}$.

choose a different route: We first extract the thermal mass results from the continuum-extrapolated results of the entropy density by mapping equation (3.49) to the continuum-extrapolated entropy density results (Figure 3.8). To do the mapping, one has to presume a particular value for d_g. Thereafter we fit the parameters λ and T_s to match the extracted results of the thermal mass.

Let us first set $d_g = 16$ and $T_s = 0$ (this is the "canonical" QCD expectation) and see to which degree will this parameterization agree with the continuum-extrapolated results. Using this parameterization and fitting the thermal mass on the entire temperature range $T \geq T_c$, we obtain the fit shown in Figure 3.9. The poor fit may be due to the strong interaction effects near the critical temperature T_c. Next, we constrain the fitting to the temperature range $T > 2\,T_c$ so as to avoid the above-mentioned strong interaction effects. The fit obtained over this high-temperature regime is shown in Figure 3.9. We see that we are able to reproduce the behavior of the thermal mass in this high-temperature regime, but the fitted $\lambda \approx 14$ is significantly larger than the unity and much different from the λ's in the other fits.

Let us next fit this high-temperature regime without constraining the gluon degeneracy to 16. The fit obtained is shown in Figure 3.10. We see that, without constraining the degeneracy to 16, we are able to fit the thermal mass down to $\approx 2\ T_c$, with the best fit values of $\lambda = 3.56$ and $d_g = 17.2$. The continuum-extrapolated results therefore cannot be understood with $d_g = 16$. Quantitatively, the deviation of $d_g = 17.2$ from 16 is small, but qualitatively it is important because it points to an imperfection in the continuum-extrapolation procedure used to obtain the continuum-extrapolated results.

To reproduce the "non-perturbative" behavior of the mass (the behavior near the critical temperature), the parameter T_s, along with λ and d_g, is utilized (see equation (3.52)) [16]. Using this, we obtain the fit shown in Figure 3.10 with the fitted values of $\lambda = 4.17$, $T_s = -2.96$ and $d_g = 17.2$. Thus by introducing the parameter T_s, one can fit the thermal mass nicely down to T_c. The negative value of T_s means that the coupling should be larger than one would expect from perturbative QCD. This perhaps indicates that non-perturbative contributions to the coupling become large as one approaches T_c.

In conclusion, an interpretation of gluon lattice data within a model of a gas of quasi-particles with effective thermal masses reproduces the lattice results of thermodynamic properties of the pure-gauge plasma [16]. The fitted value of $d_g = 17.2$ ($\neq 16$), which is the only way we were able to match the continuum extrapolated results, is perhaps due to imperfect correction (extrapolation) of finite-lattices results. In the next section, we apply this quasi-particle model to the un-corrected lattice results. This will enable us to shed some light on the interplay between finite-size and interaction effects.

Parameter / Figure	d_g	λ	T_s/T_c
3.9 (fit over all T's)	16	2.85	-
3.9 (fit over $T > 2T_c$)	16	13.92	-
3.10 (fit over all T's)	17.2	3.56	-
3.10 (fit over all T's)	17.2	4.19	-2.92 [16]

TABLE 3.2: The fitted parameters corresponding to Figures 3.9 - 3.10.

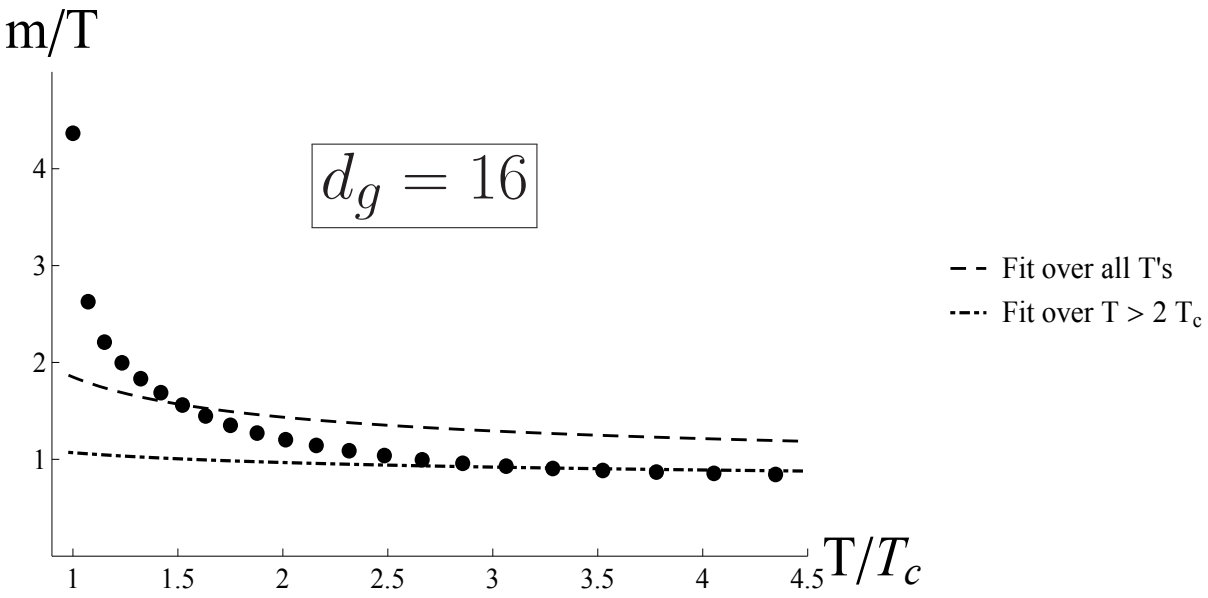

FIGURE 3.9: Symbols show m/T results obtained from mapping the lattice entropy density (Figure 3.8 [7]) to equation (3.49). The curves show the fits of m/T results corresponding to the use of $d_g = 16$ and the fit parameter λ (see Table 3.2).

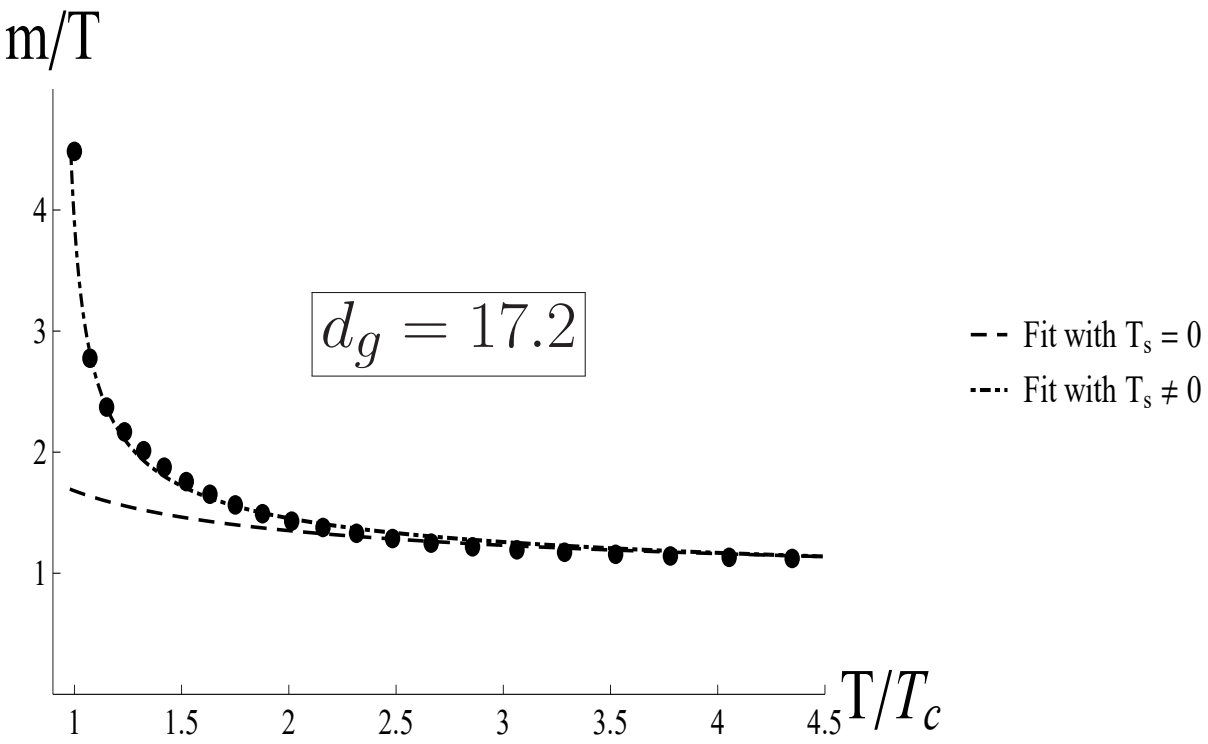

FIGURE 3.10: Symbols show m/T results obtained from mapping the lattice entropy density (Figure 3.8 [7]) to equation (3.49). The curves show the fits of m/T results corresponding to the use of the fit parameters d_g, λ and T_s (see Table 3.2).

3.10 The quasi-particle model on the lattice

We have seen that, in lattice calculations, space-time is approximated by a finite, discretized Euclidian lattice, and the results obtained on these lattices are then extrapolated to the continuum limit. But we saw in chapter 2 that finite-size effects on the thermodynamic bulk properties are significant in general. In addition, the effects of discretizing space-time are also significant, as was discussed in section 2.9. Furthermore, in the interacting SU(3) plasma, in addition to finite-size and discretization effects, there are also interaction effects. Since lattice QCD calculations aim for obtaining the continuum thermodynamic bulk properties from results on finite, discretized lattices, it is imperative to disentangle and quantify finite-size, discretization and interaction effects that are inherent to these calculations.

We saw in the previous section that the quasi-particle model we discussed is a simple, yet accurate, mean of analyzing the continuum-extrapolated lattice results. In this section, we attempt to analyze the raw (un-extrapolated) lattice QCD results with a lattice version of the quasi-particle model, in order to get some insight on the interplay between finite-size effects, discretization artifacts and genuine interaction effects.

In the previous section we saw that quasi-particle thermodynamic bulk properties (entropy density, pressure and energy density) in infinite volume (3.49), (3.53) and (3.54) are obtained from the corresponding scalar bulk properties in infinite volume. It seems natural, therefore, to assume that the quasi-particle bulk properties on the lattice should be obtained from the corresponding scalar properties on the lattice discussed in section 2.9. Thus we replace formulae (3.49), (3.53) and (3.54) by their lattice counterparts derived in section 2.9, which gives

$$s_l^{QP} = s_l^{id} , \tag{3.60}$$

$$p_l^{QP} = p_l^{id} - B(T,V) , \tag{3.61}$$

$$e_l^{QP} = e_l^{id} + B(T,V) , \tag{3.62}$$

where s_l^{id}, p_l^{id} and e_l^{id} are given in equations (2.199), (2.198) and (2.197), respectively. A further discussion of the quasi-particle energy density and pressure on the lattice is however beyond the scope of this thesis.

Let's turn our attention now to the thermal mass. Similar to the thermodynamic properties above, we assume that the quasi-particle thermal mass on the lattice can be obtained from the continuum thermal mass (3.31) by replacing the scalar propagator appearing in it by its lattice version (2.180) and discretizing the momenta accordingly.

Thus (3.31), with $N = 3$ and $N_f = 0$, and with the generalized coupling (3.52), and on a lattice with $N_\sigma^3 \times N_\tau$ and with a lattice spacing a [1], becomes

$$m_E^2(N_\sigma, N_\tau, a) = \frac{1}{2}\, G^2(T) \left[12\, \frac{1}{a^4 N_\tau N_\sigma^3} \sum_q \Delta_{0L} \right] , \tag{3.63}$$

where Δ_{0L} is the lattice propagator (2.180) and the sum is over the discretized energies and momenta (2.175) - (2.176). The subscript "E", in analogy with notation used for the un-renormalized lattice Free energy density (2.183), is to indicate that this still needs to be renormalized by subtracting from it the vacuum contribution, as discussed in section 2.9. Thus we obtain for the renormalized thermal mass

$$m(N_\sigma, N_\tau, a)^2 = \frac{1}{2}\, G^2(T)\, \theta^2 \, . \tag{3.64}$$

where

$$\theta^2 = \frac{12}{a^4} \left(\frac{1}{N_\tau N_\sigma^3} \sum_q \Delta_{0L} - \frac{1}{N_\sigma^4} \sum_q \Delta_{0L} \right) . \tag{3.65}$$

Since gluons are massless, the expression above is divergent due to the zero momentum mode ($q = 0$). This divergence does not arise in the continuum limit (equation (3.31)) because the phase space factor $d^3k/(2\pi)^3$ suppresses the integrand at small k's. To regulate this divergence, it is necessary that we revisit the process by which we obtained (3.65) and revise it: In Section 3.6 we obtained the gluon self energy by solving Dyson's equation (3.23) approximately. That lead us to the thermal mass (3.31) that contains the propagator of the free massless scalar field, whose lattice version (2.180) that appears in (3.65) is divergent. But it can be shown that, when Dyson's equation is solved self-consistently, a mass term in the free propagator will be generated [18] which will regulate this divergence. This self-consistency mass m_*, by dimensional analysis, has to be proportional to the thermal mass itself. In the analysis that will follow, we will not attempt to solve Dyson's equation self-consistently, but rather use the ansatz

$$m_*^2 = c^2\, m^2 \, , \tag{3.66}$$

as a specification of the relation between the self-consistency mass and the thermal mass (here c is a constant).

[1] Recall that lattice simulations are done on isotropic lattices ($a_\sigma = a_\tau = a$).

And hence the propagator (2.180) becomes

$$\Delta_{0l}^{-1} \longrightarrow \tilde{\Delta}_{0l}^{-1} = m_*^2 + \frac{4}{a^2}\Big\{ \sum_{\mu=1}^{3} \sin^2(\frac{1}{2}q_\mu a) + \sin^2(\frac{1}{2}q_0 a)\Big\} \ . \tag{3.67}$$

Let us now study the behavior of the thermal mass on the lattices $16^3 \times 4$, $32^3 \times 6$ and $32^3 \times 8$. Similar to what was done in the previous section, we obtain the temperature dependence of the mass on a given lattice by mapping (3.60) to the un-conrrected entropy density results on that lattice. In [7], only the continuum entropy density is given. We can however obtain the entropy density results on the various lattices by noting that the entropy density and energy density are related by

$$\frac{s}{T^3} = \frac{e-f}{T^4} = \frac{1}{T^4}\left(e - T\int_0^T dT'\ T'^2 \frac{e}{T'^4} \right) \ , \tag{3.68}$$

which we can use to obtain the entropy density results from the energy density results (Figure 3.6 [7]).

The entropy density results we obtained are shown in Figure 3.11. Figure 3.12 shows the temperature and thermal mass dependence of the quasi-particle entropy density. To fit the thermal mass results, we find it more convenient to first define

$$h = \frac{\theta}{T} \ , \tag{3.69}$$

where θ was defined in (3.65). Thus, from (3.64), we can write

$$\frac{1}{\sqrt{2}}\, G(T) = \frac{m/T}{h} \ . \tag{3.70}$$

This allows us to obtain $\frac{1}{\sqrt{2}}G$ results from m/T results. The fits we obtained are shown in Figure 3.13 and the fitted parameters are given in Table 3.3. The corresponding entropy density fits are shown in Figure 3.11. We see from the Figures that we are able to reproduce the lattice results rather accurately down to the vicinity of T_c. From Table 3.3, the parameter c, which increases as higher order corrections to the mass increase, is larger on larger lattices. That this parameter basically doubles when going from one lattice to the next suggests that the contribution of these higher order corrections are rather sensitive to finite-size effects. The parameter λ is smaller on larger lattices, meaning that the coupling is larger on larger lattices, which is is seen in Figure 3.13. One can thus infer that there is an inverse relation between interaction effects and finite-size effects. Note most crucially that the fitted d_g, for all lattices, is 16. Also, that we did

not need to use the parameter T_s to obtain these fits suggests that, in the original quasi-particle model, the parameter T_s models the effect of a self-consistent quasi-particle mass.

In conclusion, the formulation of the quasi-particle model on finite lattices can reproduce the uncorrected lattice results. The bare propagator approximation is divergent on a finite lattice and this creates the necessity of going beyond it; in particular, a self-consistent scheme would yield a regulator for this divergence which, in addition, allows us to understand the lattice QCD results in terms of the usual running coupling (without the parameter T_s). Most importantly, we were able to obtain good fits of the un-corrected lattice results by using $d_g = 16$, in contrast to what we saw in the previous section where the only way we were able to match the continuum-extrapolated results was by using $d_g = 17.2$.

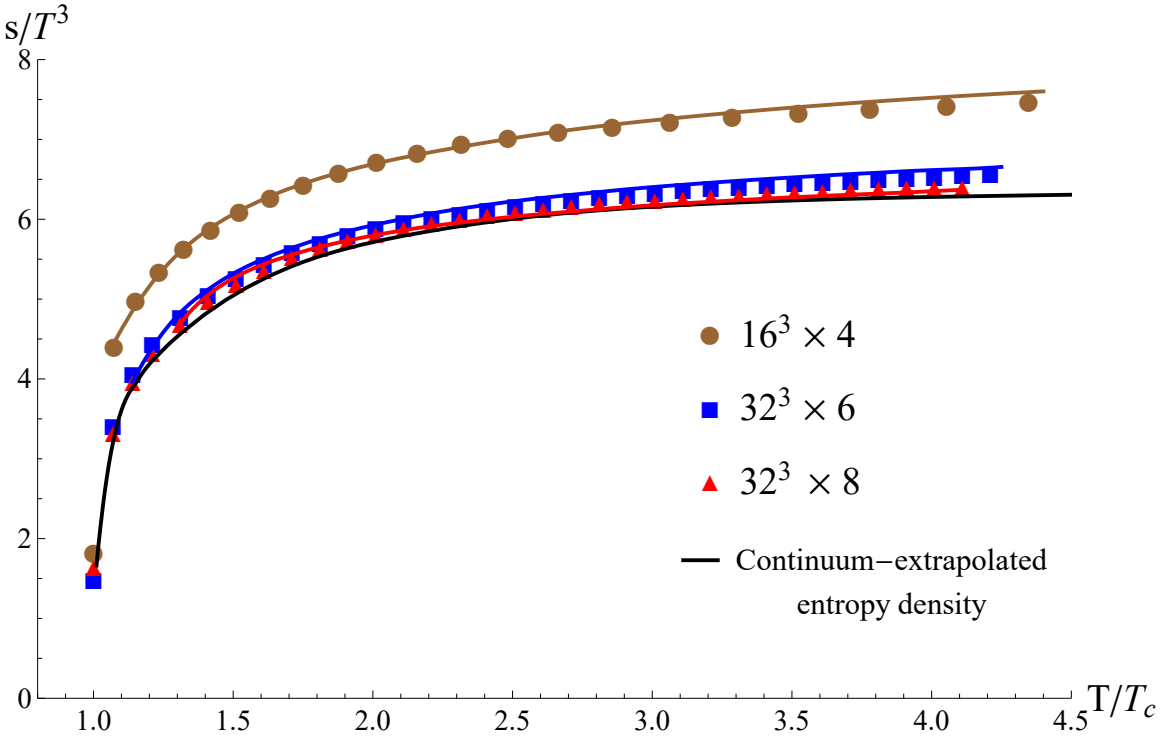

FIGURE 3.11: Symbols show the entropy density results on the various lattices, as indicated in the plot legend. These results were obtained from Figure 3.6 [7] via relation (3.68). The brown, blue and red curves are the entropy density fits corresponding to the fits shown in Figure 3.13.

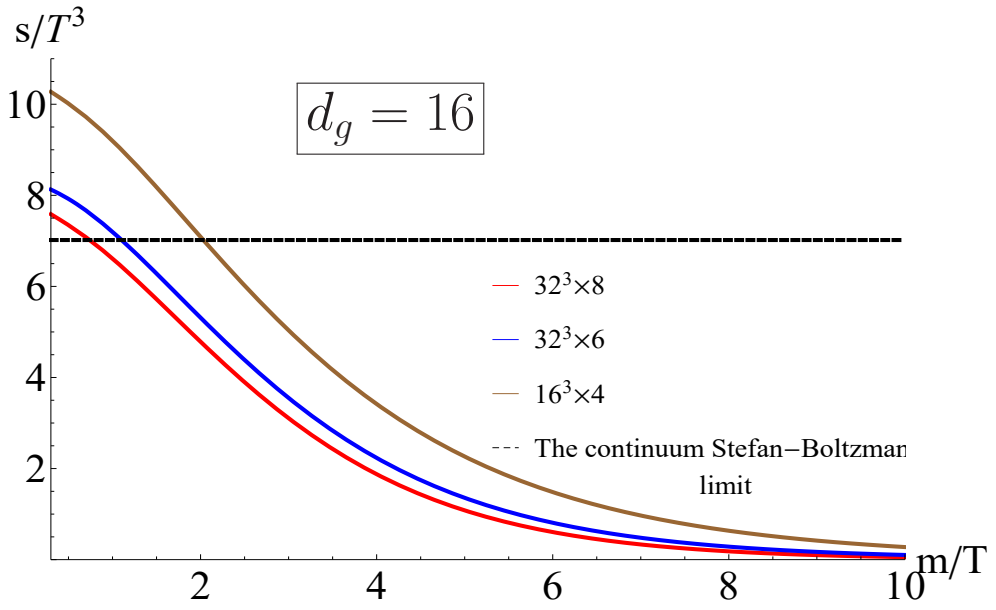

FIGURE 3.12: The quasi-particle entropy density on the various lattices as a function of m/T.

Lattice \ Parameter	d_g	c	λ	T_s/T_c
$16^3 \times 4$	16	0.21	1.16	-
$32^3 \times 6$	16	0.40	1.07	-
$32^3 \times 8$	16	0.83	0.93	-

TABLE 3.3: The fitted parameters corresponding to Figures 3.13 and 3.11.

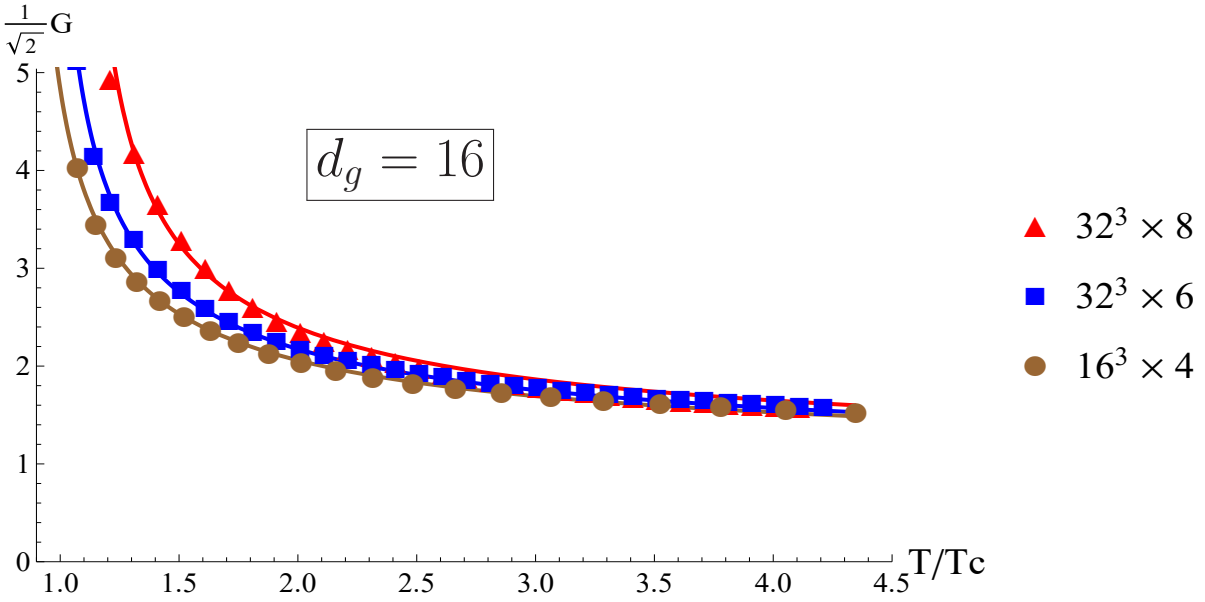

FIGURE 3.13: The thermal mass fits on the $16^3 \times 4, 32^3 \times 6$ and $32^3 \times 8$ lattices, where the fit parameters c and λ were used (see Table 3.3).

Conclusion

From our observations in chapter 2 we conclude that finite-size effects on the thermodynamic properties of the free scalar field, at $LT = \mathcal{O}(1)$, which is the regime relevant in Heavy-ion collisions, can be of order 10%. These effects, therefore, are of the same order as interaction effects in the same regime, as seen in lattice results for the SU(3) plasma we discussed in chapter 3.

We conclude as well that the quasi-particle model we discussed, initially devised to study the continuum-extrapolated SU(3) lattice results, can be adapted to study the un-extrapolated lattice results. In adapting this model to finite lattices, we encountered a divergence of the massless propagator and we proposed a self-consistency ansatz to regulate this divergence. This self-consistency ansatz has the added benefit of allowing us to model the un-extrapolated lattice results by using the usual QCD running coupling.

Furthermore, the adapted quasi-particle model allows us to model the un-extrapolated lattice results by using the canonical degeneracy $d_g = 16$, this perhaps indicates that there exists a slight imperfection in the continuum extrapolation procedure used in [7], because, as we saw, the only way we were able to match the continuum-extrapolated results was by using $d_g = 17.2$.

Suggestions for the future

There are many other areas into which our work in this thesis can be extended, for example, our discussion of finite size effects on the thermodynamic bulk properties of the free scalar field can be extended to, e.g., an interacting scalar field, fermionic systems and further geometries and boundary conditions. Also the SU(3) quasi-particle model on finite lattices can, in addition to the study of the entropy density and thermal mass which we've partly done, be used to study the behavior of the energy density and pressure of the SU(3) plasma. Furthermore, it would be immensely useful to apply this quasi-particle model to lattice results of quark-gluon systems.

Appendix A

Spherically symmetric integrals

Consider the integral

$$\mathrm{I} = \int \frac{d^d k_\perp}{(2\pi)^d} (k_\perp^2 + A^2)^m \,, \tag{A.1}$$

where $d, m, A \in \mathbb{C}$. Because of the angular independence of this integral, it can be decomposed into an angular part and a radial part:

$$\mathrm{I} = \int \frac{d\Omega_d}{(2\pi)^d} \int_0^\infty dk_\perp k_\perp^{d-1} (k_\perp^2 + A^2)^m \,, \tag{A.2}$$

where

$$\int d\Omega_d = \frac{2\pi^{\frac{d}{2}}}{\Gamma(\frac{d}{2})} \tag{A.3}$$

is the surface of unit sphere in d dimensional space. Now, for the radial part

$$\int_0^\infty dk_\perp k_\perp^{d-1} (k_\perp^2 + A^2)^m = \frac{1}{2} \int_0^\infty d(k_\perp^2)(k_\perp^2)^{\frac{d}{2}-1} (k_\perp^2 + A^2)^m \,. \tag{A.4}$$

This integral is convergent if $d < -2m$, $d\,\mathrm{Arg}[1/A^2] \leq 2\pi, \mathrm{Re}[A^2] > 0$ and $d > 0$. We make the substitution $u = A^2 \Big/ \left(k_\perp^2 + A^2\right)$ to obtain

$$\frac{1}{2} \int_0^\infty d(k_\perp^2)(k_\perp^2)^{\frac{d}{2}-1} (k_\perp^2 + A^2)^m = \frac{1}{2} A^{d+2m} \int_0^1 du\, u^{(-m-\frac{d}{2})-1} (1-u)^{\frac{d}{2}-1} \,. \tag{A.5}$$

Now

$$\int_0^1 du\, u^{(-m-\frac{d}{2})-1}(1-u)^{\frac{d}{2}-1} = \mathrm{B}\left(-m-\frac{d}{2},\frac{d}{2}\right) = \frac{\Gamma(-m-\frac{d}{2})\Gamma(\frac{d}{2})}{\Gamma(-m)}\ , \tag{A.6}$$

where B is Euler's Beta function. Thus, from (A.3) and (A.6), (A.1) becomes

$$\mathrm{I} = 2^{-d}\pi^{-d/2}A^{d+2m}\frac{\Gamma(-m-d/2)}{\Gamma(-m)}\ . \tag{A.7}$$

Appendix B

Mode sums

Consider first the one dimensional massive mode sum

$$S = \pi^{d/2}\Gamma(-\frac{d}{2}) \sum_{n=-\infty}^{\infty} \left[\left(\frac{m}{\pi}\right)^2 + \left(\frac{n}{L}\right)^2 \right]^{d/2} , \quad \mathrm{Re}[d] < -1 .$$

This sum is divergent for positive d. The objective is to find an analytic continuation of S valid for positive d [12]. By introducing the Jacobi theta function

$$\theta_J(z;,x) = \sum_{n=-\infty}^{\infty} e^{-\pi n^2 x} e^{2\pi n z} , \tag{B.1}$$

one can use the integral representation of the Gamma function to write [12]

$$S = \int_0^\infty dx x^{-d/2-1} e^{-x\frac{m^2}{\pi}} \theta_J\left(0; \frac{x}{a^2}\right) . \tag{B.2}$$

Applying Jacobi's transformation

$$\theta_J(z;,x) = \frac{1}{\sqrt{x}} e^{\pi\frac{z^2}{x}} \theta_J\left(\frac{z}{ix}; \frac{1}{x}\right) , \tag{B.3}$$

S becomes

$$S = L\left[\Gamma\left(-\frac{d+1}{2}\right)\left(\frac{m}{\sqrt{\pi}}\right)^{d+1} + \int_0^\infty dx\, x^{(d+1)/2-1} e^{-\frac{m^2}{\pi x}} [\theta(0; a^2 x) - 1]\right] , \tag{B.4}$$

and this formula is valid for all d's except the pole at $d=-1$. Performing the integral in (B.4) gives the large m expansion

$$S=\frac{Lm^{d+1}}{\pi^{(d+1)/2}}\left[\Gamma\left(-\frac{d+1}{2}\right)+2\sum_{n=-\infty}^{\infty}{}'\frac{\mathrm{K}_{\frac{(d+1)}{2}}(2m|Ln|)}{(m|Ln|)^{(d+1)/2}}\right], \tag{B.5}$$

where K is a modified Bessel function. In [12], this modified Bessel function is mistakenly reported to be of order $d+1$.

For a multi-dimensional sum

$$\mathcal{S}=\pi^{d/2}\Gamma\left(-\frac{d}{2}\right)\sum_{n_1,\ldots,n_p=-\infty}^{\infty}\left[\left(\frac{m}{\pi}\right)^2+\left(\frac{n_1}{L_1}\right)^2+\cdots+\left(\frac{n_p}{L_p}\right)^2\right]^{d/2}, \tag{B.6}$$

an analytic continuation is obtained in direct analogy with (B.4)[12] by using the generalized Jacobi Θ_J function defined by

$$\Theta_J(z_1,\ldots,z_p;x_1,\ldots,x_p)=\prod_{i=1}^{p}\theta_J(z_i;x_i), \tag{B.7}$$

to obtain [12]

$$\begin{aligned}\mathcal{S}=\frac{L_1\ldots L_p m^{d+p}}{\pi^{(d+p)/2}}&\left[\Gamma\left(-\frac{d+p}{2}\right)\right.\\&\left.+2\sum_{n_1,\ldots,n_p=-\infty}^{\infty}\frac{K_{\frac{d+p}{2}}(2m\sqrt{(L_1n_1)^2+\cdots+(L_pn_p)^2})}{(m\sqrt{(L_1n_1)^2+\cdots+(L_pn_p)^2})^{(d+p)/2}}\right].\end{aligned} \tag{B.8}$$

We note for the interested reader that there are a few typos in [12], below we list some of them.

1. In [12], the first relation in (2.15) is off by a factor of 1/2. It should be

$$E=-\frac{\pi}{24}\frac{1}{a}\approx-0.1309/a\ . \tag{B.9}$$

   (B.9) can be obtained from (2.13) in [12] (another derivation is provided in [10]).

2. The integral in the third relation in (2.18) in [12] is not well defined in the limit $m\to 0$ (when it should yield the massless Casimir energy).

3. The fourth relation in (2.18) in [12] is not correct, it does not agree with the second and third results in (2.15) in [12] (the first result in (2.15) is already incorrect, as we pointed out above).

4. Relation (7.8) in [12] is missing a factor of $\Gamma((d+1)/2)$.

5. The second relation in (7.1) is missing a factor of -1. It should be

$$E = -\frac{\partial}{\partial\beta}\ln(Z)\ . \tag{B.10}$$

References

[1] David McMahon. *Quantum Field Theory Demystified*. McGraw-Hill, 2008.

[2] Mikko Laine and Aleksi Vuorinen. Basics of thermal field theory. *Lect. Notes Phys*, 925:1, 2016.

[3] Eduardo Fradkin. *Field theories of condensed matter physics*. Cambridge University Press, 2013.

[4] Joseph I Kapusta and Charles Gale. *Finite-temperature field theory: Principles and applications*. Cambridge University Press, 2006.

[5] Michel Le Bellac. *Thermal field theory*. Cambridge University Press, 2000.

[6] Jürgen Engels, Frithjof Karsch, and Helmut Satz. Finite size effects in euclidean lattice thermodynamics for non-interacting bose and fermi systems. *Nuclear Physics B*, 205(2):239–252, 1982.

[7] G Boyd, Jürgen Engels, Frithjof Karsch, Edwin Laermann, C Legeland, M Lütgemeier, and Bengt Petersson. Thermodynamics of su (3) lattice gauge theory. *Nuclear Physics B*, 469(3):419–444, 1996.

[8] Szabolcs Borsányi, Zoltan Fodor, Christian Hoelbling, Sandor D Katz, Stefan Krieg, and Kálmán K Szabó. Full result for the qcd equation of state with 2+ 1 flavors. *Physics Letters B*, 730:99–104, 2014.

[9] Hendrick BG Casimir. On the attraction between two perfectly conducting plates. In *Proceedings of the KNAW*, volume 51, pages 793–795, 1948.

[10] Michael Bordag, Galina Leonidovna Klimchitskaya, Umar Mohideen, and Vladimir Mikhaylovich Mostepanenko. *Advances in the Casimir effect*. OUP Oxford, 2009.

[11] Harold Cohen. *Complex analysis with applications in science and engineering*. Springer Science & Business Media, 2010.

[12] Jan Ambjørn and Stephen Wolfram. Properties of the vacuum. i. mechanical and thermodynamic. *Annals of Physics*, 147(1):1–32, 1983.

[13] Viatcheslav Mukhanov. *Physical foundations of cosmology*. Cambridge university press, 2005.

[14] R. M. Ricotta. Thermodynamic properties of the free massless bose field on a lattice. *Revista Brasile ira de Fisica*, 19(2), 1989.

[15] Jürgen Engels, Frithjof Karsch, and Krzysztof Redlich. Scaling properties of the energy density in su (2) lattice gauge theory. *Nuclear Physics B*, 435(1-2):295–310, 1995.

[16] André Peshier, B Kämpfer, OP Pavlenko, and G Soff. Massive quasiparticle model of the su (3) gluon plasma. *Physical Review D*, 54(3):2399, 1996.

[17] Paolo Castorina and Massimo Mannarelli. Effective degrees of freedom and gluon condensation in the high temperature deconfined phase. *Physical Review C*, 75(5): 054901, 2007.

[18] Andre Peshier. Hard thermal loop resummation of the thermodynamic potential. *Physical Review D*, 63(10):105004, 2001.